

**University of Southern Queensland
Faculty of Health, Engineering and Sciences**



Structure and Dynamics of Solitary Waves in Fluid Media

**A thesis submitted in fulfillment of the requirements of
Doctor of Philosophy**

**Niharika Singh
BEd, MSc.**

2016

Abstract

This research deals with the study of nonlinear solitary waves in fluid media. The equations which model surface and internal waves in fluids have been studied and used in this research. The approach to study the structure and dynamics of internal solitary waves in near-critical situations is the traditional theoretical and numerical study of nonlinear wave processes based on the methods of dynamical systems. The synergetic approach has been exploited, which presumes a combination of theoretical and numerical methods. All numerical calculations were performed with the desktop personal computer. Traditional and novel methods of mathematical physics were actively used, including Fourier analysis technique, inverse scattering method, Hirota method, phase-plane analysis, analysis of integral invariants, finite-difference method, Petviashvili and Yang–Lakoba numerical iterative techniques for the numerical solution of Partial Differential Equation.

A new model equation, dubbed the Gardner–Kawahara equation, has been suggested to describe wave phenomena in the near-critical situations, when the nonlinear and dispersive coefficients become anomalously small. Such near-critical situations were not studied so far, therefore this study is very topical and innovative. Results obtained will shed a light on the structure of solitary waves in near-critical situation, which can occur in two-layer fluid with strong surface tension between the layers. A family of solitary waves was constructed numerically for the derived Gardner–Kawahara equation; their structure has been investigated analytically and numerically.

The problem of modulation stability of quasi-monochromatic wave-trains propagating in a media has also being studied. The Nonlinear Schrödinger equation (NLSE) has been derived from the unidirectional Gardner–Ostrovsky equation and a general Shrira equation which describes both surface and internal long waves in a rotating fluid. It was demonstrated that earlier obtained results (Grimshaw & Helfrich, 2008; 2012; Whitfield & Johnson, 2015a; 2015b) on modulational stability/instability

are correct within the limited range of wavenumbers where the Ostrovsky equation is applicable. In the meantime, results obtained in this Thesis and published in the paper (Nikitenkova et al., 2015) are applicable in the wider range of wavenumbers up to $k = 0$. It was shown that surface and internal oceanic waves are stable with respect to self-modulation at small wavenumbers when $k \rightarrow 0$ in contrast to what was mistakenly obtained in (Shrira, 1981).

In Chapter 4 new exact solutions of the Kadomtsev–Petviashvili equation with a positive dispersion are obtained in the form of obliquely propagating skew lumps. Specific features of such lumps were studied in details. In particular, the integral characteristics of single lumps (mass, momentum components and energy) have been calculated and presented in terms of lump velocity. It was shown that exact stationary multi-lump solutions can be constructed for this equation. As the example, the exact bi-lump solution is presented in the explicit form and illustrated graphically. The relevance of skew lumps to the real physical systems is discussed.

List of Publications and Presentations

The following publications and conference presentations were produced during the period of study:

1. Kurkina, O., Singh, N. and Stepanyants, Y. (2014) Structure of Internal Solitary Waves in Two-layer Fluid at Near-critical Situation, *Communications in Nonlinear Science and Numerical Simulation*, v. 22, n. 1–3, p. 1235–1242.
2. Kurkina, O., Singh, N. and Stepanyants, Y. (2014) Internal Solitary waves in Two-layer Fluids at Near-critical Situation. Proc. 19th Australasian Fluid Mechanics Conference, 2014, RMIT University, Melbourne, Australia, 8–11 December 2014, Paper Number 347.
3. Nikitenkova, S., Singh, N. and Stepanyants, Y. (2015) Modulational Stability of Weakly Nonlinear Wave-trains in Media with Small- and Large-scale Dispersions. *Chaos*, v. 25, 123113, 9 p.
4. Singh, N. and Stepanyants, Y. (2016) Obliquely Propagating Skew KP Lumps. *Wave Motion*, v.64, p. 92–102.

Certification of the Thesis

The work contained in this Thesis has not been previously submitted to meet the requirements for an award at this or any other higher educational institution. To the best of my knowledge and belief, the Thesis contains no material previously published or written by another person except where due reference is made.

Candidate: Niharika Singh

Signed: _____

Date: _____

ENDORSEMENT

Principal Supervisor: Professor Yury Stepanyants

Signed: _____

Date: _____

Associate Supervisor: Associate Professor Ron Addie

Signed: _____

Date: _____

Acknowledgement

I would like to express my sincere gratitude and thankfulness to my principal supervisor, Professor Yury Stepanyants for his continuous inspiration, support, patience, and individual feedback throughout the course of my PhD study. It has been a great privilege and blessing to work under his guidance and share the tremendous knowledge and experience he has in the area of our study. He has always been very approachable providing continuous motivation to obtain new and efficient results.

I would also like to express my sincere gratitude and appreciation to my associate supervisor Associate Professor Ron Addie, for his continuous encouragement, support, valuable advice, and suggestions.

I am also very thankful to all of the staff in the School of Agricultural, Computational and Environmental Sciences and former Department of Mathematics and Computing for their cooperation. I extend my gratitude and appreciation to my postgraduate colleagues for their discussions, comments and advices, especially during our group seminars.

Finally, I wish to thank my husband and especially my three children for their patience and support at all times during the course of my study.

Contents

Abstract...	i
List of Publications and Presentations	iii
Certification of the Thesis	iv
Acknowledgement	v
List of Figures	viii
Chapter 1 Introduction and Literature Review	1
1.1. Solitary Waves	2
1.2. History of Solitary Waves	3
1.3. Types of Solitary Waves	5
1.4. Applications	6
1.5. Linear and Nonlinear Equations	7
1.6. Classification of Solitons Based on Nonlinear Equations	9
1.6.1. The KdV Soliton	10
1.6.2. Kink (Topological Solitons)	11
1.6.3. The Envelope Solitons	12
1.7. Internal Waves	13
1.7.1. Oceanic Internal Waves	14
1.7.2. Internal Deep Ocean Waves	16
1.8. Research Objectives	17
1.9. Content of this Research	18
Chapter 2 Structure of Internal Solitary Waves in Two-layer Fluid	21
2.1. Introduction	21
2.2. Dispersion Relation and Stationary Solutions to the Gardner-Kawahara Equation	25
2.3. Soliton Solutions to the Gardner–Kawahara Equation	28
2.4. Discussion	34
2.5. Conclusion	35

Chapter 3	Modulational Stability of Weakly Nonlinear Wave-Trains	36
3.1.	Introduction.....	36
3.2.	The Governing Equations and Dispersion Relations	39
3.3.	The Nonlinear Schrödinger Equation and Modulation Instability	45
3.4.	Conclusion.....	54
Chapter 4	Obliquely Propagating Skew Kadomtsev–Petviashvili Lumps...56	
4.1.	Introduction.....	56
4.2.	Skew lumps	57
4.3.	Obliquely Propagating Skew Multi-lump Solutions	66
4.4.	Integral Characteristics of Skew Lumps.....	74
4.5.	Conclusion.....	76
Chapter 5	Research Outcome and Further Work.....	78
5.1.	Research Outcome.....	78
5.2.	Future Work.....	79
Appendix A	The Numerical Code for the Construction of Stationary Solutions of the Gardner–Ostrovsky Equation by the Petviashvili Method	81
Appendix B	Derivation of Nonlinear Schrödinger Equation.....	88
Appendix C	Publication Papers	91
Bibliography		119

List of Figures

Figure 1.1: Sketch of (a) a periodic wave and (b) a solitary wave.....	8
Figure 1.2a: Schematic of the soliton solution of the Kortweg-de Vries equation.....	9
Figure 1.2b: Schematic of the soliton solution of the sine-Gordon equation.....	10
Figure 1.2b: Schematic of the soliton solution of the nonlinear Schrödinger equation.....	10
Figure 1.3: Schematic plot of processes associated with the passage of a linear oceanic internal wave. Deformation of the thermocline (heavy solid line), orbital motions of the water particles (dashed lines), streamlines of the velocity field (light solid lines), surface current velocity vectors (arrows in the upper part of the image), and variation of the amplitude of the Bragg waves (wavy line at the top).....	15
Figure 1.4: Andaman Sea; The front of a packet of internal solitary waves (left-hand section of the image) interacting with the tail of another internal solitary wave packet (right-hand section of image).....	16
Figure 2.1: Sketch of internal waves at the interface between two fluid layers.....	21
Figure 2.2: The dependence of the normalised dispersion coefficient $\beta_1/(cH^4)$ on the ratio of layer thicknesses $b = h_1/h_2$ at the double critical situation.....	24
Figure 2.3: Plots of phase speed (2.4) for $B = 0$ (line 1, KdV dispersion), $B = 1$ (line 2), and $B = -1$ (line 3). Dashed horizontal line shows the object moving with a constant speed V_s and generating small amplitude wave at the resonant wavenumber κ_r	26
Figure 2.4: Schematic structure of solitary wave asymptotics for Equation (2.13) with different signs of B (frame a). If $B = 0$ only the solitons with monotonic exponential tails are possible as shown in frame b) – see exact solution Equation (2.17).	28
Figure 2.5: Solitary wave shapes as per Equation (2.17) for three values of V . Line 1 pertains to $V = 0.1$ (quasi-KdV case), line 2 pertains to $V = 0.1663$ ('fat soliton'), and line 3 pertains to $V = 0.166666$ (table-top soliton).	29
Figure 2.6: Solitary wave shapes numerically obtained for $B = 1$ and three values of V . Case a) $V = -0.3$, case b) $V = -0.5$, case c) $V = -1.0$	32
Figure 2.7: Examples of single soliton and bi-soliton representing a family of stationary multi-soliton solutions of the GK Equation (2.6).	33
Figure 2.8: Solitary wave shapes numerically obtained for the fixed soliton amplitude $A = 0.998$ and four values of B : line 1 – $B = 0$, line 2 – $B = -10$, line 3 – $B = -100$, line 4 – $B = -1000$	34
Figure 3.1: Dispersion curves as per Equations (3.14) and (3.15) for different coefficients B and Γ . Lines 1 in panels a) and b) pertain to Equation (3.14) with $\Gamma = 1$; lines 2 in panels a) and b) pertain to Equation (3.15) with the same $\Gamma = 1$	

($r = 1.46 \cdot 10^{-2}$); in panel b) line 3 pertains to Equation (3.14) and line 4 – to Equation (3.15) with $\Gamma = -1$ ($q = -1.46 \cdot 10^{-2}$). Dashed lines in panels a) and b) represent the dispersionless dependence $\omega = Ck$ 43

Figure 3.2: Group velocities as per Equation (3.16) for different coefficients B and Γ . Line 1 pertains to V_g with $B = \Gamma = 1$; line 2 pertains to V_{gO} with the same parameters B and Γ ; line 3 pertains to V_g with $B = \Gamma = -1$; line 4 pertains to V_{gO} with the same parameters B and Γ ; and line 5 pertains to V_g with $B = 1$ and $\Gamma = 0$. Dashed horizontal line illustrates the limiting dispersionless case $V_g = C$, and dashed vertical line shows the position of maximum in line 2. 44

Figure 3.3: The dispersion coefficient in the NLSE (3.18) as a function of wavenumber for different primitive equations. 47

Figure 3.4: The nonlinear coefficient in the NLS equation (3.18) as a function of a wavenumber for different basic equations. In frame a) lines 1, 2 and 3 are plotted for $B = \Gamma = 1$, lines 4, 5 and 6 are plotted for $B = \Gamma = -1$; in frame b) lines 7, 8 and 9 are plotted for $B = -\Gamma = 1$, lines 10, 11 and 12 are plotted for $B = -\Gamma = -1$ 51

Figure 3.5: Ranges of stability (when $F(k) < 0$) and instability (when $F(k) > 0$) of wave-trains against self-modulation. Frame a) pertains to $B = \Gamma = 1$; frame b) pertains to $B = \Gamma = -1$; frame c) pertains to $B = -\Gamma = 1$; and frame d) pertains to $B = -\Gamma = -1$. For the meaning of lines see the text. 53

Figure 4.1a: Contour plot of the conventional KP1. 59

Figure 4.1b: 3D plot of the conventional KP1 lump. 60

Figure 4.2: The domain of possible velocity components (shaded) of a single lump as per Equation (4.12). 62

Figure 4.3: Contour plots of lumps for different values of ν . a) $\nu = 0.5$; b) $\nu = 1.0$; c) $\nu = 1.5$; and d) $\nu = 1.9$. Arrows show maximum values, zero isolines are also indicated. 63

Figure 4.4a: Contour plot of a skew lump with $\nu = 1.5$ in the coordinate system where the zero isolines are symmetrical with respect to the coordinate axes (see the hyperbolic lines). 65

Figure 4.4b: 3D profile of the same lump in Figure 4.4a. 65

Figure 4.5a: Skew lumps as per Equation (4.18) with $a = b = 0$ and $\nu = 0$ 68

Figure 4.5b: Skew lumps as per Equation (4.18) with $a = b = 0$ and $\nu = 0.5$ 68

Figure 4.5c: Skew lumps as per Equation (4.18) with $a = b = 0$ and $\nu = 1.0$ 69

Figure 4.5d: Skew lumps as per Equation (4.18) with $a = b = 0$ and $\nu = 1.5$ 69

Figure 4.5e: Skew lumps as per Equation (4.18) with $a = b = 0$ and $\nu = 1.9$ 70

Figure 4.6a: Skew lumps as per Equation (4.18) with $a = 10$, $b = 0$ and $\nu = 0$ 70

Figure 4.6b: Skew lumps as per Equation (4.18) with $a = 10$, $b = 0$ and $\nu = 0.5$ 71

Figure 4.6c: Skew lumps as per Equation (4.18) with $a = 10$, $b = 0$ and $\nu = 0.9$ 71
Figure 4.6d: Skew lumps as per Equation (4.18) with $a = 10$, $b = 0$ and $\nu = 0.99$ 72
Figure 4.6e: Skew lumps as per Equation (4.18) with $a = 10$, $b = 0$ and $\nu = 1.01$ 72
Figure 4.6f: Skew lumps as per Equation (4.18) with $a = 10$, $b = 0$ and $\nu = 1.1$73
Figure 4.6g: Skew lumps as per Equation (4.18) with $a = 10$, $b = 0$ and $\nu = 1.5$ 73
Figure 4.6e: Skew lumps as per Equation (4.18) with $a = 10$, $b = 0$ and $\nu = 1.9$ 74

Chapter 1 Introduction and Literature Review

Internal waves in the oceans and atmosphere have been under intense experimental and theoretical studies for the last thirty years or even more (see reviews by (Ostrovsky & Stepanyants, 1989) and (Grimshaw, 1996)). It has been well understood that the density stratification can support not only the dynamics of linear dispersive wave packets, but also the propagation of relatively long and localized disturbances called solitary waves or solitons. These waves are typically single-humped isolated waves of elevation or depression and they can propagate for long distances without distortion of their shapes. Solitary waves appear in the real world in various embodiments, for instance, as the pycnocline humps or depressions, freak waves, tsunami waves, waves behind of high speed ships, tidal bores, morning glory clouds, etc. Internal waves occur in the coastal seas, fjords and lakes, as well as in the atmospheric boundary layers.

There are few ways to classify solitons, for example there are topological and nontopological solitons. Independently of the topological nature of solitons, all solitons can be divided into two groups by taking into account their profiles: permanent and time dependent. For example, kink soliton have a permanent profile (in ideal system), while all breathers have an internal dynamics, even if they are static. So their shape oscillates in time. The third way to classify the solitons is in accordance with nonlinear equations which describe their evolution and is discussed later in the chapter.

This research is devoted to further study of possible manifestations of solitary waves in fluid media, as well as conditions when they can occur. In particular, we investigate the Lighthill criterion for surface and internal waves in rotating fluids and derive the condition when a self-modulation of quasi-harmonic waves can occur. It is well-known that self-modulation leads to the formation of envelope solitons. We also study the conditions of solitary wave existence in the KdV-type systems, as well as the existence of 2D skew lumps and their properties in the KP equation.

1.1. Solitary Waves

Solitary waves (also known as the “waves of translation”) are waves which propagate without any temporal evolution in shape or size. The envelope of a solitary wave has one global peak and decays far away from the peak. Solitary waves arise in many contexts, including the elevation of the surface of water and the intensity of light in optic fibers. A soliton is a nonlinear solitary wave with the additional property that the wave retains its permanent structure, even after interacting with another soliton. For example two solitons propagating in opposite direction effectively pass through each other without breaking. One of the specific features of solitons is their stability and robustness with respect to external perturbations and interactions with other nonlinear waves. They can survive in the noisy environment, under the influence of nonstationary perturbations and in the inhomogeneous media (Ostrovsky, 2015). Namely due to such particle-like properties these waves were called solitons (Remoissenet, 1999).

Solitons form a special class of solutions of model equations, including the Korteweg–de Vries (KdV), nonlinear Schrödinger (NLS) and Kadomtsev–Petviashvili (KP) equations. These model equations are approximations, which hold under a restrictive set of conditions. The soliton solutions obtained from the model equations provide important insight into the dynamics of solitary waves, despite that they are limited by the conditions under which the model equations hold. In many cases the results obtained within the framework of approximate model equations provide a platform to construct more realistic solutions within more accurate primitive equations. Solitary waves can transmit energy and momentum at large distances with minimal dissipation, impact beaches, engineering constructions and ships. This explains the importance of study of different kind of solitary waves, their possible manifestations and conditions when they can appear.

Solitary waves usually arise due to the balance between the nonlinear and dispersive or dissipative effects. In most types of solitary waves, the pulse width depends on the amplitude. When a soliton interacts with another soliton, it emerges from the “collision” unchanged except, possibly, for a phase shift. That is, for a conservative (non-dissipative) system, a soliton is a solitary wave whose amplitude,

shape, and velocity are conserved after a collision with another soliton (Scott, 2005). Solitary waves arise in both continuous systems such as the KdV equation (Korteweg & De Vries, 1895) and discrete systems such as the Toda lattice (Toda, 1989a) and in both one and many spatial dimensions, e.g., within the framework of 2D KP equation (Kadomtsev–Petviashvili, 1970; Petviashvili & Pokhotelov, 1992).

The key issues in studying solitary waves include linear versus nonlinear, integrable versus non-integrable, persistent versus transient, asymptotic behavior, localization in physical space, and persistent against the effects of noise and other external perturbations.

Many exactly solvable models have soliton solutions, including the Korteweg–de Vries equation, nonlinear Schrödinger equation, sine-Gordon equation, etc. The soliton solutions can be typically found from the corresponding Ordinary Differential Equations, and their interactions can be studied by means of the inverse scattering transform (IST) (Ablowitz & Segur, 1981) or asymptotic methods (Gorshkov & Ostrovsky, 1981). The mathematical theory of these equations is broad and very active field of contemporary mathematical research.

1.2. History of Solitary Waves

The early history of solitons or solitary waves began in August 1834 when the Victorian Engineer John Scott Russell observed a solitary wave travelling along the Scottish canal. He then conducted controlled laboratory experiments using a wave tank and quantified the phenomenon in the Report of 1844 (Russell, 1844). He demonstrated the facts that:

- solitary waves that he observed had a bell-type shape,
- a sufficiently large initial mass of water can produce two or more independent near-solitary waves that separate in time,
- solitary waves can cross each other “without change of any kind” and
- larger-amplitude waves move faster than smaller ones.

The mathematical evolution of the theory of solitary waves is followed from its inception when analytical mechanics were developed. It was recognized that the motion of a wave differs from that of the water particles, but the first exact solution of a wave theory, published by Gerstner in 1802, assumes that both motions coincide. With Russell's experimental in 1838, his classification of solitary waves that he observed had a hyperbolic secant shape, a sufficiently large initial mass of water can produce two or more independent near-solitary waves that separate in time, solitary waves can cross each other "without change of any kind" and a larger-amplitude waves move faster than smaller ones (Russell, 1844).

The most successful contributions were brought by Airy in 1845 with a nonlinear shallow water theory of waves of non-permanent form and by Stokes in 1849 with a theory of deep water waves. The first mathematical description of waves of permanent form was obtained by Boussinesq in 1871 and it was rediscovered by another method by Rayleigh in 1876. The next steps were to improve the stationary behaviour of solitary waves. Rayleigh had remarked that in his solution the pressure distribution at the free surface is not constant, thus invalidating the stationarity of the solution.

The definitive theory of shallow water waves was first published in 1895 by Diederick Korteweg, the Dutch physicist, and his student Gustav de Vries. They derived a nonlinear partial differential equation (PDE) which currently bears their names. McCowan (1894), Korteweg & de Vries, (1895) gave more accurate results for the wave form and the maximum possible wave-height.

In 1958 solitons in plasma physics was discovered by J.H. Adlam and J.E. Allen, solitary waves in collision-less plasma containing a magnetic field (Allen, 1998). In 1965 Zabusky and Kruskal found through the numerical investigations that solitary waves in KdV equation retain their identity after collisions. This feature led these authors to introduce the term soliton to emphasise their particle-like property.

1.3. Types of Solitary Waves

After the discovery of solitons, they were investigated in both one dimension and even in two and three spatial dimensions (Scott, 2005). The most prominent examples, beside the KdV-type solitons, include the following types of solitons and corresponding equations:

- *Envelope Solitons* (Scott, 2005): Solitary waves that arise in the propagation of modulated plane waves in dispersive nonlinear media with an amplitude-dependent dispersion relation. The basic model equation describing such solitons is the nonlinear Schrödinger (NLS) equation.
- *Topological solitons* (Scott, 2005): The typical representatives of this class of solitons are solutions to the sine-Gordon equation that emerges because of topological constraints. One example is a skyrmion, which is the solitary-wave solution of a field model whose topological charge is the baryon number. Other examples include domain walls, which refer to interfaces that separate distinct regions of order and which form spontaneously when a discrete symmetry (such as time-reversal symmetry) is broken, screw dislocations in crystalline lattices, and the magnetic monopole.
- *Kinks* (Scott, 2005): The only one-dimensional topological solitary wave, it represents a twist in the value of a solution and causes a transition from one value to another. Kinks can be represented by heteroclinic orbits on the phase plane, whereas pulse-like solitary waves can be represented by homoclinic orbits. Kinks are the particular solutions of the sine-Gordon equation; they are observable in the solid state physics, crystal dislocations in Josephson junctions and many other physical areas.
- *Vortex solitons* (Scott, 2005): A term often applied to the phenomena such as *vortex rings* (a moving, rotating, toroidal fluid objects) and *vortex lines*. One of the good examples of a vortex soliton is the Hill vortex (Lamb, 1932) or its plane analog, the Lamb–Chaplygin vortex (Chaplygin, 2007).
- *Dissipative solitons* (Scott, 2005): Stable localized structures that arise in spatially extended dissipative systems. They are often studied in the context of nonlinear

reaction-diffusion systems and are known as the autosolitons (Kerner, Osipov, 1994). One of the most popular equations in this field is the Kuramoto–Sivashinsky equation (Scott, 2005).

- *Gap solitons* (Scott, 2005): Solitary waves that occur in finite gaps in the spectrum of continuous systems. For example, gap solitons have been studied rather thoroughly in the NLS equations with spatially periodic potentials and have been observed experimentally in the context of both nonlinear optics and Bose–Einstein condensation.
- *Higher-dimensional solitary waves* (Scott, 2005), (Petviashvili & Pokhotelov, 1992): Solitary waves and other localized structures have also been studied in higher-dimensional settings. One example of a genuine two-dimensional soliton is a “lump” solution of the Kadomtsev–Petviashvili (KP) equation of the first type (i.e., the KP1 equation). This type of solitons decays algebraically rather than exponentially and is sometimes described as “weakly localized”. The KP equation of the second type (i.e., the KP2 equation) differs from the KP1 equation in that it has the opposite sign in front of its dispersion term. The KP2 equation has stable line-soliton solutions, which (unlike line solitons in the KP1 equation) can merge with each other to form a single line soliton, which can, in turn, disintegrate into two separate line solitons (Ablowitz & Segur, 1981).

1.4. Applications

Solitary waves are present in fluid mechanics, optics, atomic physics, biophysics, and other physical areas (Scott, 2005), (Ablowitz & Segur, 1981). Solitons in biology may occur in proteins and DNA and are related to the low frequency collective motions. A recently developed model in neuroscience proposes that signals are conducted within neurons in the form of solitons. In magnets, there also exist different types of solitons and other nonlinear waves. These magnetic solitons are exact solutions of classical nonlinear differential equations (magnetic equations).

Envelope solitary waves are omnipresent in nonlinear optics (Scott, 2005). There have been extensive experimental and theoretical investigations about both

spatial solitary waves, in which the nonlinearity balances diffraction, and temporal solitary waves, in which the nonlinearity balances dispersion. From the mathematical perspective, continuous nonlinear Schrödinger equations are among the hallmark models in nonlinear optics, as they describe dispersive envelope waves (via solitary-wave solutions of the NLS equation) of the electromagnetic field in optical fibers, and discrete NLS (DNLS) equations can be used to describe the dynamics of pulses in optical waveguide arrays and photorefractive crystals.

1.5. Linear and Nonlinear Equations

For a long time linear equations have been used for describing different phenomena. For example, Newtons, Maxwells and Schrödinger equations are linear and they take into account only a linear response of a system to an external disturbance. However, the majority of real systems are nonlinear. Most of the theoretical models are still relying on a linear description, corrected as much as possible for nonlinearities which are treated as small perturbations (Mourachkine, 2004). It is well known that such an approach can be absolutely wrong. The linear approach can sometimes miss completely some essential behaviours of the system.

Nonlinearity has to do with threshold, with multi-stability, with hysteresis, with phenomena which are changed quantitatively as the excitations are changed. In a linear system, the ultimate effect of the combined action of two different causes is merely the superposition of the effects of each cause taken individually. But in a nonlinear system adding two elementary actions to one another can induce dramatic new effects reflecting the onset of cooperativity between the constituent elements. To understand nonlinearity, one should first understand linearity. Consider linear waves. In general, a wave may be defined as a progression through matter of a state of motion. Characteristic properties of any linear wave are:

- The shape and velocity of a linear wave are independent of its amplitude
- The sum of two linear waves is also a linear and
- Small amplitude waves are linear.

Large amplitude waves may become nonlinear. The fate of a wave travelling in a medium is determined by properties of the medium. Nonlinearity results in the distortion of the shape of large amplitude waves for example in turbulence. However, there is another source of distortion the dispersion of a wave.

More than 100 years ago the mathematical equations describing solitary wave were solved, at which point it was recognized that the solitary wave, shown in Figure 1.1(b), may exist due to a precise balance between the effects of nonlinearity and dispersion (Mourachkine, 2004). Nonlinearity tends to make the hill steeper Figure 1.1 while dispersion flattens it.

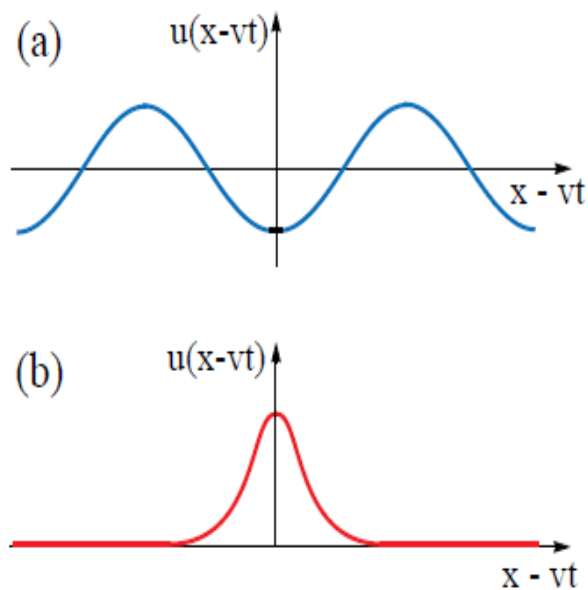


Figure 1.1: Sketch of (a) a periodic wave and (b) a solitary wave.

A solitary wave lives between these two dangerous destructive forces. Thus the balance between nonlinearity and dispersion is responsible for the existence of solitary waves.

1.6. Classification of Solitons Based on Nonlinear Equations

The three nonlinear equations which is used to describe soliton solutions are the KdV equation, the sine-Gordon equation and the nonlinear Schrödinger (NLS) equation. General summary of these equations are as follows:

Kortweg-de Vries equation,

$$u_t = 6uu_x - u_{xxx} \quad (1.1)$$

the sine-Gordon equation

$$u_{tt} = u_{xx} - \sin u \quad (1.2)$$

and the nonlinear Schrödinger equation

$$iu_t = -u_{xx} \pm |u|^2 u. \quad (1.3)$$

For simplicity, the equations are written for dimensionless function depending on the dimensionless time and space variable. Simple sketch of these equations are shown in Figure 1.2.

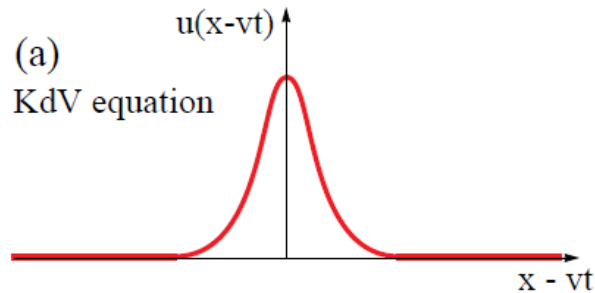


Figure 1.2a: Schematic of the soliton solution of the Kortweg-de Vries equation

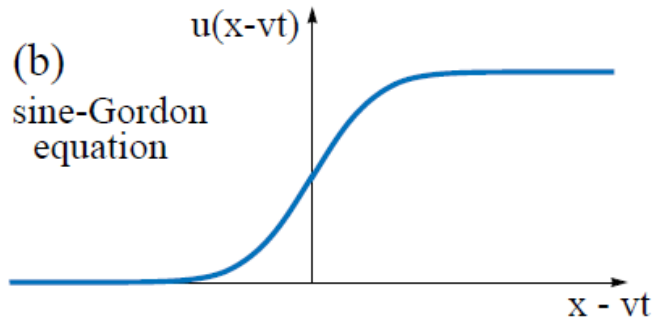


Figure 1.2b: Schematic of the soliton solution of the sine-Gordon equation.

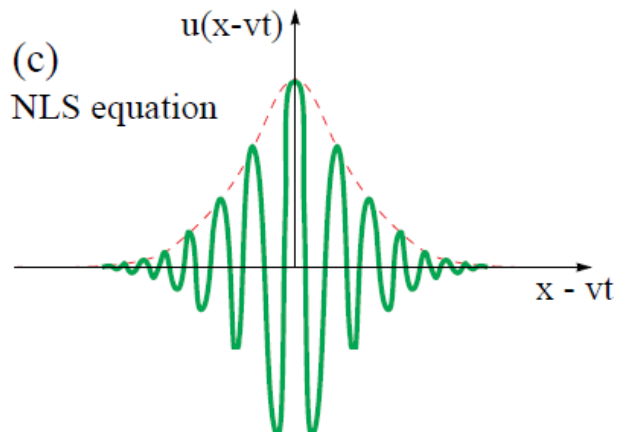


Figure 1.2c: Schematic of the soliton solution of the nonlinear Schrödinger equation.

There are many other nonlinear equations (i.e. Boussinesq equation) which can be used for evaluating solitary waves; however these three equations are particularly important for the physical applications. They exhibit the most famous solitons: the KdV (pulse) solitons, the sine-Gordon (topological) solitons and NLS (envelope) solitons. Common features and individual differences of these solitons is discussed below.

1.6.1. The KdV Soliton

The exact solution for a KdV soliton Equation (1.1) is given as

$$u(x,t) = u_0 \operatorname{sech}^2\left(\frac{x-vt}{l}\right) \quad (1.4)$$

where u_0 is the initial height of the soliton, $v = \sqrt{gh(1 + \frac{u_0}{2h})}$ and $2l$ is the width of the soliton.

The basic properties of KdV solitons can be summarized as:

- Its amplitude increases with its velocity (and vice versa). Thus they cannot exist at rest.
- Its width is inversely proportional to the square root of its velocity.
- It is a unidirectional wave pulse, i.e. its velocity cannot be negative for solutions of the KdV equation.
- The sign of the soliton solution depends on the sign of the nonlinear coefficient in the KdV equation.

The KdV solitons are nontopological, and they exist in physical systems with weakly nonlinear and with dispersive waves. When a wave impulse breaks up into several KdV solitons, they all move in the same direction. In presence of dissipation (friction), the KdV solitons gradually decelerate and become smaller and longer and thus decrease (Mourachkine, 2004).

1.6.2. Kink (Topological Solitons)

The exact solution of the sine-Gordon equation is given as

$$u(x - vt) = 4 \arctan \left[\exp \left(\pm \frac{\omega_0}{c_0} \frac{x - vt}{\sqrt{1 - v^2/c_0^2}} \right) \right] \quad (1.5)$$

The basic properties of a kink (topological) soliton can be summarized as:

- Its amplitude is independent of its velocity- it is constant and remains the same for zero velocity, thus the kink may be static.
- Its width gets narrower as its velocity increases, owing to Lorentz contraction.

- It has the properties of a relativistic particle.
- The topological kink which has a different screw sense is called an antikink.

Topological solitons are extremely stable. Under the influence of friction, these solitons only slow down and eventually stop and at rest, they can live ‘eternally’. In a finite system, the topological soliton can only be destroyed by moving a semi-infinite segment of the above a potential maximum which will require an infinite energy (Remoissenet, 1999).

1.6.3. The Envelope Solitons

The nonlinear Schrödinger (NLS) equation is formally similar to the Schrödinger equation of quantum mechanics which is given as:

$$\left(i\hbar \frac{\partial}{\partial t} + \frac{\hbar^2}{2m} \frac{\partial^2}{\partial x^2} \right) \psi(x, t) = 0 \quad (1.6)$$

where U is the potential and $\psi(x, t)$ is the wave function. The NLS equation describes self-focusing phenomena in nonlinear optics, one-dimensional self-modulation of monochromatic waves in nonlinear plasma etc. In the NLS equation the potential U is replaced by $|u|^2$ which brings into the system self-interaction. The second term of the NLS equation is responsible for the dispersion and the third one for the nonlinearity. The solution of NLS solution is shown schematically in Figure 1.2(c). The shape of the enveloping curve in Figure 1.2(c) (the red dashed line) is given by

$$u(x, t) = u_0 \operatorname{sech} \left(\frac{x - vt}{l} \right) \quad (1.7)$$

where $2l$ determines the width of the soliton. Its amplitude u_0 depends on l , but the velocity v is independent of the amplitude distinct from the KdV soliton. The shapes of the envelope and KdV solitons are different, the KdV soliton has a sech^2 shape. Thus the envelope soliton has a slightly wider shape. However, other properties of the

envelope solitons are similar to KdV as they are ‘mortal’ and can be regarded as particles.

In an envelope soliton the stable group has normally from 14 to 20 humps under the envelope, the central one being the highest one. The groups with more humps are unstable and break up into smaller ones. The waves inside the envelope move with a velocity that differs from the velocity of the soliton thus, the envelope soliton has an internal dynamics. The relative motion of the envelope and the carrier wave is responsible for the internal dynamics of the NLS soliton. The NLS equation is inseparable part of the nonlinear optics where the envelope solitons are usually called dark and bright solitons and become quasi-three-dimensional.

1.7. Internal Waves

Internal tides, namely internal waves of a tidal period, were first observed in the ocean by Helland-Hansen and Nansen (1909) in the Norwegian Sea by means of hydrographic observations using Nansen bottles repeated at short intervals. They have since been observed in many places in the World’s ocean both in the mid-ocean and near coasts, over continental shelves and slopes.

Internal ocean waves are waves which occur within the subsurface layers of the ocean where the density gradient is strong and are generated when the interface between layers is disturbed. Disturbances are caused by tidal flow passing over shallow underwater obstacles such as a sill or a shallow ridge. The favorable place for the generation of intensive oceanic internal waves is where there is complex coastline geometry and bathymetry, narrow passages, stratified waters and strong tidal current. Internal waves are commonly observed in the Lombok Strait one of the outflow straits of the Indonesian through flow, which transports water from the Pacific to the Indian Ocean.

1.7.1. Oceanic Internal Waves

Oceanic internal waves are waves in the interior of the ocean. They exist when the water body consists of layers of different density. This difference in water density is mostly due to a difference in water temperature, but can also be due to a difference in salinity. Often the density structure of the ocean can be approximated by two layers. The interface between layers of different densities is called pycnocline. When the density difference is due to temperature it is called thermocline, and when it is due to salinity it is called halocline.

Just like ocean surface waves, which are waves at the interface of two media of different density, that is of water and air, the internal waves are waves at the interface between two water layers of different density. In both cases the restoring force is gravity, which is the reason why both waves sometimes are called gravity waves. These waves are generated when the interface is disturbed. In the case of surface waves, this disturbance can be caused by a stone thrown into the water or by wind blowing over the water surface. In the case of internal waves, this disturbance is usually caused by tidal flow pushing the layered water body over shallow underwater obstacles, e. g., over shallow sills or shallow ridges (Maxworthy, 1979), (Helfrich & Melville, 1986) and (Lamb, 1994).

Internal waves in the ocean typically have wavelengths from hundreds of meters to tens of kilometers and periods from tens of minutes to several hours. Their amplitude (peak-to trough distance) often exceeds 50 m. Associated with internal waves are orbital motions of the water particles as shown in Figure 1.1 (the dashed circular lines). The radius of the circular motion of the water particles is largest at the pycnocline (or thermocline) depth and decreases downwards as well as upwards from this depth. To first order, the internal waves do not give rise to an elevation of the sea surface as the familiar surface waves do, but they do give rise to a variable (horizontal) surface current. The current velocity at the sea surface varies in magnitude and direction giving rise to convergent and divergent flow regimes at the sea surface as shown in Figure 1.3.

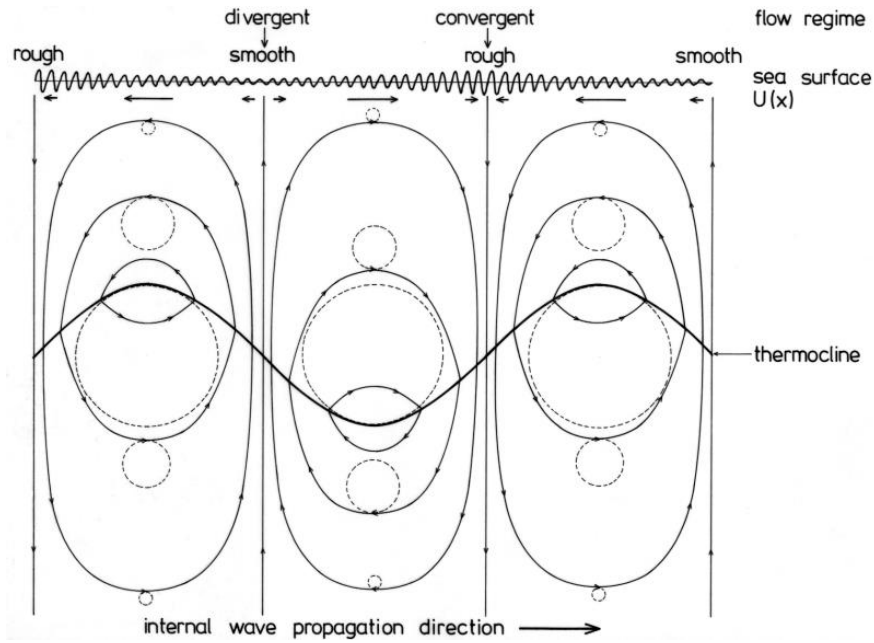


Figure 1.3: Schematic plot of processes associated with the passage of a linear oceanic internal wave. Deformation of the thermocline (heavy solid line), orbital motions of the water particles (dashed lines), streamlines of the velocity field (light solid lines), surface current velocity vectors (arrows in the upper part of the image), and variation of the amplitude of the Bragg waves (wavy line at the top).

The variable surface current interacts with the surface waves and modulates the sea surface roughness (Hughes, 1978), (Alpers, 1985). This interaction is the reason why oceanic internal waves become visible on radar images of the sea surface and, in some cases, also on images acquired in the visible ultraviolet or infrared wavelength band (see Apel, *et al.*, 1975).

Due to the hydrodynamic interaction of the variable surface current with the surface waves, the amplitude of the Bragg waves is increased in convergent flow regions and is decreased in divergent flow regions. As a consequence, the radar signatures of oceanic internal waves consist of alternating bright and dark bands on a uniform background.

But there exist also other radar signatures of internal waves: Sometimes they consist only of bright lines or only of dark bands. When the wind speed is below threshold for Bragg wave generation, only bright bands are encountered and when surface slicks are present, only dark lines are seen (da Silva *et al.*, 1998). However,

radar imaging theories capable of explaining these exceptional radar signatures of internal waves quantitatively still do not exist.

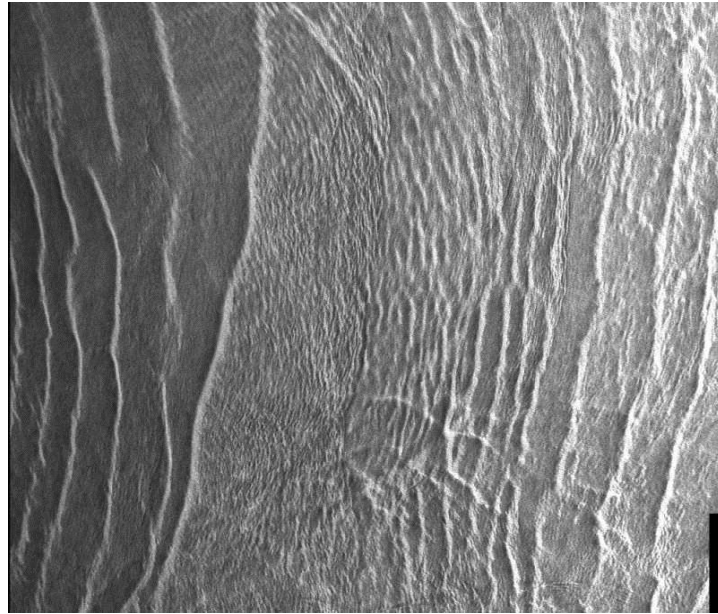


Figure 1.4: Andaman Sea; The front of a packet of internal solitary waves (left-hand section of the image) interacting with the tail of another internal solitary wave packet (right-hand section of the image).

1.7.2. Internal Deep Ocean Waves

Internal solitary waves occur in a wide range of deep-ocean locales, in region at least as far as 500 kilometers from the shore or even further. Deep water solitons are typically formed during strong tidal flow over relatively shallow underwater sills that protrude up into the permanent thermocline, for example, 300 to 500 meters. The Strait of Gibraltar is one of the most thoroughly studied cases (Farmer & Armi, 1988). Packets of internal solitons regularly propagate into the Western Mediterranean Sea following the generation at the Gibraltar sill by the combined tidal, surface and subsurface flow of Mediterranean water out of the Atlantic ocean (Apel, *et al.*, 2006).

The amplitudes of these waves are of the order of 50 meters and their inter-soliton distance or wavelength varies from 500 to 2000 meters. These solitons can have larger amplitudes in a deep ocean and much larger scales both across and along their fronts. At the same time due to a deeper pycnocline position and smoother stratification,

the effective nonlinearity in such solitons may remain relatively small, whereas in the shelf zone it can reach significant values (Ostrovsky & Stepanyants, 1989), (Apel, *et al.*, 2006), (Ostrovsky, *et al.*, 2015).

1.8. Research Objectives

The aim of the research of this Thesis is threefold:

- 1) To derive a model equation describing the dynamics of internal waves in two-layer fluid with surface tension between the layers at the near critical situation, when both the coefficients of quadratic nonlinearity and cubic dispersion are close to zero. The corresponding model equation, dubbed the Gardner–Kawahara equation, was not derived so far, and its properties were not studied, whereas the particular cases, the Gardner equation and Kawahara equation are well-known (see, for example (Ostrovsky *et al.*, 2015) and references therein). Possible solitary type solutions of the Gardner–Kawahara equation will be investigated by means of an elaborated numerical scheme. The structure of solitary waves will be studied and the range of parameters where they can exist will be determined.
- 2) To derive the NLS equation describing long surface and internal waves in a rotating fluid. The derivation of this equation and study its properties provides a basis for the investigation of conditions for the existence of envelop solitons in natural oceanic conditions (as well as in some other media where the large-scale dispersion occurs). There is a number of papers devoted to derivation of NLS equation for shallow waves in rotating fluids, but the results obtained are contradictory and doubtful. Therefore, here we revisit the problem of modulation stability of quasi-monochromatic wave-trains propagating in different media with the double dispersion occurring both at small and large wavenumbers. We derive the nonlinear Schrödinger equation and determine conditions when the modulation instability can occur. The NLSE derived here

has a wider range of applicability than in the previously considered cases (Shrira, 1981), (Grimshaw & Helfrich, 2008; 2012), (Whitfield & Johnson, 2015a, b). We present the analysis of coefficients of the NLSE for different signs of coefficients of the governing equation and compare them with those derived from the Ostrovsky equation (Grimshaw & Helfrich, 2008; 2012) or Gardner–Ostrovsky equation (Whitfield & Johnson, 2015a, b).

- 3) To derive exact analytical solution in the form of skew lumps of the KP1 equation. Lump solutions of the Kadomtsev–Petviashvili equation with a positive dispersion (the KP1 equation) are well known (Ablowitz & Segur, 1981), (Petviashvili & Pokhotelov, 1992). In recent years even more general skew lumps were derived for this equation (Lu et al., 2004), (Ma, 2015). However, their properties were not studied thoroughly. Here we derive exact solutions describing not only single skew lumps, but even more general multi-lumps. We calculate the integral characteristics of single lumps (mass, momentum components and energy) and present them in terms of lump velocity. As an example, the bi-lump solution is presented in the explicit form, analysed and illustrated graphically.

1.9. Content of this Research

The outline of the research is as follows:

- Chapter 2: A new model equation describing weakly nonlinear long internal waves at the interface between two thin layers of different density is derived for the specific relationships between the densities, layer thicknesses and surface tension between the layers. The equation derived and dubbed here the Gardner–Kawahara equation represents a natural generalisation of the well-known Korteweg–de Vries (KdV) equation containing the cubic nonlinear term, as well as the fifth-order dispersion term. Solitary wave solutions are investigated numerically and categorised in terms of two dimensionless parameters, the wave

speed and fifth-order dispersion. The equation derived may be applicable to wave description not only in a fluid, but in other nonlinear media.

- Chapter 3: Revisits the problem of modulation stability of quasi-monochromatic wave-trains propagating in a media with the double dispersion occurring both at small and large wavenumbers. It starts with the shallow-water equations derived by Shrira (1981) for the description of both surface and internal long waves in a rotating fluid. The small-scale (Boussinesq-type) dispersion is assumed to be weak, whereas the large-scale (Coriolis-type) dispersion is considered as is without any restriction. For unidirectional waves propagating in one direction only the considered set of equations reduces to the Gardner–Ostrovsky equation which is applicable only within a finite range of wavenumbers. Then the nonlinear Schrödinger equation is derived, which describes the evolution of narrow-band wave-trains. It is shown that within the more general bi-directional equation the wave-trains, similar to that derived from the Ostrovsky equation, are also modulationally stable at relatively small wavenumbers $k < k_c$ and unstable at $k > k_c$, where k_c is some critical wavenumber specified below. The NLS equation derived here has a wider range of applicability at small wavenumbers than the equations derived in other papers (Grimshaw & Helfrich, 2008; 2012), (Whitfield & Johnson, 2015a, b). This chapter presents the analysis of coefficients of the NLS equation for different signs of coefficients of the governing equation. The governing equation is presented in the dimensionless form, containing the dispersion parameters of either sign, so that the equation is applicable not only to water waves in a rotating fluid, but to a wider class of nonlinear waves of any nature. The derived NLS equation determines the criterion of modulational stability/instability for all possible signs of dispersion coefficients. From the results obtained it follows that the findings of Grimshaw & Helfrich (2008; 2012) and Whitfield & Johnson (2015a, b) are correct within the range of validity of the Ostrovsky or Gardner–Ostrovsky equations, correspondingly, but contradict to the results obtained by Shrira (1981) at small k .

- Chapter 4: Contains a study of obliquely propagating skew lumps within the framework of the Kadomtsev–Petviashvili equation with a positive dispersion (the KP1 equation). The specific features of such lumps are analysed in details. It is shown that the skew multi-lump solutions can be also constructed within the framework of that equation. As an example, the bi-lump solution is presented in the explicit form, analysed and illustrated graphically. The relevance of skew lumps to the real physical systems is discussed.
- Chapter 5: Contains conclusion and discussions of results obtained in the Thesis. It also highlights further avenues of research in this field.

Chapter 2 Structure of Internal Solitary Waves in Two-layer Fluid

2.1. Introduction

The governing equation describing long internal waves of small amplitude at the interface in a two-layer fluid is, in general the well-known Korteweg–de Vries (KdV) equation [see, e.g., (Ablowitz & Segur, 1981; Apel, *et al.*, 2007) and references therein]:

$$\frac{\partial u}{\partial t} + c \frac{\partial u}{\partial x} + \alpha u \frac{\partial u}{\partial x} + \beta \frac{\partial^3 u}{\partial x^3} = 0. \quad (2.1)$$

Here the coefficients are:

$$c^2 = \frac{g(\rho_2 - \rho_1)h_1h_2}{\rho_1h_2 + \rho_2h_1}, \quad \alpha = \frac{3c}{2h_1h_2} \frac{\rho_2h_1^2 - \rho_1h_2^2}{\rho_1h_2 + \rho_2h_1}, \quad \beta = \frac{h_1h_2}{6} c \frac{\rho_1h_1 + \rho_2h_2 - 3\sigma/c^2}{\rho_1h_2 + \rho_2h_1}, \quad (2.2)$$

where index 1 pertains to the upper layer, index 2 – to the lower layer (see Figure 2.1), $\rho_{1,2}$ are densities of the layers, $h_{1,2}$ are thicknesses of the layers, and σ is the surface tension between the layers. For the sake of simplicity the assumption here is that the ‘rigid lid’ approximation is used to filter the surface mode (Brekhovskikh & Goncharov, 1994).

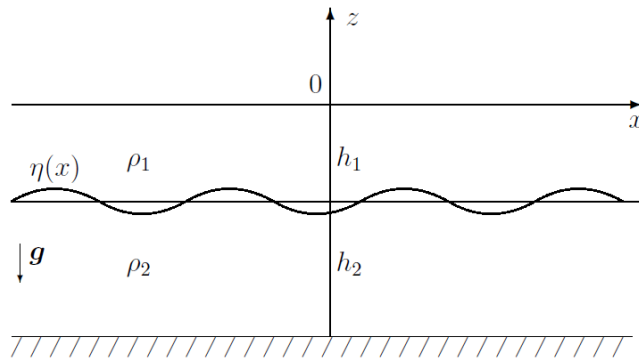


Figure 2.1: Sketch of internal waves at the interface between two fluid layers

However, at certain conditions Equation (2.1) degenerates because some of its coefficients vanish. In particular, the generalisation is required when the density interface is located near the half-depth of the fluid. In this case the coefficient of quadratic nonlinearity α becomes anomalously small, then the next order nonlinear term is taken into consideration, the cubic term, to balance the dispersion effect (Apel, *et al.*, 2007). The corresponding equation is known as the Gardner equation (alias the extended KdV or combKdV equation):

$$\frac{\partial u}{\partial t} + c \frac{\partial u}{\partial x} + \alpha u \frac{\partial u}{\partial x} - \alpha_1 u^2 \frac{\partial u}{\partial x} + \beta \frac{\partial^3 u}{\partial x^3} = 0 \quad (2.3)$$

where the cubic nonlinear coefficient is

$$\alpha_1 = \frac{21}{8c} \left[\frac{8}{7} \left(\frac{c}{h_1 h_2} \right)^2 \frac{\rho_2 h_1^3 + \rho_1 h_2^3}{\rho_1 h_2 + \rho_2 h_1} - \left(\frac{2\alpha}{3} \right)^2 \right]. \quad (2.4)$$

The KdV and Gardner equations are completely integrable (Ablowitz & Segur, 1981); they possess, in particular, soliton solutions (Apel, *et al.*, 2007) which attract a special interest due to their specific particle-like properties, e.g., they restore their shapes after the interaction with each other and asymptotically evolve from arbitrary pulse-type perturbations. In a two layer fluid the structure of Gardner solitons is very well studied, it varies from the bell-shaped KdV solitons for small amplitude waves to table-top solitons for large-amplitude waves (Apel, *et al.*, 2007).

There are also situations when the dispersion coefficient β vanishes. Such cases are known, for example for gravity-capillary waves with strong surface tension and magnetosonic waves in plasma (Karpman, 1975). In the near critical situation when the dispersive coefficient β becomes anomalously small, the next-order dispersion should be taken into consideration. This leads to the fifth-order KdV equation with the quadratic nonlinearity:

$$\frac{\partial u}{\partial t} + c \frac{\partial u}{\partial x} + \alpha u \frac{\partial u}{\partial x} + \beta \frac{\partial^3 u}{\partial x^3} + \beta_1 \frac{\partial^5 u}{\partial x^5} = 0 \quad (2.5)$$

This equation was derived for the first time by (Kakutani & Ono, 1969) for magnetosonic waves in plasma and then it was derived for many other types of waves, including gravity-capillary waves on the surface of thin liquid films (Hasimoto, 1970); (Stepanyants, 2005), electromagnetic waves in nonlinear electric transmission lines (Gorshkov & Papko, 1977) (Nagashima, 1979), etc. Recently the similar equation was derived for internal waves in two-layer fluid (Giniyatullin *et al.*, 2014) and it was obtained the expression for the coefficient β_1 :

$$\frac{\beta_1}{cH^4} = \frac{b \left[4a(1+b^4) + 19b(1+a^2b^2) + 30ab^2 \right]}{360(a+b)^2(1+b)^4} - \frac{sb^2(1+a)}{32(1+b)^3(a+b)^2} \left[\frac{4}{3}(1+ab) + s(1+a)(1+b) \right] \quad (2.6)$$

where $a = \rho_1/\rho_2$, $b = h_1/h_2$, $H = h_1 + h_2$, and $s = 2\sigma[(\rho_1 + \rho_2)Hc^2]^{-1}$.

Equation (2.5) is currently known as the Kawahara equation, although it was derived by other authors cited above. However, (Kawahara, 1972) investigated its solitary solutions and obtained numerically a family of solitons with non-monotonic, but oscillatory tails.

In the meantime, as has been recently shown (Giniyatullin *et al.*, 2014) in the case of internal waves in two-layer fluid with strong surface tension at the interface the double-critical situation is also possible when both the coefficients of quadratic nonlinearity α and third-order dispersion β become so small that the next order corrections with the coefficients α_1 and β_1 should be taken into consideration. The double-critical situation is irrelevant to oceanic conditions, but it can be relevant to laboratory experiments and some technological processes when there are flows of relatively thin layers of immiscible fluids of different physical properties. In such cases the surface tension between the layers can be important leading to vanishing of the conventional third-order dispersion (particular estimates are presented below at the end of this Chapter).

As per Equation (2.2), in the double critical situation both coefficients α and β vanish when $\rho_1 = \rho_2(h_1/h_2)^2$ and $\sigma = c^2\rho_2h_2[1 + (h_1/h_2)^3]/3$. In this case the coefficients α_1 and β_1 take simple forms:

$$\alpha_1 = \frac{3c}{h_1h_2}, \quad \beta_1 = cH^4 \frac{1+b^5}{90(1+b)^5} \quad (2.7)$$

The coefficient β_1 is always positive and has the minimum value at $b = 1$ (i.e. when the thicknesses of the upper and lower layers are equal); its plot is shown in Figure 2.2.

In the vicinity of the double critical situation the governing equation reads:

$$\frac{\partial u}{\partial t} + c \frac{\partial u}{\partial x} + \alpha u \frac{\partial u}{\partial x} - \alpha_1 u^2 \frac{\partial u}{\partial x} + \beta \frac{\partial^3 u}{\partial x^3} + \beta_1 \frac{\partial^5 u}{\partial x^5} = 0 \quad (2.8)$$

This equation is called the Gardner–Kawahara equation.

Now consider stationary solutions of Equation (2.8) in the form of solitary waves. A family of soliton solutions are constructed numerically by means of the Petviashvili method (Petviashvili & Pokhotelov, 1992) (Pelinovsky & Stepanyants, 2004) and Yang–Lakoba AITEM (A.N.) method (Yang & Lakoba, 2008). The properties of such solutions are investigated and discussed.

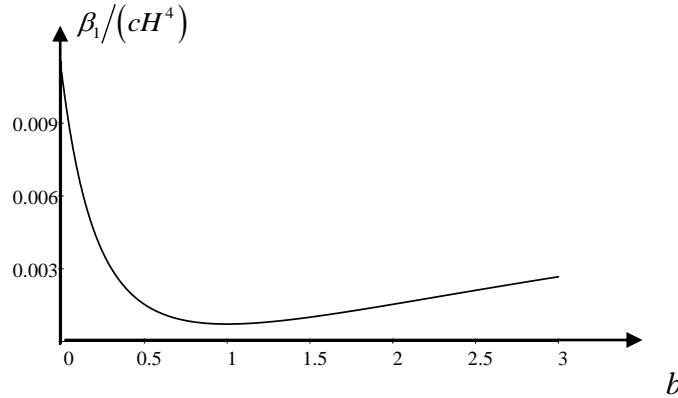


Figure 2.2: The dependence of the normalised dispersion coefficient $\beta_1/(cH^4)$ on the ratio of layer thicknesses $b = h_1/h_2$ at the double critical situation.

2.2. Dispersion Relation and Stationary Solutions to the Gardner–Kawahara Equation

First, present Equation (2.8) in the dimensionless form using change of variables:

$$\tau = \frac{\alpha^3 t}{\alpha_1 \sqrt{\alpha_1 \beta}}, \quad \xi = \frac{\alpha(x - ct)}{\sqrt{\alpha_1 \beta}}, \quad v = \frac{\alpha_1}{\alpha} u. \quad (2.9)$$

After that the main equation reads:

$$\frac{\partial v}{\partial \tau} + v \frac{\partial v}{\partial \xi} - v^2 \frac{\partial v}{\partial \xi} + \frac{\partial^3 v}{\partial \xi^3} + B \frac{\partial^5 v}{\partial \xi^5} = 0 \quad (2.10)$$

where $B = (\beta_1/\alpha_1)(\alpha/\beta)^2$.

For waves of infinitesimal amplitude, $v \rightarrow 0$, the solution in the form $v \sim e^{i(\tilde{\omega}\tau - \kappa\xi)}$ gives the dispersion relation

$$\tilde{\omega} = -\kappa^3 + B\kappa^5. \quad (2.11)$$

Then, it follows that the phase speed of small-amplitude waves is

$$V_{ph}(\kappa) \equiv \frac{\tilde{\omega}}{\kappa} = -\kappa^2 + B\kappa^4. \quad (2.12)$$

The plot of phase speed is shown in Figure 2.3 for three values of the parameter B .

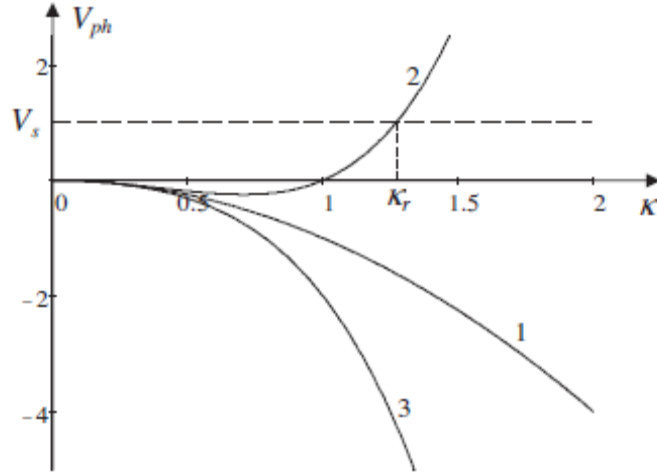


Figure 2.3: Plots of phase speed (2.4) for $B = 0$ (line 1, KdV dispersion), $B = 1$ (line 2), and $B = -1$ (line 3). Dashed horizontal line shows the object moving with a constant speed V_s and generating small amplitude wave at the resonant wavenumber κ_r .

In the case $B \leq 0$ the phase speed is a monotonic function of κ , whereas at $B > 0$ it has a minimum, $V_{min} = -1/(4B)$ at the point $\kappa_c = (2B)^{-1/2}$ (see Figure 2.3). The concept of phase speed is very important in understanding the process of interaction of a moving source with waves. In particular, if the speed of a source is such that there is no resonance with any wave, i.e. there is no intersection of the dashed line in Figure 2.3 with the dispersion curve (e.g., with lines 1 or 3), then the source does not loose energy for wave excitation. Otherwise, in the case of the resonance (see the intersection of dashed line with line 2), the source experiences energy losses for wave generation and, as a result, it experiences wave resistance. Without external compensation of energy losses such source cannot move stationary.

Consider now stationary solutions to the wave Equation (2.10) depending on one variable only $\zeta = \xi - V\tau$. In this case Equation (2.10) reduces to the Ordinary Differential Equation:

$$\frac{d}{d\zeta} \left[-Vv + \frac{v^2}{2} - \frac{v^3}{3} + \frac{d^2v}{d\zeta^2} + B \frac{d^4v}{d\zeta^4} \right] = 0 \quad (2.13)$$

Further the focus is on the solitary solutions only; therefore assuming zero asymptotics at the infinity, integrate Equation (2.13) once with the zero integration constant:

$$B \frac{d^4 v}{d\zeta^4} + \frac{d^2 v}{d\zeta^2} - Vv + \frac{v^2}{2} - \frac{v^3}{3} = 0 \quad (2.14)$$

It follows from this equation that the shape of a solitary wave is determined by two parameters, B and V . Considering an asymptotic solution of Equation (2.13) when $\zeta \rightarrow \infty$ and $v \rightarrow 0$, we linearise it (simply omit the nonlinear terms) and seek for its solution in the form $v \sim e^{\mu\zeta}$. Substituting this trial solution into linearised Equation (2.13), gives the equation determining the exponent μ :

$$B\mu^4 + \mu^2 - V = 0 \quad (2.15)$$

The roots to this bi-quadratic equation are:

$$\mu_{1,2} = \pm \sqrt{\frac{-1 + \sqrt{1 + 4BV}}{2B}}; \quad \mu_{3,4} = \pm \sqrt{\frac{-1 - \sqrt{1 + 4BV}}{2B}}. \quad (2.16)$$

Analysing the roots in detail: first assume that B is negative, then for $V < 0$, $\sqrt{1 + 4BV} > 1$; therefore the roots $\mu_{1,2}$ are purely imaginary, and the roots $\mu_{3,4}$ are real. Solutions corresponding to purely imaginary roots are not decaying and cannot represent solitary waves with the zero asymptotics. If $V = 0$, then $\mu_{1,2} = 0$ and again the solution is with non-decaying asymptotics. If $0 < V < -1/(4B)$, then $\sqrt{1 + 4BV} > 0$, and all four roots $\mu_{1,2,3,4}$ are real. In this case the soliton solutions are possible with the exponential asymptotics $v \sim \exp(-|\mu_1\zeta|)$. And at last, if $V > -1/(4B)$, then $\sqrt{1 + 4BV}$ is complex; all roots are complex-conjugate in pairs $\mu_{1,2} = \pm(p_1 \pm iq_1)$, $\mu_{3,4} = \pm(p_2 \pm iq_2)$. Due to presence of the real parts of the roots $p_{1,2}$, the soliton solutions are also possible with the oscillatory asymptotics. The decay rate of a solitary wave in the far field is determined by the root with the smallest value of $|p_{1,2}|$.

Assume now that B is positive, then it follows from the similar analysis as above that solitary waves with the oscillatory asymptotics are possible only when $V < V_{min} \equiv -1/(4B)$. In the particular case of $B = 0$, Equation (2.15) has two real roots $\mu_{1,2} = \pm\sqrt{V}$ corresponding to soliton solutions, provided that $V > 0$.

These findings can be summarised with the help of a schematic diagram shown in Figure 2.4. It should be noticed that the analysis of roots only predicts possible asymptotics of solitons provided that they exist, but it does not guarantee their existence. In particular, if $B = 0$, then soliton solutions with monotonically decaying exponential asymptotics could exist for any $V > 0$ (see case b) in the diagram), but in fact they exist only for $0 \leq V \leq 1/6$ (see the exact solution Equation (2.17) of the Gardner equation below).

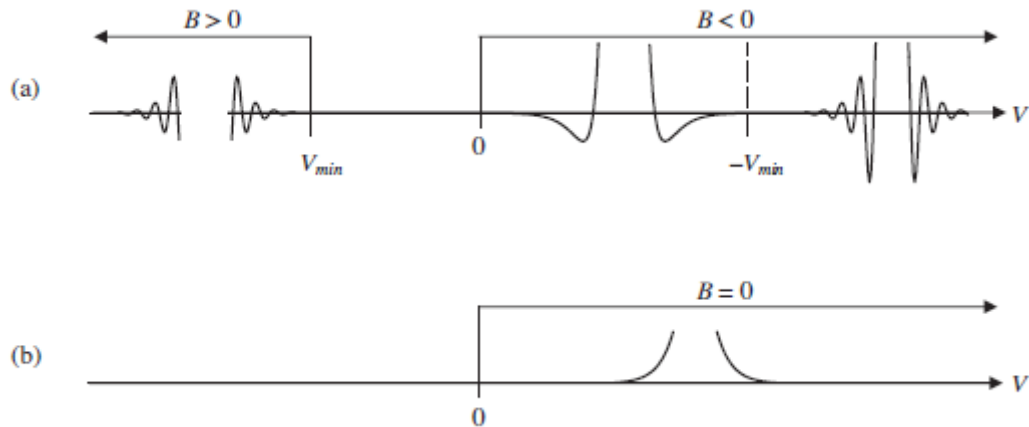


Figure 2.4: Schematic structure of solitary wave asymptotics for Equation (2.13) with different signs of B (frame a). If $B = 0$ only the solitons with monotonic exponential tails are possible as shown in frame b) – see exact solution Equation (2.17).

2.3. Soliton Solutions to the Gardner–Kawahara Equation

Consider first the limiting case of $B = 0$ when Equation (2.14) reduces to the completely integrable Gardner equation. It has a family of soliton solutions which is determined by only one parameter V varying in the interval $0 \leq V \leq 1/6$ (a soliton solution does not exist beyond this interval):

$$v(\zeta) = \frac{\sqrt{6V}}{2} \left[\tanh\left(\frac{\sqrt{V}}{2}\zeta + \phi\right) - \tanh\left(\frac{\sqrt{V}}{2}\zeta - \phi\right) \right] \quad (2.17)$$

where $\phi(V) = (1/4)\ln[(1 + \sqrt{6V})/(1 - \sqrt{6V})]$, and the amplitude of a soliton $A = 1 - \sqrt{1 - 6V}$.

The family of solitons varies from KdV-type bell-shaped solitons, when $V \rightarrow 0$, to table-top solitons, when $V \rightarrow 1/6$ (see e.g., (Apel, *et al.*, 2007)) the typical solitons are shown in Figure 2.5 for three values of V .

If $B \neq 0$, then exact analytical solutions of Equation (2.14) are not known. However it can be constructed numerically using, for example, a modified Petviashvili method (Petviashvili & Pokhotelov, 1992) (Pelinovsky & Stepanyants, 2004) or even more effective Yang–Lakoba method (Yang & Lakoba, 2008). To this end make a Fourier transform of Equation (2.14) on the variable ζ denoting the Fourier spectrum of function v by $\hat{F}(v)$:

$$(B\kappa^4 - \kappa^2 - V)\hat{F}(v) = \frac{1}{3}\hat{F}(v^3) - \frac{1}{2}\hat{F}(v^2) \quad (2.18)$$

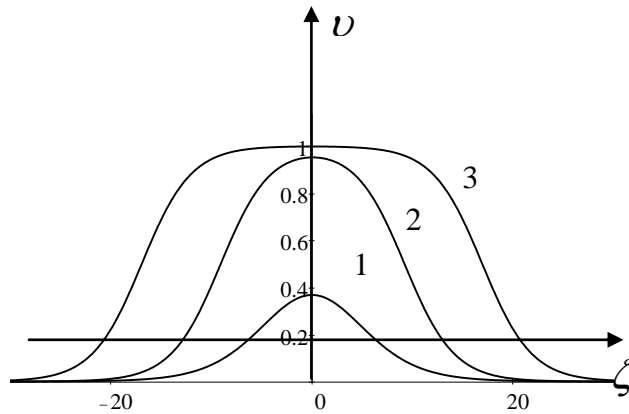


Figure 2.5: Solitary wave shapes as per Equation (2.17) for three values of V . Line 1 pertains to $V = 0.1$ (quasi-KdV case), line 2 pertains to $V = 0.1663$ ('fat soliton'), and line 3 pertains to $V = 0.16666$ (table-top soliton).

If we multiply Equation (2.18) by $\hat{F}(\nu)$ and integrate it over κ from minus to plus infinity, we then obtain the equality:

$$\int_{-\infty}^{+\infty} (B\kappa^4 - \kappa^2 - V) \hat{F}(\nu) \hat{F}(\nu) d\kappa = \int_{-\infty}^{+\infty} \left[\frac{1}{3} \hat{F}(\nu^3) - \frac{1}{2} \hat{F}(\nu^2) \right] \hat{F}(\nu) d\kappa \quad (2.19)$$

If $\nu(\zeta)$ is an exact solution of Equation (2.14) and $\hat{F}(\nu)$ is its Fourier spectrum satisfying Equation (2.18), then it follows from Equation (2.19) that the quantity M (the stabilising factor) as defined below should be equal to one:

$$M[\nu] \equiv \frac{\int_{-\infty}^{+\infty} (B\kappa^4 - \kappa^2 - V) \hat{F}(\nu) \hat{F}(\nu) d\kappa}{\int_{-\infty}^{+\infty} \left[\frac{1}{3} \hat{F}(\nu^3) - \frac{1}{2} \hat{F}(\nu^2) \right] \hat{F}(\nu) d\kappa} = 1 \quad (2.20)$$

However, in general, if $\nu(\zeta)$ is not a solution of Equation (2.14), then $M[\nu]$ is a functional of ν . In the spirit of the Petviashvili method constructs the iteration scheme (for details see (Petviashvili & Pokhotelov, 1992)):

$$\hat{F}(\nu_{n+1}) = M^r[\nu_n] \frac{\frac{1}{3} \hat{F}(\nu_n^3) - \frac{1}{2} \hat{F}(\nu_n^2)}{V_{ph}(\kappa) - V} \quad (2.21)$$

where $V_{ph}(\kappa)$ is the phase speed of infinitesimal perturbation as per Equation (2.12), and the exponent r should be taken in the range $r = [3/2, 2]$ to provide a convergence of the numerical scheme. As has been shown in (Pelinovsky & Stepanyants, 2004), $r = 3/2$ provides the fastest convergence for pure cubic nonlinearity, whereas $r = 2$ provides the fastest convergence for pure quadratic nonlinearity. In our calculations it was taken $r = 7/4$ which provided the fastest convergence to the stationary solution for the mixed

quadratic and cubic nonlinearity. The convergence is controlled by the closeness of parameter M to unity. Starting from the arbitrary pulse function $\upsilon_0(z)$ we conducted calculations with the given parameters B and V on the basis of iteration scheme Equation (2.21) until the parameter M attained a unity up to small quantity ε (in our calculations we have chosen $\varepsilon = 10^{-6}$). To avoid a singularity in Equation (2.21) the speed of a solitary wave should be taken such that at the given value of V_{ph} the fourth-degree polynomial in the denominator of Equation (2.12) does not have real roots.

As the test case the Gardner Equation (2.14) considered with $B = 0$. As seen here there is no singularity in Equation (2.21) if $V > 0$; this is in agreement with the condition of existence of Gardner solitons Equation (2.17). For relatively small $V \leq 0.1663$ the obtained numerical solutions are in a complete agreement with the analytical solution Equation (2.17). But for larger values of V it failed to obtain any solution by means of the modified Petviashvili method as the iteration procedure Equation (2.21) did not converge to something. In the meantime, application of the Yang–Lakoba method (Yang & Lakoba, 2008) enabled us to construct soliton solutions in the complete agreement with the analytical solution (2.17) for any positive value of $V < 1/6$. Thus, it has been confirmed that the Yang–Lakoba method is even more efficient and converges faster than the Petviashvili method.

In the case of $B > 0$ the denominator of Equation (2.21) is positive when $V < V_{min}$. Then, depending on the value of V we have obtained various shapes of solitary waves by the Petviashvili method; as illustrated by Figure 2.6 for $B = 1$. For other positive values of B the soliton structures are qualitatively the same as shown in this figure, but solitons become narrower when $B \rightarrow 0$ and wider when $B \rightarrow \infty$. Their asymptotic behaviour is in agreement with the prediction shown in Figure 2.4 for $B > 0$; the oscillatory tails of solitons are clearly seen in this figure.

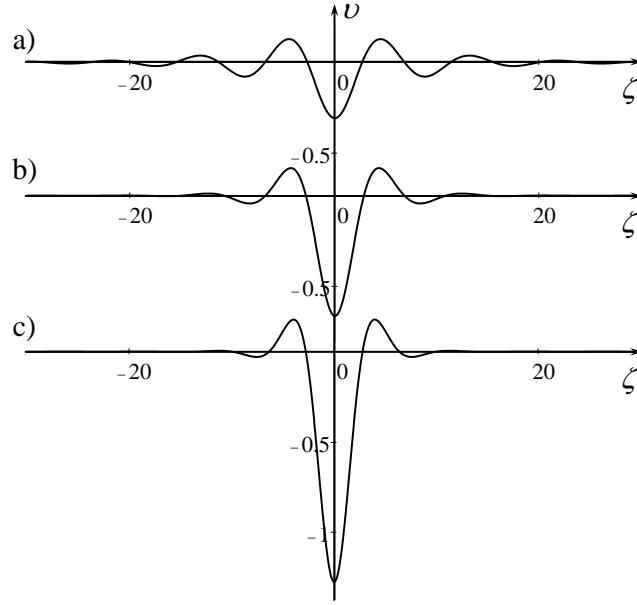


Figure 2.6: Solitary wave shapes numerically obtained for $B = 1$ and three values of V where $V_{min} = -0.25$. Case a) $V = -0.3$, case b) $V = -0.5$, case c) $V = -1.0$.

It is worth noting two features of these solitons. Firstly, at small amplitudes, when $V \rightarrow (V_{min})^-$, solitons reduce to stationary moving wavetrains. Such wavetrains can be described by the higher-order non-linear Schrödinger equation; similar solutions in the form of envelope solitons have been earlier obtained for the Ostrovsky equation (Obregon & Stepanyants, 1998; Grimshaw & Helfrich, The effect of rotation on internal solitary waves, 2012).

Secondly, due to oscillatory character of soliton tails, solitons can form the bound states – stationary propagating bi-solitons and even more complicated multi-solitons (Gorshkov *et al.*, 1979; Obregon & Stepanyants, 1998). These structures are not considered in details here, but is present in only one example in Figure 2.7. In frame a) a single soliton with oscillating tails, whereas in frame b) the bi-soliton is depicted for the same parameters $B = 1$ and $V = -0.5$.

For the sake of completeness, the structure of soliton solutions for the negative parameter B was also investigated, although in the context of interfacial waves in the two-layer fluid this parameter is always positive. When $B < 0$, the denominator of Equation (2.21) is non-singular, if $V > 0$. With the help of Petviashvili and Yang–Lakoba numerical methods it has obtained a family of soliton solutions only in the finite

range of the parameter V : $0 < V \leq V_{cr}$, where V_{cr} depends on B , but only slightly differs from $1/6$. We did not investigate in details the dependence of soliton speed on its amplitude for different values of B , this can be a matter of a separate study. Figure 2.8 presents several soliton solutions constructed numerically for the fixed amplitude $A = 0.998$ and different values of parameter B .

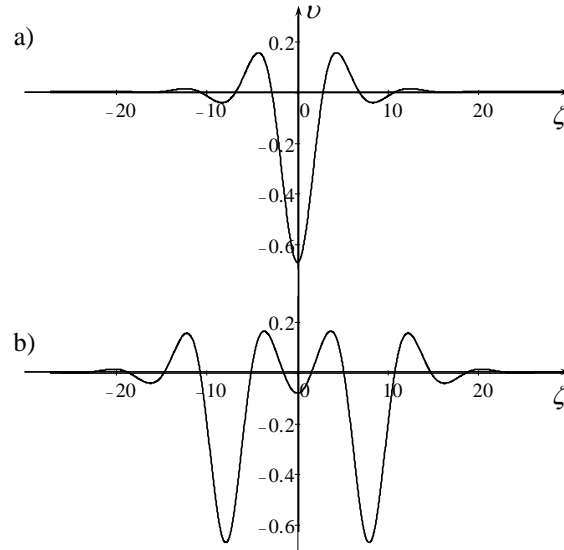


Figure 2.7: Examples of single soliton and bi-soliton representing a family of stationary multi-soliton solutions of the GK Equation (2.6).

As from this Figure, the greater the B , the wider the soliton. Again, in accordance with the prediction, soliton asymptotics changes from the exponential aperiodic, when $V < -1/(4B)$, to oscillatory decaying, when $V > -1/(4B)$ (see Figure 2.4). However, the oscillations are so small and they decay so fast that are hardly visible in soliton profile. In the insertion one can see the magnified portion of corresponding soliton tails.

Due to oscillatory character of soliton tails the bounded bi-soliton and multi-soliton solutions may exist in this case too. Moreover, even more complicated infinite chains of bounded solitons are possible. Such chains may be both regular and irregular representing quasi-random sequences of bounded solitons (Gorshkov *et al.*, 2010).

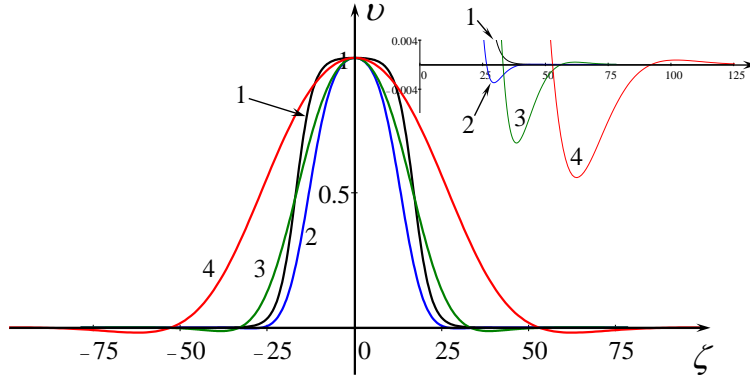


Figure 2.8: Solitary wave shapes numerically obtained for the fixed soliton amplitude $A = 0.998$ and four values of B : line 1 – $B = 0$, line 2 – $B = -10$, line 3 – $B = -100$, line 4 – $B = -1000$.

2.4. Discussion

Let us make an estimate of physical applicability of the Gardner–Kawahara equation to the real case of two-layer system consisting of kerosene in the upper layer and water in the lower layer. Take the following parameters for the kerosene and water at 20°C : the density of kerosene is $\rho_1 = 0.82 \text{ g/cm}^3$, the density of water is $\rho_2 = 0.998 \text{ g/cm}^3$, and the surface tension at the interface between them is $\sigma = 48 \text{ dyn/cm}$. Then the double critical condition occurs, if the layer thicknesses are $h_1 = 0.82 \text{ cm}$ and $h_2 = 0.9 \text{ cm}$ with the total fluid depth $H = h_1 + h_2 = 1.72 \text{ cm}$. If we choose $h_1 = 0.62 \text{ cm}$ and $h_2 = 1.1 \text{ cm}$ with the same total depth, we will have a near critical condition with $h_1/h_2 \approx 0.56$. In this case the coefficient β_1 is positive and close to its minimum value (see Figure 2.2); the dimensionless coefficient B in Equations (2.10), (2.14) is also positive and Equation (2.14) possesses soliton solutions of negative polarity with the oscillatory tails as shown in Figure 2.6. The shapes of such solitons may vary from quasi-sinusoidal wave-trains, when the amplitude goes to zero, up to narrow pulses, when the amplitude increases. The negative speeds of these solitons (see the diagram in Figure 2.4) imply that they travel with the speeds less than the speed of long linear waves c in the immovable coordinate frame (see Equation (2.2)).

2.5. Conclusion

Thus, in this Chapter it has been shown that in the study of interfacial waves between two immiscible fluids there are such situations, when the double critical conditions can occur, i.e. when both the coefficients of quadratic nonlinearity and third-order dispersion vanish simultaneously. In the near-critical situation the basic governing equation is the Gardner–Kawahara Equation (2.8).

Apparently, the similar Gardner–Kawahara equation can be applicable for the description of other types of waves in continuous media, for example, in plasma physics. The equation can be further generalised to take into account weak medium rotation in the spirit of the Ostrovsky equation (Apel et al., 2007; Grimshaw *et al.*, 1998) and weak wave diffraction in the spirit of the Kadomtsev–Petviashvili equation (Petviashvili & Pokhotelov, 1992). In the latter case two-dimensional lump solitons with oscillatory tails can be possible. Such solutions were constructed numerically for the two-dimensional version of the Kawahara Equation (2.3) in (Abramyan & Stepanyants, 1985).

Chapter 3 Modulational Stability of Weakly Nonlinear Wave-Trains

3.1. Introduction

It is a well-known fact that unidirectional trains of shallow-water waves (both surface and internal) are modulationally stable except in the case of very strong surface tension (Ablowitz & Segur, 1981). This result formally agrees with what follows from the Korteweg–de Vries (KdV) equation:

$$\frac{\partial \eta}{\partial t} + c_0 \frac{\partial \eta}{\partial x} + \alpha \eta \frac{\partial \eta}{\partial x} + \beta \frac{\partial^3 \eta}{\partial x^3} = 0 \quad (3.1)$$

which is applicable to the description of weakly nonlinear long waves. The coefficients α and β may be of either sign depending on the nature of waves. In particular, for the surface gravity-capillary waves the coefficients are (Karpman, 1975)

$$\alpha = \frac{3 c_0}{2 h}, \quad \beta = \frac{c_0 h^2}{6} \left(1 - \frac{3\sigma}{\rho g h^2} \right), \quad (3.2)$$

where $c_0 = (gh)^{1/2}$ is the speed of long linear waves, g is the acceleration due to gravity, h is the fluid depth, σ is the surface tension, and ρ is the fluid density. The dispersion relation between the wave frequency ω and wavenumber k for infinitesimal amplitude waves in the linearised Equation (3.1) is well-known (see, e.g., (Ablowitz & Segur, 1981; Karpman, 1973; Ostrovsky *et al.*, 2015)):

$$\omega(k) = c_0 k - \beta k^3. \quad (3.3)$$

It shows that the dispersion appears at relatively large k (small wavelength λ), when the influence of the second term in the right-hand side is not negligibly small. Such small-scale (“Boussinesq”) dispersion is typical for long water waves. The derivation of Equation (3.1) is based on the assumption that the dispersion is weak, so

that $\beta k^3 \ll c_0 k$ or $k \ll k_1$, where $k_1 = (c_0/|\beta|)^{1/2}$. Depending on the sign of coefficient β , one can distinguish between the negative dispersion, if $\beta > 0$ (the phase speed $V_p \equiv \omega(k)/k = c_0 - \beta k^2$ decreases with k in this case), and positive dispersion, if $\beta < 0$ (the phase speed increases with k).

There are also physical systems containing the large-scale (“Coriolis-type”) dispersion which manifests when $k \rightarrow 0$ and disappears when $k \rightarrow \infty$. In many physical situations the large-scale dispersion is small and of the same order of smallness as the small-scale dispersion, so that the combined dispersion relation can be presented in the form (Grimshaw *et al.*, 1998b; Ostrovsky *et al.*, 2015):

$$\omega(k) = c_0 k - \beta k^3 + \gamma/k \quad (3.4)$$

where γ is some constant which can be of either sign, and $\gamma/k \ll c_0 k$, so that $k \gg k_2$, where $k_2 = (|\gamma|/c_0)^{1/2}$. The corresponding weakly nonlinear evolution equation generalising the KdV equation (3.1) is known as the Ostrovsky equation (Ostrovsky, 1978; Grimshaw *et al.*, 1998; Grimshaw & Helfrich, 2008; 2012; Ostrovsky *et al.*, 2015):

$$\frac{\partial}{\partial x} \left(\frac{\partial \eta}{\partial t} + c_0 \frac{\partial \eta}{\partial x} + \alpha \eta \frac{\partial \eta}{\partial x} + \beta \frac{\partial^3 \eta}{\partial x^3} \right) = \gamma \eta. \quad (3.5)$$

This equation is applicable for waves of intermediate spatial scales

$$\sqrt{|\gamma|/c_0} \ll k \ll \sqrt{c_0/|\beta|} \quad (3.6)$$

when both small-scale and large-scale dispersions are relatively small. (Grimshaw & Helfrich, 2008, 2012), using Ostrovsky Equation (3.5) with $\beta > 0$ and $\gamma > 0$ have shown that the large scale dispersion drastically changes the modulation stability of quasi-harmonic wave-trains. The nonlinear correction to the wave frequency remains negative for all wavenumbers as in the case of KdV equation, but the dispersion coefficient in the

non-linear Schrödinger equation (NLSE) changes its sign at $k = k_c \equiv (\gamma/3\beta)^{1/4}$ when the group velocity $c_g = d\omega/dk$ attains maximum. Therefore, the corresponding NLSE remains modulationally stable for $k < k_c$, but becomes unstable for $k > k_c$. This is in a sharp contrast to the intuition based on the NLSE derived from the KdV equation (3.1). Indeed, at a first glance one can expect an influence of Coriolis-type dispersion at large scales only, as it vanishes when $k \rightarrow \infty$. At this limit, $k \rightarrow \infty$, the small-scale dispersion predominates, and wave-trains should be modulationally stable as in the case of KdV equation.

The physical explanation of this apparent contradiction is in the crucial role of a zero harmonic (the “mean flow”) generated by the basic wave-train. The nonlinear coefficient in the NLSE usually consists of contributions from both the second and zero harmonics. However, the zero harmonic is beyond the range of applicability of the Ostrovsky equation (3.5), which formally requires the zero total “mass” of a perturbation (see, e.g., (Grimshaw *et al.*, 1998)). Therefore the zero harmonic cannot contribute to the nonlinear coefficient, and the second harmonic provides the nonlinear coefficient in the NLSE of the opposite sign in comparison with that derived from the KdV equation, where both zero and second harmonics contribute jointly (this will be clearly seen from the analysis presented in this Appendix).

As the Ostrovsky equation is approximate and has a limited range of validity, the issue of modulation stability of wave-trains remained uncertain thus far, because at very small wavenumbers the situation with the modulation stability could be different, and contribution of the zero harmonic into the nonlinear coefficient of NLSE might be important again. Therefore the problem of modulation stability of wave-trains should be resolved within the framework of more accurate equations in the long-wave limit. Moreover, for the analysis of modulation stability of waves in the real physical systems (e.g., water waves, or plasma waves) the KdV model equation is, obviously, insufficient, because it contains only the quadratic nonlinear term, whereas cubic nonlinear terms usually provide the same order contribution to the nonlinear coefficient of NLSE.

The analysis of modulation stability of long water waves in a rotating fluid was undertaken as earlier as 1981 by Shrira, who derived a set of shallow-water equations and investigated modulation stability of quasi-monochromatic waves, ignoring however the small-scale dispersion. His analysis predicts the modulation instability of wave-trains at very small wavenumbers; this does not match with the result of Grimshaw & Helfrich (2008; 2012). Thus, the problem of modulation stability of water waves requires thorough consideration which motivates the current study.

Below the problem of modulation stability of quasi-monochromatic wave-trains is re-examined on the basis of the 2D shallow-water model set of equations derived by (Shrira, 1981) and augmented by the terms representing the Boussinesq dispersion. We derive the 2D NLSE and study a stability of quasi-monochromatic wave-trains with respect to longitudinal and transverse modulations for various signs of coefficients of the NLSE. The results obtained can be applicable not only to water waves, but in the wider context, including plasma waves, waves in solids, in optical media, etc.

3.2. The Governing Equations and Dispersion Relations

The following set of equations are applicable (after appropriate scaling) to both surface and internal waves in the Boussinesq approximation (Ostrovsky, 1978; Shrira, 1981; Grimshaw *et al.*, 1998):

$$\frac{\partial \eta}{\partial t} + \nabla_{\perp} [(h + \eta) \mathbf{q}] = 0 \quad (3.7)$$

$$\frac{\partial \mathbf{q}}{\partial t} + (\mathbf{q} \cdot \nabla_{\perp}) \mathbf{q} + [\mathbf{f} \times \mathbf{q}] + \frac{c_0^2}{h} \nabla_{\perp} \eta + s h \frac{\partial^2 \nabla_{\perp} \eta}{\partial t^2} = 0, \quad (3.8)$$

where η is the perturbation of a free surface in a non-stratified fluid or perturbation of an isopycnal surface (surface of equal density) in a stratified fluid, $\mathbf{q} = (u, v)$ is the depth averaged fluid velocity with two horizontal components, longitudinal u and transverse v , $\mathbf{f} = f \mathbf{n}$, where $f = 2\Omega \sin \varphi$ is the Coriolis parameter, Ω is the angular

frequency of Earth rotation, φ is the local geographic latitude, \mathbf{n} is the unit vector normal to the Earth surface, and $\nabla_{\perp} = (\partial/\partial x, \partial/\partial y)$. Other parameters in Equations (3.7), (3.8) are c_0 – the speed of long linear waves, h – the fluid depth, and s – the dispersion parameter. In the case of surface waves the long-wave speed $c_0 = (gh)^{1/2}$, and $s = (1 - 3\sigma/\rho gh^2)/3$; whereas for internal waves in two-layer fluid $c_0 = \sqrt{\frac{\Delta\rho}{\rho} g \frac{h_1 h_2}{h_1 + h_2}}$ and $s = h_1 h_2 / 3h^2$, where h_1 and h_2 are thicknesses of the upper and lower layers correspondingly, and $\Delta\rho = \rho_2 - \rho_1$ is the difference of layer densities (in the Boussinesq approximation both these densities are assumed close to each other ($\rho_1 \approx \rho_2 = \rho$), while the product $\Delta\rho g$ is assumed to be finite).

In the one-dimensional case when all variables depend on one spatial coordinate x this set of equations can be reduced to one bi-directional equation for the transverse velocity v (Shrira, 1981).

If

$$\eta = \frac{h}{f} \frac{\partial v}{\partial x}, \quad u = -\frac{1}{f + v_x} \frac{\partial v}{\partial t}, \quad (3.9)$$

where indices t and x here and below stand for the corresponding derivatives, then we obtain:

$$v_{tt} - c_0^2 v_{xx} + f^2 v - s h^2 v_{ttxx} = \left(\frac{v_t v_x}{f + v_x} \right)_t + \frac{f}{2} \left[\frac{(v_t)^2}{(f + v_x)^2} \right]_x. \quad (3.10)$$

For perturbations of relatively small amplitude the nonlinear terms in the right-hand side can be simplified, and Equation (3.10) can be reduced to

$$v_{tt} - c_0^2 v_{xx} + f^2 v - s h^2 v_{ttxx} \approx \frac{1}{f} (v_{tt} v_x + 2v_t v_{xt}) - \frac{1}{f^2} [v_{tt} (v_x)^2 + 4v_t v_x v_{xt} + (v_t)^2 v_{xx}]. \quad (3.11)$$

By introducing new variables $\tau = ft/\sqrt{|\Gamma|}$, $\xi = (x/h)(|B/s|)^{1/2}$, $w = v_{\perp}(|B/s|)^{1/2}/(Ahf)$, where $A = B = \Gamma = 1$, one can present Equation (3.11) in the dimensionless form:

$$w_{\tau\tau} - C^2 w_{\xi\xi} + \Gamma w - B w_{\tau\xi\xi} = A \left(w_{\tau\tau} w_{\xi} + 2w_{\tau} w_{\tau\xi} \right) - \Phi \left[w_{\tau\tau} \left(w_{\xi} \right)^2 + 4w_{\tau} w_{\xi} w_{\tau\xi} + \left(w_{\tau} \right)^2 w_{\xi\xi} \right] \quad (3.12)$$

where $C^2 = (c_0/hf)^2(|B\Gamma/s|)$ stands for the normalised characteristic wave speed, and $\Phi = A^2$ (we prefer to keep letter Φ rather than A^2 to track the contribution of nonlinear terms in the final equation). For further estimates we put $C = 34.3$ assuming that $h = 1000$ m, $g = 9.8$ m/s ($c_0 = 99$ m/s), $f = 5 \cdot 10^{-3}$ s⁻¹, $s = 1/3$, and $B = \Gamma = 1$.

In what follows we will not restrict ourselves to the particular choice of dimensionless coefficients $A = B = \Gamma = 1$ as above, but will assume that these coefficients can be of either sign with the moduli equal to unity. Then Equation (3.12) or its unidirectional analogue, the Ostrovsky equation (see below), can be considered in a much wider context. In particular, the coefficient B can be negative for magnetosonic waves in a rotating plasma (Obregon & Stepanyants, 1998) or for capillary waves in a liquid fluid layer (Karpman, 1973) (see Equation (3.2); the coefficient Γ is usually positive, but can be negative in a rotating stratified ocean with shear flows (Alias *et al.*, 2014a,b).

For unidirectional waves propagating, for instance, to the right only, one can derive from Equation (3.12) the following Gardner–Ostrovsky equation (Ostrovsky, 1978; Grimshaw *et al.*, 1998; Ostrovsky *et al.*, 2015):

$$\frac{\partial}{\partial \xi} \left(\frac{\partial w}{\partial t} + C \frac{\partial w}{\partial \xi} + a \zeta \frac{\partial \zeta}{\partial \xi} - a_1 \zeta^2 \frac{\partial \zeta}{\partial \xi} + b \frac{\partial^3 \zeta}{\partial \xi^3} \right) = r \zeta \quad (3.13)$$

where $\zeta = \partial w / \partial \xi$ (in terms of Equation (3.9) this is just the normalised variable η : $\zeta = (\eta/Afh)(B\Gamma/s)^{1/2}$], $a = 3AC/2$, $a_1 = 3\Phi C$, $b = BC/2$, and $r = \Gamma/2C$.

For perturbations of infinitesimal amplitudes the nonlinear terms on the right-hand side of Equation (3.12) can be omitted, then the following dispersion relation of the linearised equation can be obtained for $\nu \sim \exp[i(\omega t - kx)]$:

$$\omega^2 = \frac{C^2 k^2 + \Gamma}{1 + Bk^2}. \quad (3.14)$$

In the intermediate range of wavenumbers where $\sqrt{|\Gamma|/C} \ll k \ll 1/\sqrt{|B|}$, the dispersion relation can be approximated by the first three terms of the Laurent series Equation (3.4):

$$\omega = Ck - bk^3 + \frac{r}{k} \equiv Ck - \frac{BC}{2} k^3 + \frac{\Gamma}{2Ck}. \quad (3.15)$$

In particular, when $r = 0$ ($\Gamma = 0$) then from Equation (3.15) the dispersion relation Equation (3.3) in the dimensionless variables is obtained. Plots of the dispersion relations Equations (3.14) and (3.15) are shown in Figure 3.1 for different values of parameters B and Γ and $C = 34.3$. As from these plots, the dispersion relation Equation (3.15) approximates well the dispersion relation Equation (3.14) in the intermediate range of wave numbers indicated above. Therefore the non-physical singularity which appears at $k = 0$ in Equation (3.15) with $|\Gamma| = 1$ is actually beyond the range of its applicability and is just an artefact of approximate character of the dispersion relation. The more accurate Equation (3.14) does not have such singularity and is valid up to $k = 0$ inclusive.

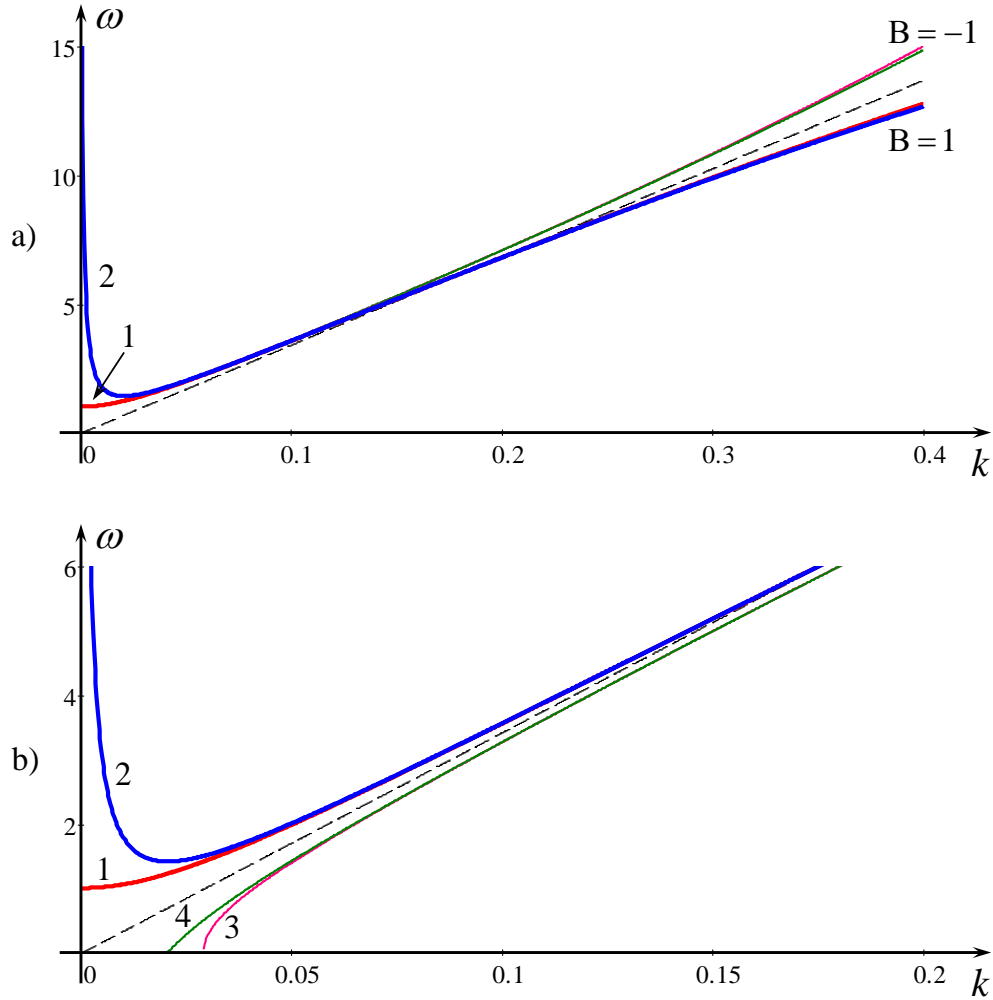


Figure 3.1: Dispersion curves as per Equations (3.14) and (3.15) for different coefficients B and Γ . Lines 1 in panels a) and b) pertain to Equation (3.14) with $\Gamma = 1$; lines 2 in panels a) and b) pertain to Equation (3.15) with the same $\Gamma = 1$ ($r = 1.46 \cdot 10^{-2}$); in panel b) line 3 pertains to Equation (3.14) and line 4 – to Equation (3.15) with $\Gamma = -1$ ($q = -1.46 \cdot 10^{-2}$). Dashed lines in panels a) and b) represent the dispersionless dependence $\omega = Ck$.

From dispersion relations Equations (3.14) and (3.15) one can readily obtain the group velocities $V_g \equiv d\omega/dk$:

$$V_g = \frac{k(C^2 - B\Gamma)}{(1+Bk^2)^{3/2} \sqrt{C^2k^2 + \Gamma}}; \quad V_{g0} = C - 3bk^2 - \frac{r}{k^2}, \quad (3.16)$$

where V_g pertains to Equation (3.14) and V_{g0} pertains to Equation (3.15).

Plots of group velocities are shown in Figure 3.2 for $B = \Gamma = 1$ and $B = \Gamma = -1$. All other combinations of signs are not shown in the figure to avoid confusion.

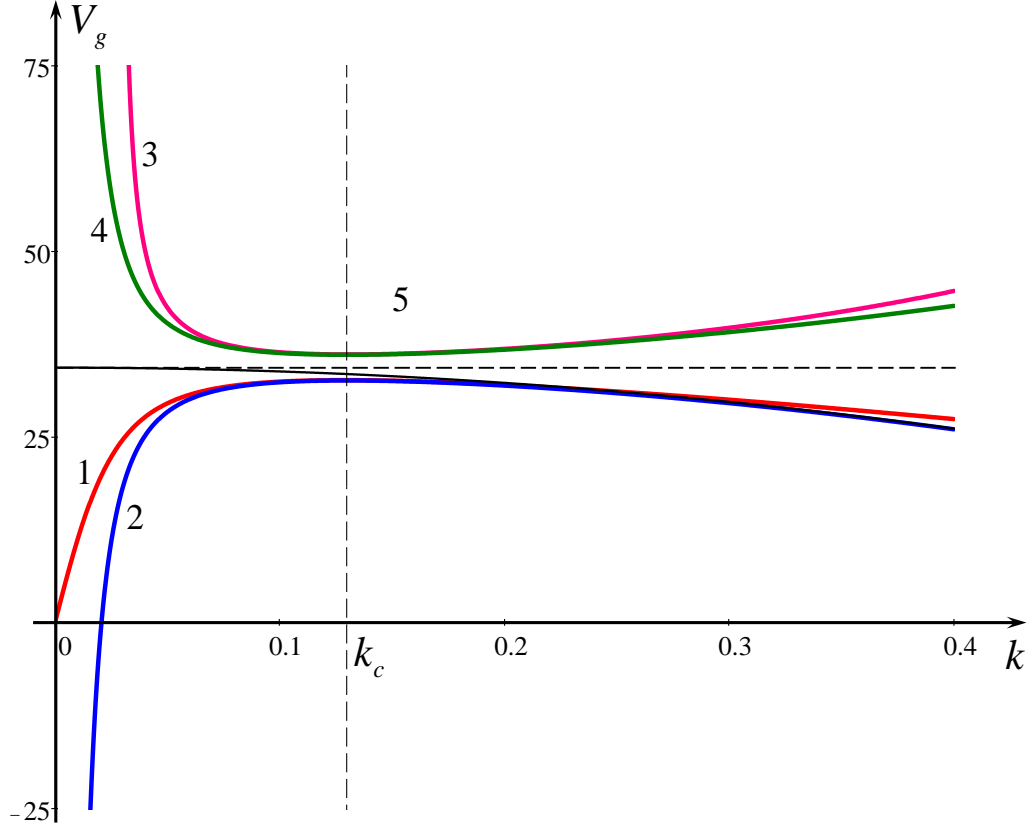


Figure 3.2: Group velocities as per Equation (3.16) for different coefficients B and Γ . Line 1 pertains to V_g with $B = \Gamma = 1$; line 2 pertains to V_{g0} with the same parameters B and Γ ; line 3 pertains to V_g with $B = \Gamma = -1$; line 4 pertains to V_{g0} with the same parameters B and Γ ; and line 5 pertains to V_g with $B = 1$ and $\Gamma = 0$. Dashed horizontal line illustrates the limiting dispersionless case $V_g = C$, and dashed vertical line shows the position of maximum in line 2.

Critical points of group velocities, Equation (3.16) (maxima, minima or inflection points depending on signs of parameters B and Γ) occur at $k = k_c$ and $k = k_{c0}$ respectively, where

$$k_c = \sqrt{\frac{1}{C} \left[\sqrt{\frac{\Gamma}{3B} \left(1 + \frac{B\Gamma}{3C} \right)} \right] - \frac{\Gamma}{C}}; \quad k_{c0} = \sqrt{\frac{1}{C} \sqrt{\frac{\Gamma}{3B}}} \quad (3.17)$$

(notice that the critical points are real if $\Gamma/B > 0$).

3.3. The Nonlinear Schrödinger Equation and Modulation Instability

This section analyses the stability of quasi-monochromatic wave-trains of small amplitude $\psi \ll 1$ within the framework of NLSE written for the dimensionless variable $\zeta = \partial w / \partial \xi$ in the form:

$$i \frac{\partial \psi}{\partial \tau} + p \frac{\partial^2 \psi}{\partial \xi^2} + q |\psi|^2 \psi = 0, \quad (3.18)$$

where $p(k)$ and $q(k)$ are the dispersion and nonlinear coefficients, respectively; they depend on the central wavenumber of the carrier wave and coefficients of the governing equation. The details of the derivation of this equation from Equation (3.12) are presented in the Appendix. Notice that the dispersion coefficient $p(k)$ can be readily obtained directly from the dispersion relations (14), $p(k) = (1/2)(\partial^2 \omega / \partial k^2)$ (see, e.g., (Karpman, 1973; Ablowitz & Segur, 1981; Ostrovsky & Potapov, 1999)). When the NLSE (3.18) is derived from the Gardner–Ostrovsky equation (3.13), then the corresponding dispersion coefficient $p_o(k)$ can be obtained from the dispersion relations Equation (3.15). Thus we have:

$$p(k) = \frac{C^2 - B\Gamma}{2} \frac{\Gamma - 2B\Gamma k^2 - 3BC^2 k^4}{(1 + Bk^2)^{5/2} (C^2 k^2 + \Gamma)^{3/2}} \quad (3.19a)$$

$$p_o(k) = -3bk + \frac{r}{k^3} \equiv \frac{C}{2k} \left(-3Bk^2 + \frac{\Gamma}{C^2 k^2} \right) \quad (3.19b)$$

The expression for the coefficient $p_o(k)$ can be obtained from Equation (3.19a) as the first terms of Taylor series on small parameters $Bk^2 \ll 1$ and $\Gamma/C^2 k^2 \ll 1$. Figure 3.3 shows the comparison of coefficients $p(k)$ and $p_o(k)$ with each other and with the coefficient $p_k(k) = -3bk \equiv -3BCK/2$ that follows from NLSE derived from the KdV equation.

In frame a) lines 1 and 2 pertain to $p(k)$ and $p_o(k)$ as per Equations (3.19a) and (3.19b), correspondingly, with $B = \Gamma = 1$; lines 3 and 4 pertain to the case when $B = 1$

and $\Gamma = -1$; line 5 shows the coefficient $p_{\kappa}(k)$. The insertion in frame a) shows the same lines in the different scale.

It clearly shows that when k increases, lines 2 and 4 asymptotically approach line 5, whereas lines 1 and 3 become indistinguishable and both approach zero.

In frame b) lines 1 and 2 pertain to $p(k)$ and $p_o(k)$, correspondingly, with $B = -1$ and $\Gamma = 1$; lines 3 and 4 pertain to the case of $B = \Gamma = -1$; line 5 shows the coefficient $p_{\kappa}(k)$. The insertion in frame b) shows the same lines in the different scale. Again when k increases, lines 2 and 4 asymptotically approach line 5, whereas lines 1 and 3 become indistinguishable and both of them infinitely increase with k .

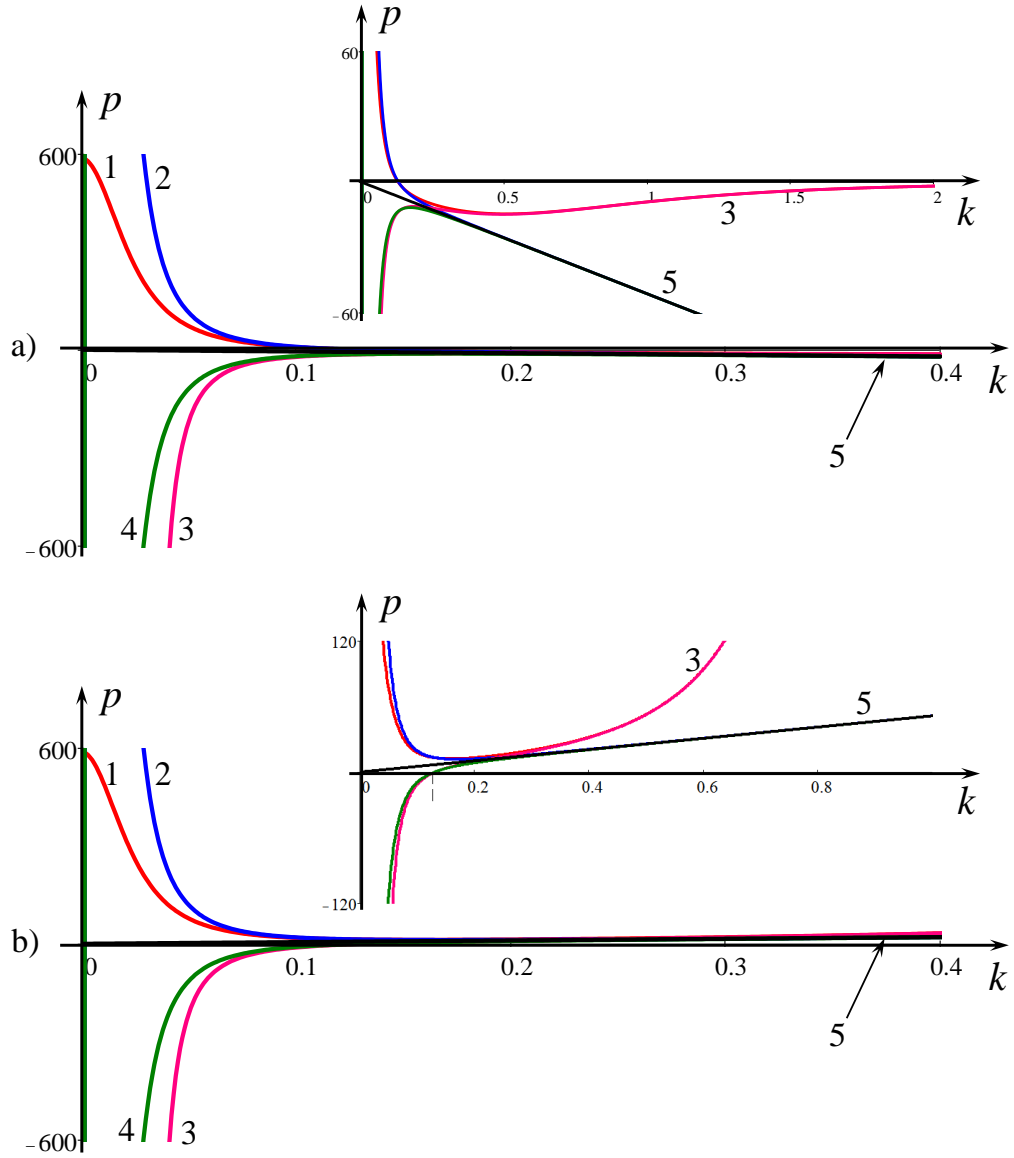


Figure 3.3: The dispersion coefficient in the NLSE (3.18) as a function of wavenumber for different primitive equations.

As one can see, in some cases the dispersion coefficient vanishes at $k = k_{c1,2}$ for Equation (3.14) and $k = k_o \approx k_{c1,2}$ for Equation (3.15), respectively, where

$$k_{c1,2} = \sqrt{\frac{1}{C} \left[\sqrt{\frac{\Gamma}{3B} \left(1 + \frac{B\Gamma}{3C} \right)} - \frac{\Gamma}{C} \right]}, \quad k_o = \sqrt{\frac{1}{C} \sqrt{\frac{\Gamma}{3B}}} \quad (3.20)$$

k_{c1} pertains to the case $B = \Gamma = 1$, whereas k_{c2} pertains to the case $B = \Gamma = -1$, and $k_{c1} < k_O < k_{c2}$. In such cases the NLSE degenerates and it should be augmented by the terms of the next-order of smallness; then the generalised NLSE can be derived for wavenumbers in the vicinity of such points (see, e.g., (Obregon & Stepanyants, 1998; Grimshaw & Helfrich, 2008; 2012)).

Now analyse the nonlinear coefficient $q(k)$. Its formal derivation from Equation (3.12) yields:

$$q(k) = \frac{-3\sqrt{C^2k^2 + \Gamma} \left[\Gamma(A^2 - \Phi) + C^2k^2A^2 - B\Phi k^2(5\Gamma + 4C^2k^2) \right]}{(1+Bk^2)^{3/2} \left[4BC^2k^4 + \Gamma(1+5Bk^2) \right]} \quad (3.21a)$$

Knowing that $\Phi = A^2$ (see after Equation (3.12)), Equation (3.21a) can be presented as:

$$q_c(k) = \frac{-3k^2A^2\sqrt{C^2k^2 + \Gamma} \left[C^2(1-4Bk^2) - 5B\Gamma \right]}{(1+Bk^2)^{3/2} \left[4BC^2k^4 + \Gamma(1+5Bk^2) \right]} \quad (3.21b)$$

This expression can be compared with the case when the cubic nonlinearity in Equation (3.12) is omitted ($\Phi = 0$):

$$q_q(k) = \frac{-3A^2(C^2k^2 + \Gamma)^{3/2}}{(1+Bk^2)^{3/2} \left[4BC^2k^4 + \Gamma(1+5Bk^2) \right]} \quad (3.21c)$$

As the coefficients (3.21b) and (3.21c) are different, in general, and contribution of the cubic nonlinear term in Equation (3.12) into the nonlinear coefficient of NLSE is important. Moreover, in some cases the quadratic nonlinear coefficient can vanish (this occurs, in particular, for internal waves in two-layer fluid with equal layer thicknesses (see, e.g., Grimshaw *et al.*, 1998)), then the only cubic nonlinear term contributes into the NLSE coefficient $q(k)$, which reduces to:

$$q_{pc}(k) = \frac{3\Phi\sqrt{C^2k^2 + \Gamma} \left[\Gamma + Bk^2(5\Gamma + 4C^2k^2) \right]}{(1+Bk^2)^{3/2} \left[4BC^2k^4 + \Gamma(1+5Bk^2) \right]}. \quad (3.21d)$$

If considering, however the range of wavenumbers when the Ostrovsky equation is applicable, i.e. $\sqrt{|\Gamma|/C} \ll k \ll 1/\sqrt{|B|}$ (see above), then from Equations (3.21b) and (3.21c) the coefficients of NLSE up to the first-order terms is obtained on small parameters ($Bk^2 \sim \Gamma/C^2 k^2 \ll 1$):

$$q_{Go}(k) \approx \frac{-3CkA^2}{4Bk^2 + \Gamma/C^2 k^2} \left[1 + \frac{\Gamma}{C^2 k^2} \left(\frac{3}{2} - \frac{\Phi}{A^2} \right) - \frac{3}{2} Bk^2 \left(1 + \frac{8}{3} \frac{\Phi}{A^2} \right) \right] \quad (3.22a)$$

if the cubic terms in Equation (3.12) are taken into consideration,

$$q_o(k) \approx \frac{-3CkA^2}{4Bk^2 + \Gamma/C^2 k^2} \left[1 + \frac{3}{2} \left(\frac{\Gamma}{C^2 k^2} - Bk^2 \right) \right] \quad (3.22b)$$

if the cubic terms in Equation (3.12) are neglected ($\Phi = 0$), and

$$q_{pc}(k) \approx 3Ck\Phi \left[1 + \frac{B\Gamma/C^2 + \Gamma^2/C^4 k^4 - 12B^2 k^4}{2(\Gamma/C^2 k^2 + 4Bk^2)} \right] \quad (3.22c)$$

if only the cubic terms in Equation (3.12) are taken into consideration and the quadratic terms are ignored.

As shown that, if the quadratic terms are not ignored, then in the lowest order on small parameters the coefficients $q_{Go}(k)$ and $q_o(k)$ do not depend on the cubic terms in Equation (3.13) and exactly coincide with the coefficient derived in (Grimshaw & Helfrich, 2008; 2012; Whitfield & Johnson, 2015a) directly from the Ostrovsky Equation (3.13) without cubic nonlinear term ($a_1 = 0$):

$$q_o(k) = q_{Go}(k) = -\frac{2}{3} \frac{a^2 k^3}{4bk^4 + r} \equiv \frac{-3CkA^2}{4Bk^2 + \Gamma/C^2 k^2} \quad (3.22d)$$

However, in the next order on small parameters the corrections depend on the cubic terms in the primitive Equation (3.12).

Notices that in the recent paper by (Whitfield & Johnson, 2015b) the NLSE was derived from the Gardner–Ostrovsky equation (3.15) which was formally considered

without the restrictions on the range of its validity. The nonlinear coefficient in that paper formally follows from Equation (3.22a) if we assume that $Bk^2 \sim \Gamma/C^2k^2 \ll 1$, but $Bk^2\Phi/A^2 \sim \Gamma\Phi/(ACk)^2 \sim 1$.

Figure 3.4 illustrates the dependence of the nonlinear coefficient in NLSE on the wavenumber k for different models. The first big difference in the dependences of the coefficients $q(k)$ is seen when $B = \Gamma = 1$. The coefficient $q_c(k)$ changes its sign at the point $k_0 = (C^2/B - 5\Gamma)^{1/2}/2C$ (see line 1 in frame a), whereas neither $q_q(k)$ nor $q_o(k)$ changes their signs (see lines 2 and 3 in frame a). However, at very small $k \ll 1$ the dependences $q_c(k)$, $q_q(k)$ and $q_o(k)$ are close to each other.

In the case $B = \Gamma = -1$ line 5 for $q_q(k)$ is qualitatively similar to line 4 for $q_c(k)$, but there is an obvious quantitative difference between these curves for relatively big values of $k > 0.2$ (both these lines go to infinity when $k \rightarrow 1/\sqrt{-B} = 1$). As in the first case, at small $k \ll 1$ the dependences $q_c(k)$, $q_q(k)$ and $q_o(k)$ are close to each other.

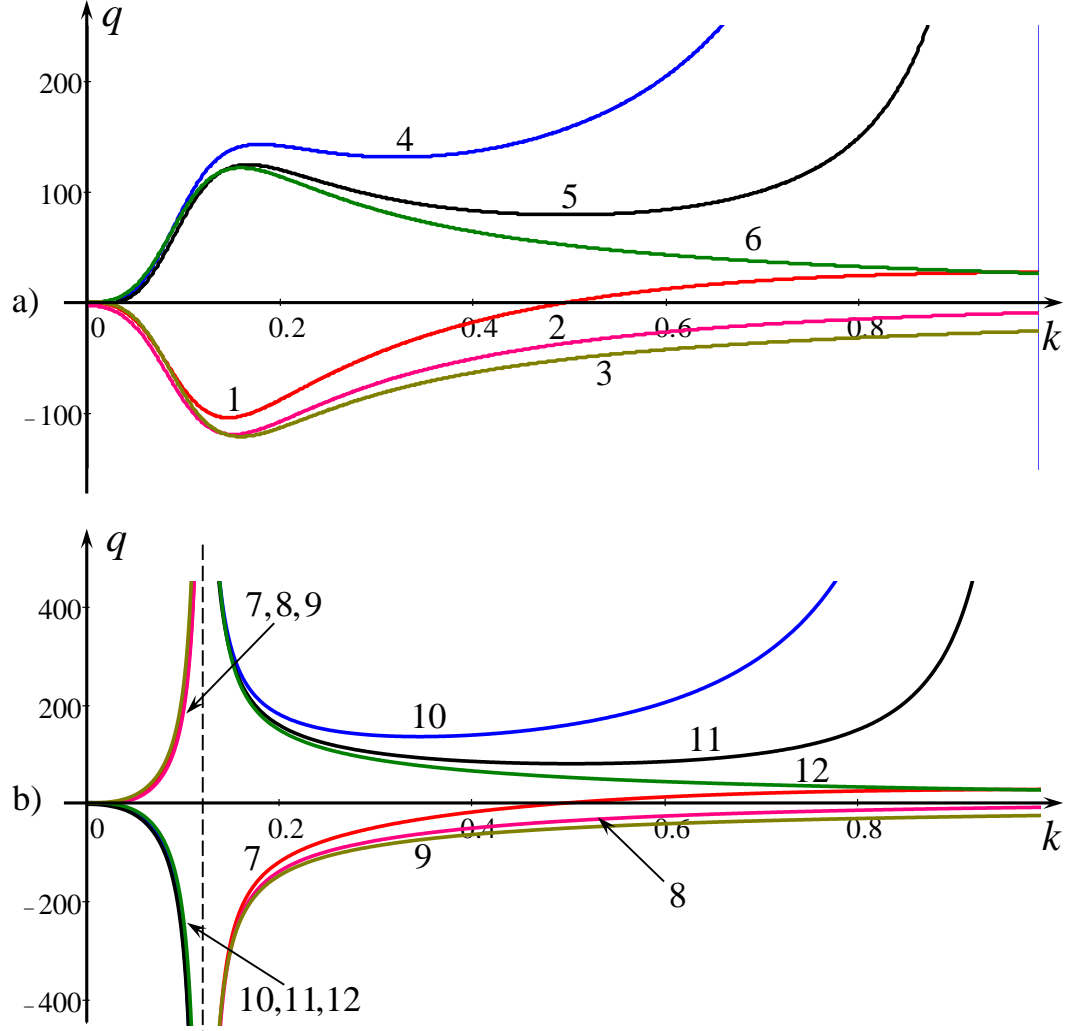


Figure 3.4: The nonlinear coefficient in the NLS Equation (3.18) as a function of a wavenumber for different basic equations. In frame a) lines 1, 2 and 3 are plotted for $B = \Gamma = 1$, lines 4, 5 and 6 are plotted for $B = \Gamma = -1$; in frame b) lines 7, 8 and 9 are plotted for $B = -\Gamma = 1$, lines 10, 11 and 12 are plotted for $B = -\Gamma = -1$.

When the coefficients B and Γ are of opposite sign, then the nonlinear coefficients change their signs at the point of singularity $k = K_{1,2}$ and $k = K_0$, where

$$K_{1,2} = \sqrt{\frac{1}{2C} \sqrt{-\frac{\Gamma}{B} \left(1 - \frac{25B\Gamma}{16C^2}\right)} - \frac{5\Gamma}{8C^2}}, \quad K_0 = \sqrt{\frac{1}{2C} \sqrt{-\frac{\Gamma}{B}}} \quad (3.23)$$

K_1 pertains to the case $B = -1$, $\Gamma = 1$, whereas K_2 pertains to the case $B = 1$, $\Gamma = -1$ and K_0 pertains to Equation (3.22d). These three singular points are very close to each other, although they are ordered in the following way $K_1 < K_0 < K_2$.

For the wavenumbers greater than the singular point all corresponding lines, except line 7, do not change their signs any more, but line 7 changes its sign at $k_0 = \frac{1}{2C} \sqrt{C^2/B - 5\Gamma}$. The points where the coefficients $p(k)$ and $q(k)$ change their signs are very important from the point of view of wave-trains stability with respect to self-modulation; this will be discussed later in this chapter.

In the case when the NLSE is derived directly from the KdV equation the nonlinear coefficient $q_{KdV}(k) = 9A^2C/Bk$ depends on the sign of coefficient B and is either positive, when $B > 0$, or negative, when $B < 0$. Notice that the expression for this coefficient does not follow from Equation (3.22d), if one formally puts $\Gamma = 0$. As explained above, the nonlinear coefficient in the NLSE derived from the KdV equation contains contributions from both the second harmonic and zero harmonic terms. However, as shown in Appendix, when $\Gamma \neq 0$ the zero harmonic contributes only into the higher-order terms (see also (Grimshaw & Helfrich, 2008; 2012)).

As well known (see, e.g., (Karpman, 1973; Ablowitz & Segur, 1981; Ostrovsky & Potapov, 1999)), the stability of quasi-monochromatic wave-trains with respect to small modulations is determined in the NLSE (3.18) by the relative sign of nonlinear and dispersive coefficients. The stability occurs when $p(k)q(k) < 0$, otherwise, when $p(k)q(k) > 0$, the wave-trains are unstable. In the latter case the “bright” envelope soliton can exist, whereas in the former case only “dark” solitons can exist on the background of a sinusoidal wave (see the references cited above). To determine the range of wave-train stability/instability for the particular choice of parameters B and Γ and present it in the vivid form, let us define function $F(k) = S \text{sign}[p(k)q(k)]$, where function $\text{sign}(x) = 1$ if $x > 0$ and $\text{sign}(x) = -1$ if $x < 0$, S is the “amplitude” of function $\text{sign}(x)$ which will help us to distinguish between different lines. Figure 3.5 illustrates the behavior of function $F(k)$ for different sets of parameters B and Γ .

Lines 1 in all frames pertain to the NLSE derived from Equation (3.12) with the cubic nonlinear term, whereas lines 2 pertain to the NLSE derived from Equation (3.12)

without cubic nonlinear term ($\Phi = 0$), and lines 3 pertain to the NLSE derived from the Ostrovsky equation (3.13) without cubic nonlinear term ($a_1 = 0$).

As one can see from this figure, in the case shown in frame a), the models based on Equation (3.12) both with and without cubic nonlinear term predict the stability of wave trains at $k < k_p \equiv \sqrt{\sqrt{(3C^2 + B\Gamma)\Gamma/B} - \Gamma} / C\sqrt{3}$ and instability at $k > k_p$. In the meantime, the model based on the Ostrovsky Equation (3.13) without the cubic nonlinear term predicts the boundary between the stability and instability at $k = k_{o1} \equiv \sqrt[4]{\Gamma/3BC^2}$. Then, the more accurate model (3.12) with the cubic nonlinear term predicts one more boundary between the stability and instability at $k = k_{o1} \equiv \sqrt{C^2/B - 5\Gamma}/2C$ (see line 1 in frame a), whereas two other models do not predict stability at high wavenumbers. Note that the case shown in frame a) pertains to gravity water waves in a rotating fluid.

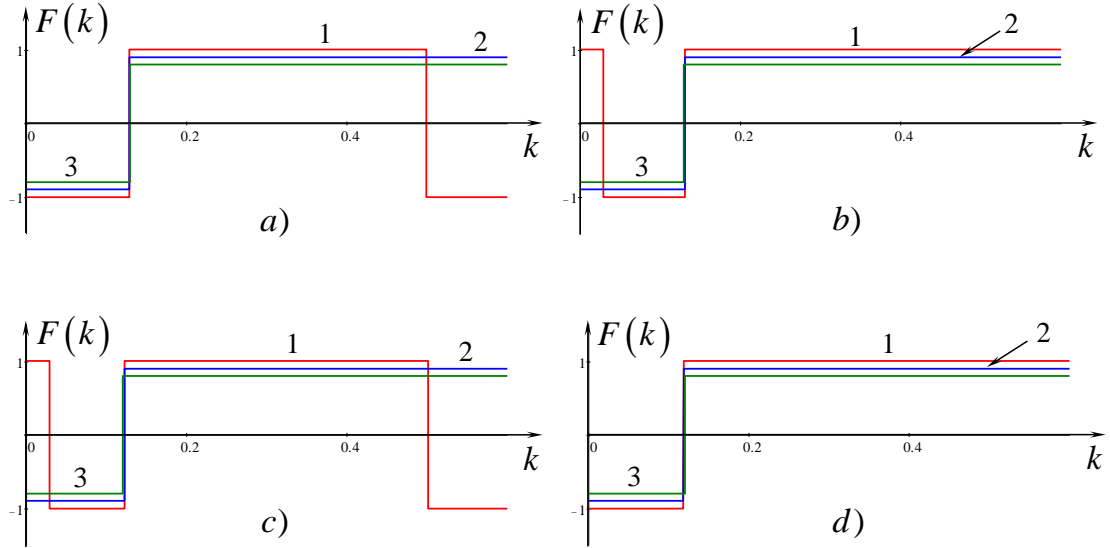


Figure 3.5: Ranges of stability (when $F(k) < 0$) and instability (when $F(k) > 0$) of wave-trains against self-modulation. Frame a) pertains to $B = \Gamma = 1$; frame b) pertains to $B = \Gamma = -1$; frame c) pertains to $B = -\Gamma = 1$; and frame d) pertains to $B = -\Gamma = -1$. For the meaning of lines see the text.

In the case shown in frame b), the model equation (3.12) with the cubic nonlinearity predicts modulation instability at very small $k < k_{o2} \equiv \sqrt{-\Gamma}/C$, whereas other models do not predict such instability. Then, there is the range of instability at $k > k_p$ predicted by the models based on Equation (3.12) both with and without cubic

nonlinear term, as well as by the model based on Ostrovsky equation (3.13) without cubic nonlinear term at wavenumbers $k > k_{O1}$.

In the case shown in frame c), the model equation (3.12) with the cubic nonlinearity predicts two regions of modulation instability, $0 < k < k_{O2}$ and $k_p < k < k_{O1}$, and two regions of stability, $k_{O2} < k < k_p$ and $k > k_{O1}$ (see line 1 in frame c). In the meantime, other two models predict only one boundary between the stability, $k < k_p$ ($k < k_{O2}$), and instability, $k > k_p$ ($k > k_{O2}$), regions (here $k_{O1} \equiv \sqrt[4]{-\Gamma/4BC^2}$).

And, at last, in the case shown in frame d), the models with and without cubic nonlinearity predict the same regions of wave-train stability $k < k_p$ ($k < k_{O2}$), and instability, $k > k_p$ ($k > k_{O2}$).

In the case when the NLSE is derived from the KdV equation the product $p(k)q(k) = -27(AC)^2/2 < 0$, so that the wave-trains are stable against self-modulations for all k .

3.4. Conclusion

Thus, it has been shown that the NLSE derived from the unidirectional Gardner–Ostrovsky equation (3.13) agrees well with the NLSE derived from the more general Shrira equation (3.12) within the range of validity of the Gardner–Ostrovsky equation. Moreover, within this range the coefficients of NLSE can be correctly obtained even without the cubic nonlinear terms in the governing Equation (3.12). Beyond the range of validity of the Gardner–Ostrovsky equation the existence of ranges of modulation stability/instability is rather non-trivial and depends on the signs of small-scale and large-scale dispersions characterised by dimensionless coefficients B and Γ . All possible signs of nonlinear and dispersive coefficient has been considered and presented the complete analysis of the problem for media with double dispersion. Therefore, this analysis is applicable not only to water waves in rotating or non-rotating fluids (e.g., various oceanic waves), but also to plasma waves, waves in solids, optical fibers and others.

In application to surface and internal waves in a rotating ocean (see Figure 3.5, frame a) our analysis shows that wave-trains are stable against self-modulation at small wavenumbers less than some critical value $k < k_p \equiv \sqrt{\sqrt{(3C^2 + B\Gamma)\Gamma/B - \Gamma}} / C\sqrt{3}$ ($k < k_{o1} \equiv \sqrt[4]{\Gamma/3BC^2}$) which depends on the dispersion coefficients of the governing equations. This is in agreement with the results obtained in (Grimshaw & Helfrich, 2008; 2012; Whitfield & Johnson 2015a), where the analysis was performed without cubic nonlinear terms in the limited range of wavenumbers as per Equation (3.6).

Chapter 4 Obliquely Propagating Skew Kadomtsev– Petviashvili Lumps

4.1. Introduction

The Kadomtsev–Petviashvili (KP) equation is one of the well-studied models of nonlinear waves in dispersive media (see, e.g., (Ablowitz & Segur, 1981) (Petviashvili & Pokhotelov, 1992)). In the immovable “laboratory” coordinate frame it can be presented in the form

$$\frac{\partial}{\partial x} \left(\frac{\partial u}{\partial t} + c \frac{\partial u}{\partial x} + \alpha u \frac{\partial u}{\partial x} - \beta \frac{\partial^3 u}{\partial x^3} \right) = -\frac{c}{2} \frac{\partial^2 u}{\partial y^2} \quad (4.1)$$

where c is the velocity of long linear perturbations, and α and β are the nonlinear and dispersive coefficients which are determined by the specific type of wave and medium properties.

The properties of solutions to this equation depend on the sign of the dispersion coefficient β . In media with positive dispersion ($\beta > 0$) the equation possesses fully localised solitary wave solutions which are dubbed the lumps (Ablowitz & Segur, 1981). V.I. Petviashvili was the first who discovered such solutions numerically and suggested very effective numerical method to construct stationary solutions of nonlinear wave equations (Petviashvili V. , 1976) (the method was rigorously substantiated later in (Pelinovsky & Stepanyants, 2004)). Then, symmetric lump solutions were found analytically (Manakov, *et al.*, 1977) and (Ablowitz & Satsuma, 1978), and more general solutions representing skew lumps were obtained in (Lu, *et al.*, 2004) and (Ma W. -X., 2015). Later, even more complex analytical solutions (bi-solitons, triple solitons, etc) were found in (Pelinovsky & Stepanyants, 1993) and (Gorshkov, *et al.*, 1993). Then it was developed a symbolic computation approach to search for lumps, and more generally, rational solutions as seen in (Ma W. -X., 2015), (Ma, Qin, & Lü, 2015) and (Zhang & Ma, 2015).

Lump solutions describe nonlinear patterns in plasma (Ablowitz & Segur, 1981) (Karpman, 1975) (Petviashvili & Pokhotelov, 1992), on the surface of a shallow water with the dominated surface tension (Karpman, 1975) (Abramyan & Stepanyants, 1985) (Falcon, *et al.*, 2002), in nonlinear optic media (Pelinovsky, *et al.*, 1995), in the Bose–Einstein condensate (Mironov, *et al.*, 2010), in solids with inner microstructure (Tauchert & Guzelsu, 1972), etc. They can play a role of elementary wave excitations, and their ensembles with nontrivial internal interaction between lumps can represent a model of strong wave turbulence.

However, even in the simplest case of one-lump solution (Manakov, *et al.*, 1977) (Ablowitz & Satsuma, 1978) (Lu, *et al.*, 2004) (Ma W. -X., 2015), the properties of such solution were not thoroughly analysed so far. Meanwhile, it is of interest to analyse lump solutions in details in the view of their physical applicability to different areas. In this paper such analysis is presented and some interesting features are found for skew lumps and bi-lumps obliquely propagating with respect to the main axis of motion. In isotropic media the main axis of motion can be chosen arbitrarily (Berger & Milewski, 2000), therefore skew lumps, apparently, can co-exist with the symmetrical lumps forming a wide class of three-dimensional patterns. The role of skew lumps in the dynamics of localised initial perturbation is not clear yet; it will be studied in the nearest future. The main aim is to describe the characteristic features of elementary skew lumps and draw attention to their possible role in the dynamic of arbitrary initial perturbations.

4.2. Skew lumps

Considering the KP1 equation (4.1) with the positive dispersion parameter β , a stationary solution representing a pulse fully localised in the space can be studied. Assume that the pulse moves in the x,y -plane with the constant velocity $\mathbf{V} = (V_x, V_y)$. For such solution function $u(x, y, t)$ in Equation (4.1) depends only on two variables $\xi = x - V_x t$ and $\eta = y - V_y t$, and the equation can be rewritten in the form

$$(c - V_x) \frac{\partial^2 u}{\partial \xi^2} + \frac{c}{2} \frac{\partial^2 u}{\partial \eta^2} - V_y \frac{\partial^2 u}{\partial \xi \partial \eta} = -\frac{\partial^2}{\partial \xi^2} \left[\frac{\alpha u^2}{2} - \beta \frac{\partial^2 u}{\partial \xi^2} \right]. \quad (4.2)$$

This equation under the transformation

$$\xi_n = \xi + V_y \eta, \quad \eta_n = \eta \quad (4.3)$$

can be reduced to the form which does not contain the mixed second derivative, but contains effective velocity along the ξ_n -axis only $V_{eff} = V_x + V_y^2/2c$. Notice that the transformation is not orthogonal, therefore it does not represent just a rotation of the coordinate system.

For further study it is convenient to convert Equation (4.2) to the dimensionless form:

$$\frac{\partial^2 v}{\partial X^2} + \frac{\partial^2 v}{\partial Y^2} - \nu \frac{\partial^2 v}{\partial X \partial Y} = \frac{\partial^2}{\partial X^2} \left[v^2 + \frac{\partial^2 v}{\partial X^2} \right] \quad (4.4)$$

where $\nu = \frac{V_y}{c} \sqrt{\frac{2}{1 - V_x/c}}$ with the help of transformation

$$X = \xi \sqrt{\frac{c - V_x}{\beta}}; \quad Y = \eta \sqrt{\frac{2(c - V_x)^2}{\beta c}}; \quad v = \frac{-\alpha u}{2(c - V_x)}. \quad (4.5)$$

From the transformation it follows the important relationships between the solitary wave amplitude A , velocity component V_x and characteristic widths along axes x and y , Δ_x and Δ_y respectively:

$$V_x = c \left(1 + \frac{1}{2c} \frac{\alpha A}{v_{\max}} \right); \quad \Delta_x = \delta_x \sqrt{-2\beta \frac{v_{\max}}{\alpha A}}; \quad \Delta_y = -\delta_y \sqrt{2\beta c} \frac{v_{\max}}{\alpha A} \quad (4.6)$$

Here the dimensionless amplitude v_{\max} and characteristic widths δ_x and δ_y depend on the parameter ν . Note that in the case of a positive dispersion, $\beta > 0$, we have $V_x < c$, and $v_{\max}/(\alpha A) < 0$ [see Equations (4.5) and (4.6)]. Then, the larger the amplitude

of a solitary wave $|A|$ the smaller its characteristic widths both in the x - and y -directions, but $\Delta_y \sim |A|^{-1}$ decreases faster than $\Delta_x \sim |A|^{-1/2}$ when $|A|$ increases.

For a lump moving along the x -axis, the parameter ν is zero; then, the well-known symmetrical lump solution to the KP1 equation is (Manakov, *et al.*, 1977) (Ablowitz & Satsuma, 1978) (Ablowitz & Segur, 1981) (Pelinovsky & Stepanyants, 1993) (see Figure 4.1):

$$\nu(X, Y) = 4 \frac{1 - \frac{1}{3}(X^2 - Y^2)}{\left[1 + \frac{1}{3}(X^2 + Y^2)\right]^2} \quad (4.7)$$

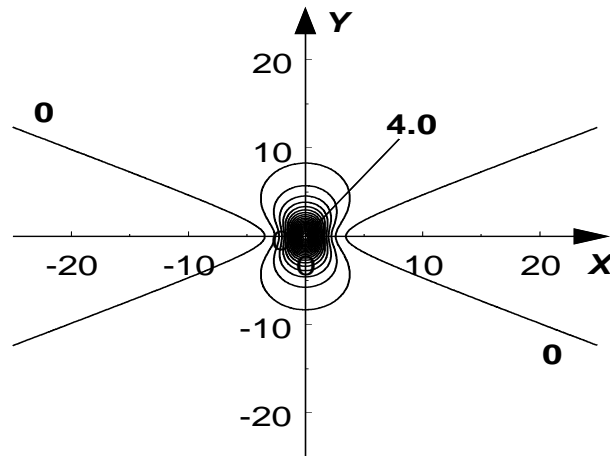


Figure 4.1a: Contour plot of the conventional KP1 lump

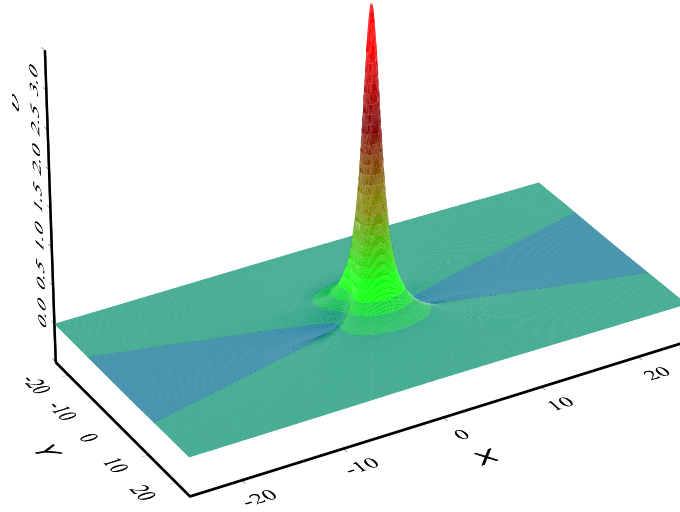


Figure 4.2b: 3D plot of the conventional KP1 lump

This solution does not contain any free parameter and can be treated as the nonlinear eigen function of Equation (4.4) with $\nu = 0$. In the dimensionless variables the lump amplitude and characteristic widths are $v_{\max} = 4$, $\delta_x = \sqrt{3}$; $\delta_y = \sqrt{3}$. The corresponding dimensional parameters are

$$V_x = c \left(1 + \frac{\alpha A}{8c} \right) < c; \quad \Delta_x = \sqrt{\frac{-24\beta}{\alpha A}}; \quad \Delta_y = -\frac{4}{\alpha A} \sqrt{6\beta c}. \quad (4.8)$$

In general for the obliquely propagating lumps, i.e., when $\nu \neq 0$, all these parameters are functions of ν .

To find a lump solution in the general case, let us use the Hirota ansatz $v = 6 \frac{\partial^2 \ln f(X, Y)}{\partial X^2}$ and transform Equation (4.4) into the bilinear form (Ablowitz & Satsuma, 1978) (Ablowitz & Segur, 1981) (Lu, *et al*, 2004) (Ma W. -X., 2015) :

$$f(f_{xx} + f_{yy} - \nu f_{xy}) - (f_x)^2 - (f_y)^2 + \nu f_x f_y = 3(f_{xx})^2 + ff_{xxxx} - 4f_x f_{xxx} \quad (4.9)$$

Substitute into this equation the quadratic function $f = (X - X_0)^2 + p(Y - Y_0)^2 + qXY + r$, where X_0 and Y_0 are arbitrary constants which determine the initial position of the lump (they are omitted further without loss of generality), p , q , and r are some unknown parameters which can be determined after substitution of the trial quadratic function into Equation (4.9). The substitution gives a set of equations for the coefficients:

$$2(p - 1) + q(\nu - q) = 0; \quad (4.10a)$$

$$2p(p - 1) + q(q - p\nu) = 0; \quad (4.10b)$$

$$2\nu p - q(p + 1) = 0; \quad (4.10c)$$

$$2r(p + 1) - \nu qr - 12 = 0. \quad (4.10d)$$

A solution of this system can be readily found: $p = 1$; $q = \nu$; $r = 12/(4 - \nu^2)$, which yields $f(X, Y) = X^2 + Y^2 + \nu XY + 12/(4 - \nu^2)$. The corresponding function $\nu(X, Y)$ generalises the known lump solution (4.7) and reduces to it when $\nu = 0$ (see also (Lu, *et al.*, 2004) (Ma W. -X., 2015)):

$$\nu(X, Y) = (4 - \nu^2) \frac{1 + \frac{4 - \nu^2}{12} \left[\frac{4 - \nu^2}{4} Y^2 - \left(X + \frac{\nu}{2} Y \right)^2 \right]}{\left\{ 1 + \frac{4 - \nu^2}{12} \left[\frac{4 - \nu^2}{4} Y^2 + \left(X + \frac{\nu}{2} Y \right)^2 \right] \right\}^2} \quad (4.11a)$$

Alternatively, this solution can be presented in another form which is useful for calculation of integral lump characteristics (the total lump mass, momentum, energy, etc):

$$\nu(X, Y) = \frac{-6}{\left(X + \frac{\nu}{2} Y - i \sqrt{\frac{12}{4 - \nu^2} + \frac{4 - \nu^2}{12} Y^2} \right)^2} + \frac{-6}{\left(X + \frac{\nu}{2} Y + i \sqrt{\frac{12}{4 - \nu^2} + \frac{4 - \nu^2}{12} Y^2} \right)^2} \quad (4.11b)$$

where i is the imaginary unit.

The solution is non-singular when ν varies in the range $-2 \leq \nu \leq 2$. This condition together with the definition of ν [see Equation (4.4)] imposes the restriction on the possible velocity components in the dimensional variables:

$$\frac{V_x}{c} < 1 - \frac{1}{2} \left(\frac{V_y}{c} \right)^2 \quad (4.12)$$

The domain of possible velocity components of a single lump is shown in Figure 4.2.

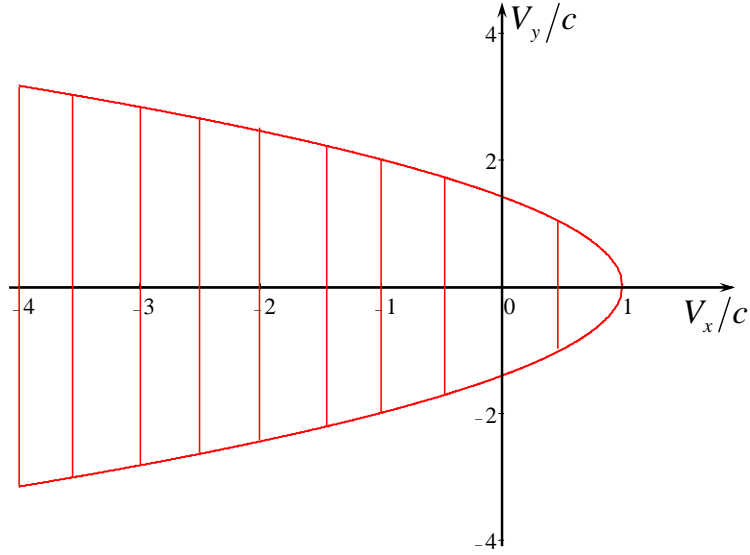


Figure 4.2: The domain of possible velocity components (shaded) of a single lump as per Equation (4.12).

The dimensionless amplitude of the obliquely moving lump is $v_{\max} = 4 - v^2$. Thus, the lump amplitude is maximal and equals 4 when $v = 0$, i.e., when it moves along the axis x . The lump has an asymmetrical shape (it is skew) and moves obliquely with respect to the axes x ; the angle of lump inclination depends on the parameter v . The similar skew-lump solution has been obtained in (Lu, *et al.*, 2004), (Ma W. -X., 2015) but as has been mentioned above, the properties of such solution were not discussed in details. Figure 4.3 shows the contour plots of skew lumps for various values of v .

Note that the parameter v does not reflect precisely the direction of motion although it pertains to the oblique lump motion; it determines the orientation of the lump on the X,Y -plane (or, correspondingly, on the physical x,y -plane). The inclination

of the lump trajectory to the axis x is determined by the angle θ , which is such that $\tan\theta = V_y/V_x$. As follows from the definition of the parameter ν [see Equation (4.4)],

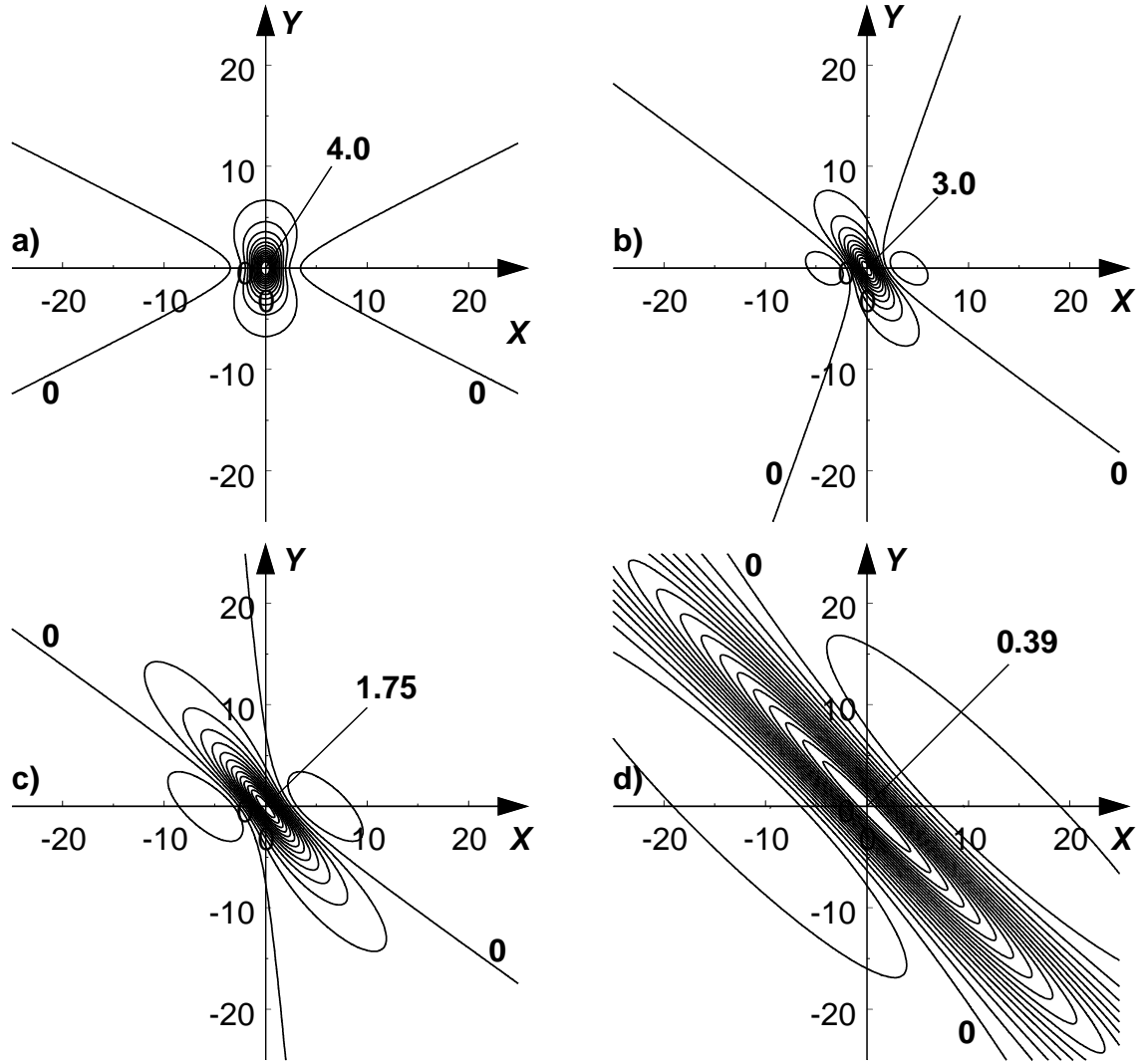


Figure 4.3: Contour plots of lumps for different values of ν . a) $\nu = 0.5$; b) $\nu = 1.0$; c) $\nu = 1.5$; and d) $\nu = 1.9$. Arrows show maximum values, zero isolines are also indicated.

$$\tan^2 \theta = \frac{\nu^2}{2} \left(\frac{c}{V_x} \right)^2 \left(1 - \frac{V_x}{c} \right) \quad (4.13)$$

Thus, the oblique lumps with $\nu \neq 0$ move at certain angles to the axes x and y and; as will be shown below, they are antisymmetric in the moving coordinate system.

The isolines of lump zeros are determined by the equation:

$$X^2 - \left(1 - \frac{\nu^2}{2}\right)Y^2 + \nu XY = \frac{12}{4 - \nu^2} \quad (4.14)$$

With the help of the orthogonal transformation of coordinates $X = X_n \cos \varphi - Y_n \sin \varphi$,

$Y = X_n \sin \varphi + Y_n \cos \varphi$ this equation can be reduced to the canonical form $\frac{X_n^2}{A^2} - \frac{Y_n^2}{B^2} = 1$

which represents the hyperbola. The angle φ between old and new coordinate systems is

determined in this case by the equation $\tan 2\varphi = \frac{2\nu}{4 - \nu^2}$; it can vary in the range $-\pi/4 \leq$

$\varphi \leq \pi/4$ when ν varies from -2 to 2 . The parameters A and B determining the ‘semi-axes’ of the hyperbola are functions of ν :

$$A^2 = \frac{48\sqrt{(4 - \nu^2)^2 + 4\nu^2}}{(4 - \nu^2)\left[\nu^2\sqrt{(4 - \nu^2)^2 + 4\nu^2} + (4 - \nu^2)^2 - 4\nu^2\right]}, \quad B^2 = \frac{48\sqrt{(4 - \nu^2)^2 + 4\nu^2}}{\nu^4\sqrt{(4 - \nu^2)^2 + 4\nu^2} + (4 - \nu^2)^3} \quad (4.15)$$

However even in this coordinate system where the zero line level of the lump is symmetrical with respect to the new coordinate axes X_n and Y_n , the lump itself is antisymmetric in the X_n, Y_n -plane as shown in Figure 4.4 for the particular value of $\nu = 1.5$ (verily skew lump!). In the meantime, in the non-orthogonal coordinates as per Equation (4.3) the lump looks symmetrical in the main cross-sections.

Having got a solution (4.11) in the dimensionless variables, one can present skew lump solution of the KP1 equation in the original variables:

$$u(x, y, t) = -\frac{2c}{\alpha} \left(1 - \frac{V_x}{c}\right) \nu \left[\sqrt{\frac{c}{\beta} \left(1 - \frac{V_x}{c}\right)} (x - V_x t), \sqrt{\frac{2c}{\beta} \left(1 - \frac{V_x}{c}\right)} (y - V_y t) \right] \quad (4.16)$$

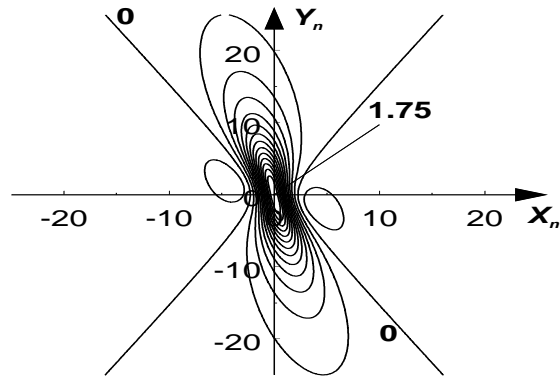


Figure 4.4a: Contour plot of a skew lump with $\nu = 1.5$ in the coordinate system where the zero isolines are symmetrical with respect to the coordinate axes (see the hyperbolic lines).

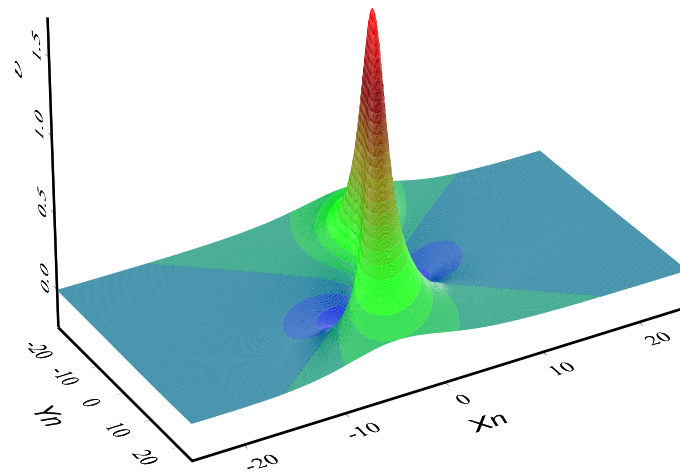


Figure 4.4b: 3D profile of the same lump in Figure 4.6a.

To illustrate the oblique and skew character of lump motion, let us consider a particular case when $V_x = 0$. Then, the lump can be either in the rest in the coordinate system moving with the speed c or it may move along axis y with any velocity in the range $-\sqrt{2} < V_y/c < \sqrt{2}$ (see Figure 4.2). For the moving lump the parameter $\nu \neq 0$, therefore the lump is inclined to the axes x and y . The lump shape is very close to the shape of the conventional symmetric lump (see Figure 4.1), if its velocity V_y is small, but it propagates in the y - rather than in the x -direction.

4.3. Obliquely Propagating Skew Multi-lump Solutions

In the similar way one can construct more complicated skew bi-lump, triple lump, ..., multi-lump solutions in the spirit of papers (Pelinsonsky & Stepanyants, 1993) (Gorshkov, *et al.*, 1993). It can be shown (see (Gorshkov, *et al.*, 1993) and references therein) that the number of lumps M constituting a multi-lump solution is $M = N(N + 1)/2 = 1, 3, 6, 10 \dots$, where N is an integer number. Such multi-lump solutions are described by Equation (4.9) with a polynomial function $f(X, Y)$ of the degree $2M$. The simplest nontrivial rational solution of Equation (4.9) after that quadratic function which describes the single lump (see above) can be constructed on the basis of six degree polynomial of X and Y with undetermined coefficients. Substituting such polynomial into Equation (4.9) and equating to zero the coefficients of like terms can find the solution containing two arbitrary parameters, a and b :

$$\begin{aligned}
 f(X, Y) = & X^6 + Y^6 + \frac{100}{4-\nu^2} X^4 + 4 \frac{17+14\nu^2-3\nu^4}{4-\nu^2} Y^4 + bX^3 + aY^3 - \frac{2000}{(4-\nu^2)^2} X^2 + \\
 & 400 \frac{19-6\nu^2}{(4-\nu^2)^2} Y^2 - \frac{4b}{4-\nu^2} X - 4 \frac{5a+8b\nu-3b\nu^3}{(4-\nu^2)(1-\nu^2)} Y - \frac{2000\nu}{(4-\nu^2)^2} XY + 60 \frac{6+\nu^2}{4-\nu^2} X^2 Y^2 + \\
 & \nu(6+\nu) X^3 Y^3 + 3XY \left[\nu(X^4 + Y^4) + (1+\nu^2) XY(X^2 + Y^2) + \frac{40\nu}{3} \frac{5X^2 + (9-\nu^2)Y^2}{4-\nu^2} - \right. \\
 & \left. \frac{(a+b\nu)X + (b+a\nu)Y}{1-\nu^2} \right] + \frac{1}{4-\nu^2} \left[\frac{ab\nu(3-\nu^2) + (a^2 + b^2)}{(1-\nu^2)^2} + \frac{120000}{(4-\nu^2)^2} \right] \quad (4.17)
 \end{aligned}$$

Depending on the parameters a , b and ν , this solution can represent either bi- or triple-lump. In the particular case $\nu = 0$, solution (4.17) reduces to the solution found in (Gorshkov, *et al.*, 1993).

Playing with the parameters a and b , one can obtain a big variety of interesting stationary solutions representing coupled lumps moving at some angles to the axis x . Choosing in particular $a = b = 0$, we obtain from Equation (4.17)

$$\begin{aligned}
f = & X^6 + Y^6 + \frac{100}{4-\nu^2} X^4 + 4 \frac{17+14\nu^2-3\nu^4}{4-\nu^2} Y^4 - \frac{2000}{(4-\nu^2)^2} X^2 + 400 \frac{19-6\nu^2}{(4-\nu^2)^2} Y^2 \\
& - \frac{4b}{4-\nu^2} X - \frac{2000\nu}{(4-\nu^2)^2} XY + 60 \frac{6+\nu^2}{4-\nu^2} X^2 Y^2 + \nu(6+\nu) X^3 Y^3 + \\
& 3XY \left[\nu(X^4 + Y^4) + (1+\nu^2)XY(X^2 + Y^2) + \frac{40\nu}{3} \frac{5X^2 + (9-\nu^2)Y^2}{4-\nu^2} \right] + \frac{120000}{(4-\nu^2)^3} \quad (4.18)
\end{aligned}$$

In this case function $f(X, Y)$ has singularities only at $\nu = \pm 2$, but when $|\nu| \rightarrow 2$, the solution for $\nu(X, Y)$ reduces to a very wide bi-lump of small amplitude (as in Figures 4.5e), which completely vanishes in the limit $|\nu| = 2$. Figure 4.5 illustrates a solution as per Equation (4.18) presented in terms of the variable $\nu(X, Y)$. This solution represents a bi-lump whose shape monotonically depends on the parameter ν .

If however $a^2 + b^2 \neq 0$, then function $f(X, Y)$ has two more singularities at $\nu = \pm 1$. The structure of the solution changes around these singular values. Figure 4.6 illustrates the function changes for the particular case of $a = 10, b = 0$. When ν increases and approaches 1, the solution being quasi-symmetrical at $\nu = 0$ and having two strongly pronounced maxima (see Figure 4.6a), becomes more and more asymmetrical. The third small maximum appears at $\nu \approx 0.9$ (see Figure 4.6c) and gradually grows when $\nu \rightarrow 1$ (see Figure 4.6d), but the distances between the maxima increase. In the limit $\nu = 1$, the distance becomes infinite, so that all three humps move off to the infinity, and the wave field between them goes to zero; the solution degenerates to zero at this value of ν .

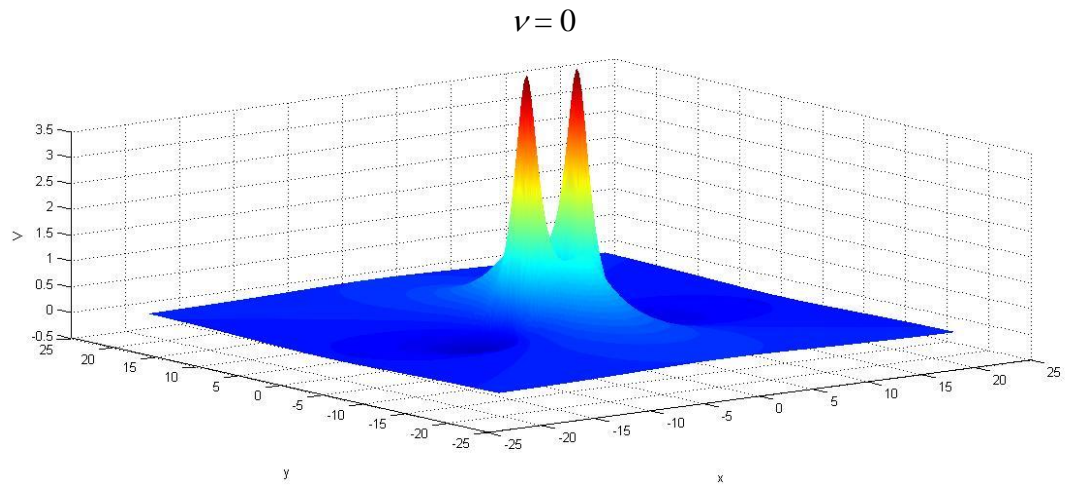


Figure 4.5a: Skew lumps as per Equation (4.18) with $a = b = 0$ and $\nu = 0$.

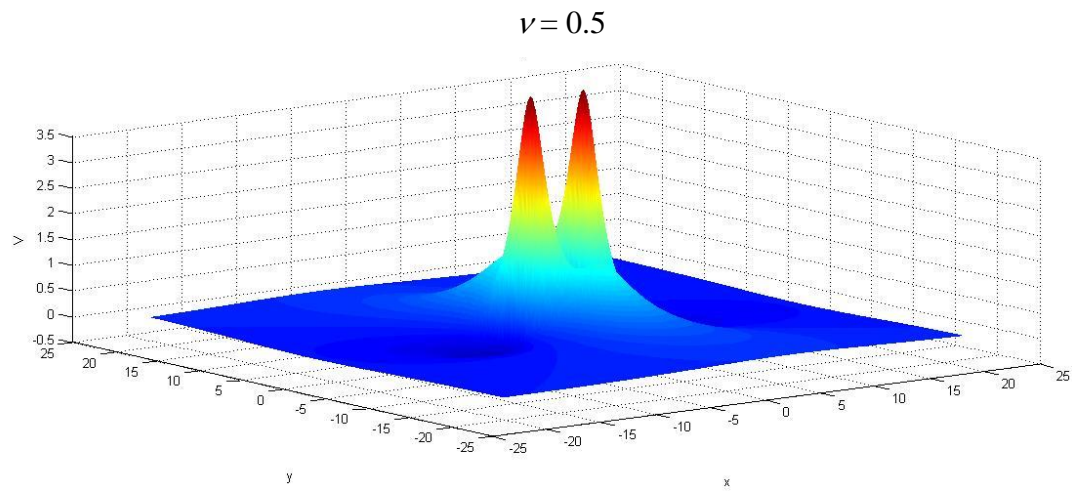


Figure 4.5b: Skew lumps as per Equation (4.18) with $a = b = 0$ and $\nu = 0.5$.

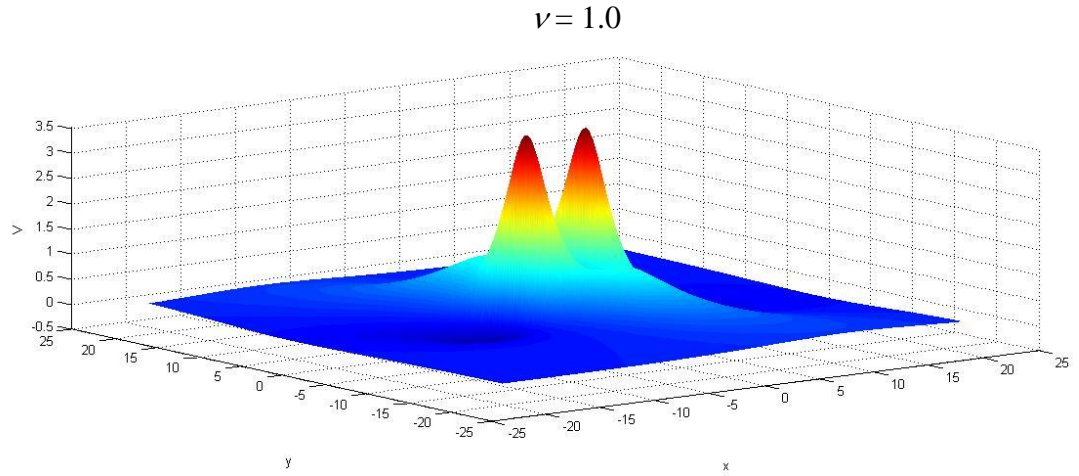


Figure 4.5c: Skew lumps as per Equation (4.18) with $a = b = 0$ and $\nu = 1.0$.

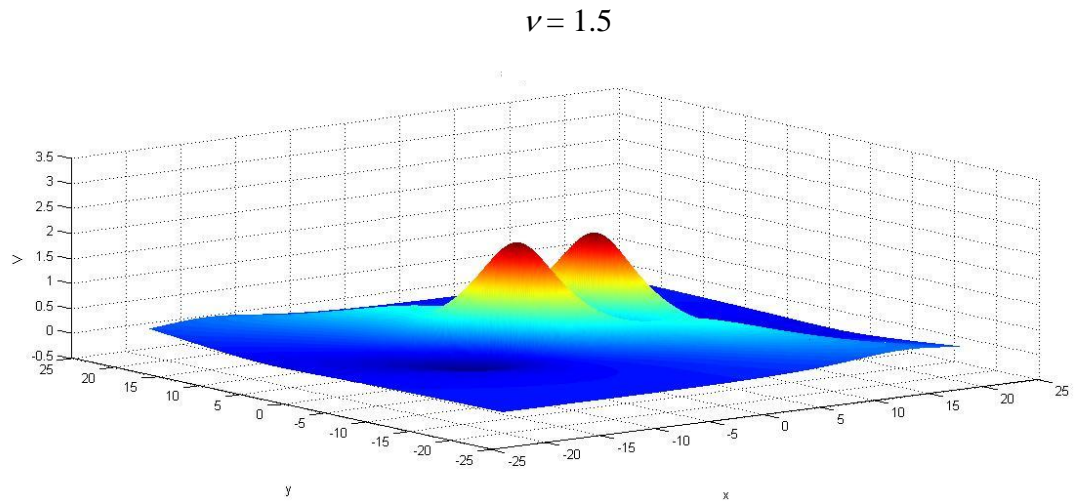


Figure 4.5d: Skew lumps as per Equation (4.18) with $a = b = 0$ and $\nu = 1.5$.

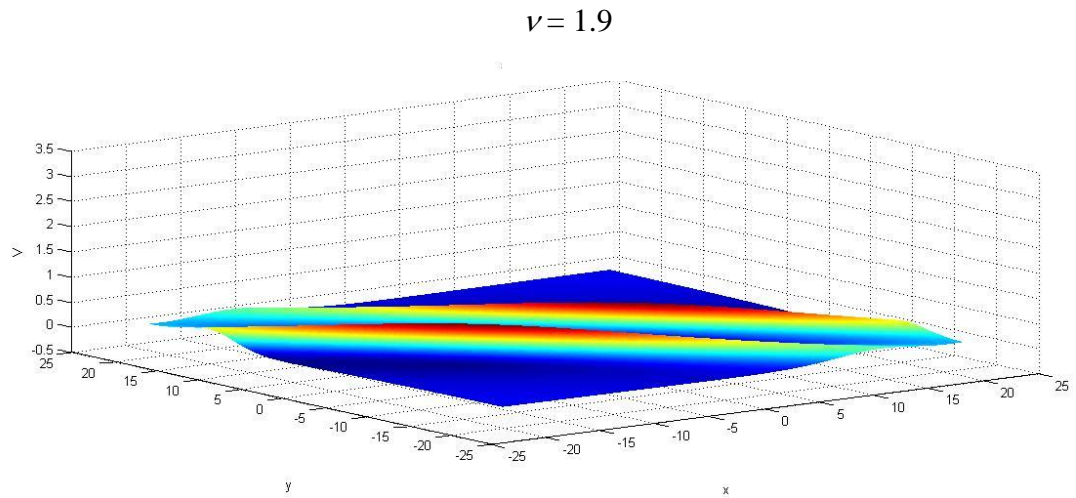


Figure 4.5e: Skew lumps as per Equation (4.18) with $a = b = 0$ and $\nu = 1.9$.

When ν is slightly greater than one, then the solution represents again the three-hump pattern with a big distance between the humps ($\nu = 0$ see Figure 4.6e). The distance decreases when ν increases; one of the humps becomes smaller than two others and gradually disappears at $\nu > 1.1$ (see Figure 4.6f). When ν increases further from 1 to 2, the solution becomes more and more symmetrical (see Figure 4.6g); eventually it reduces to a very wide bi-lump of a small amplitude (see Figure 4.6h), which completely vanishes in the limit $|\nu| = 2$.

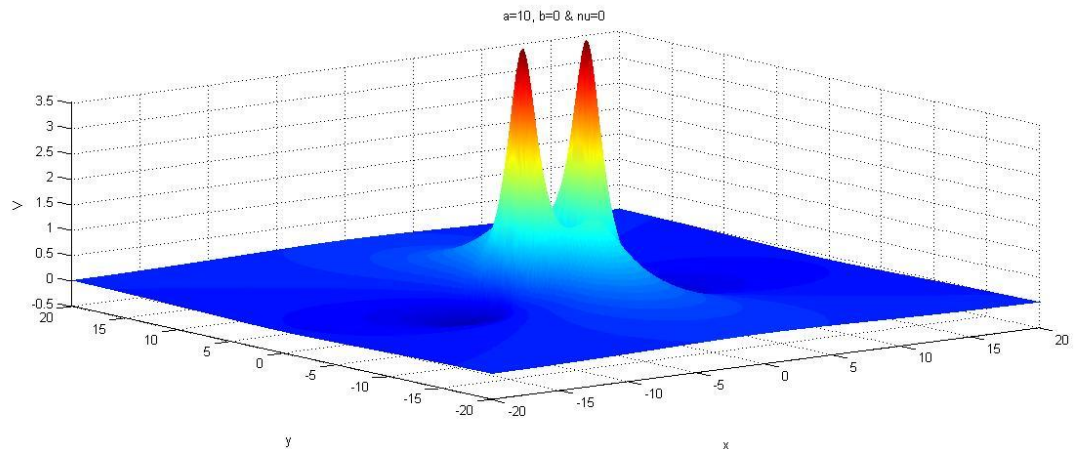


Figure 4.6a: Skew lumps as per Equation (4.18) with $a = 10$, $b = 0$ and $\nu = 0$.

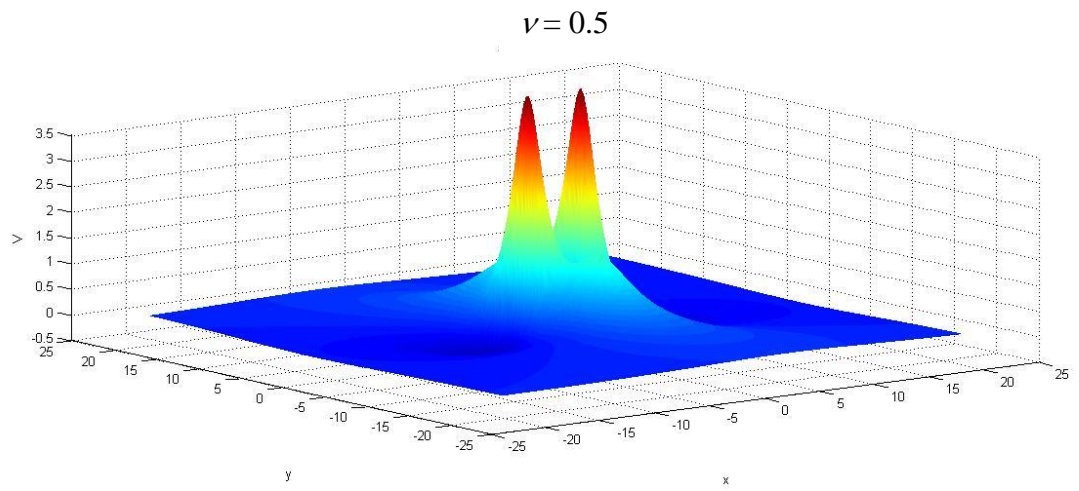


Figure 4.6b: Skew lumps as per Equation (4.18) with $a = 10$, $b = 0$ and $\nu = 0.5$.

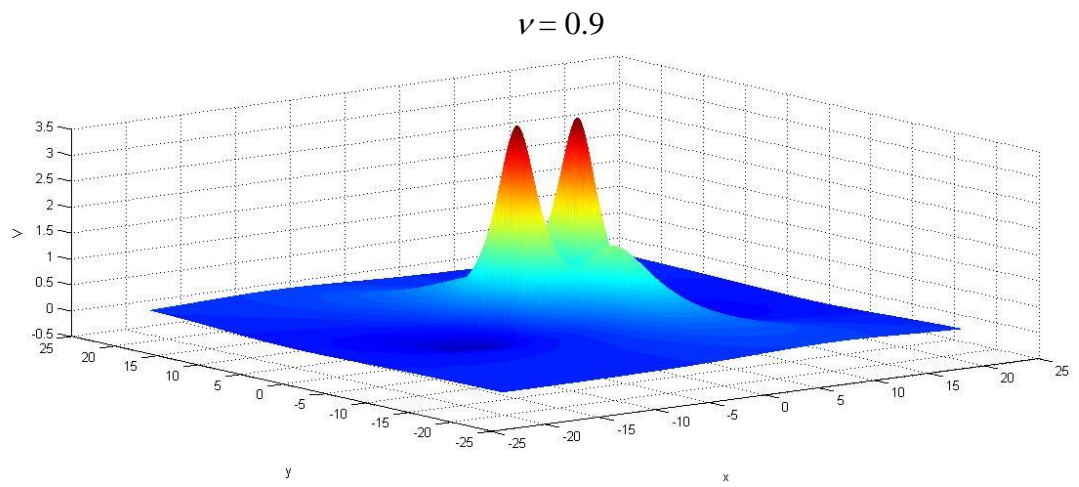


Figure 4.6c: Skew lumps as per Equation (4.18) with $a = 10$, $b = 0$ and $\nu = 0.9$.

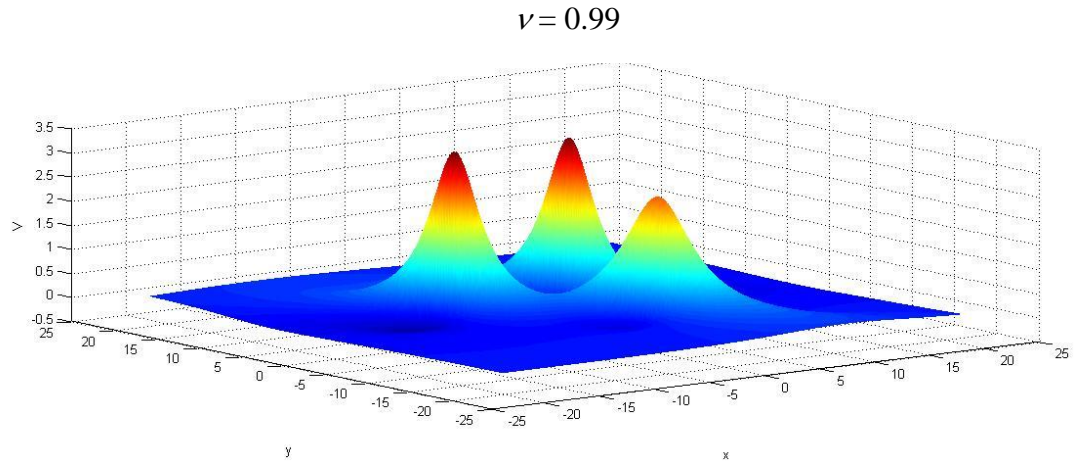


Figure 4.6d: Skew lumps as per Equation (4.18) with $a = 10$, $b = 0$ and $\nu = 0.99$.

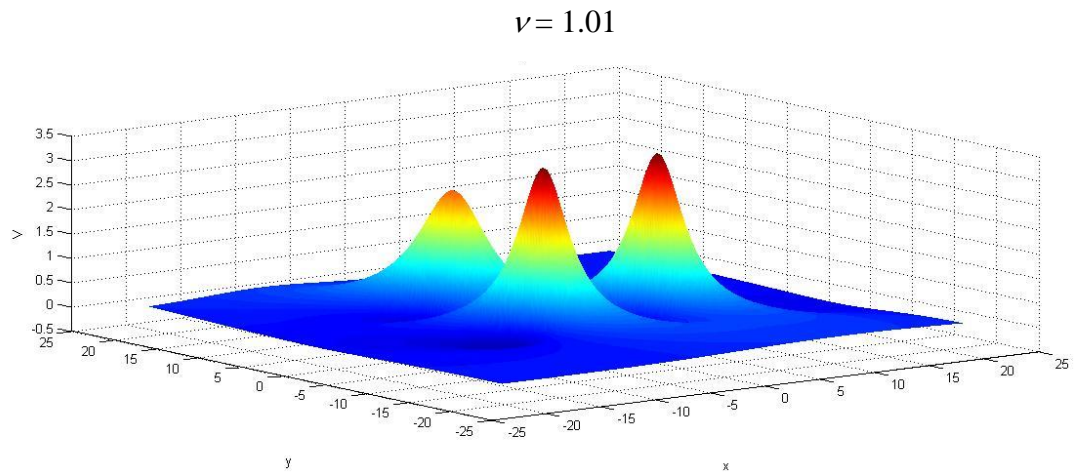


Figure 4.6e: Skew lumps as per Equation (4.18) with $a = 10$, $b = 0$ and $\nu = 1.01$.

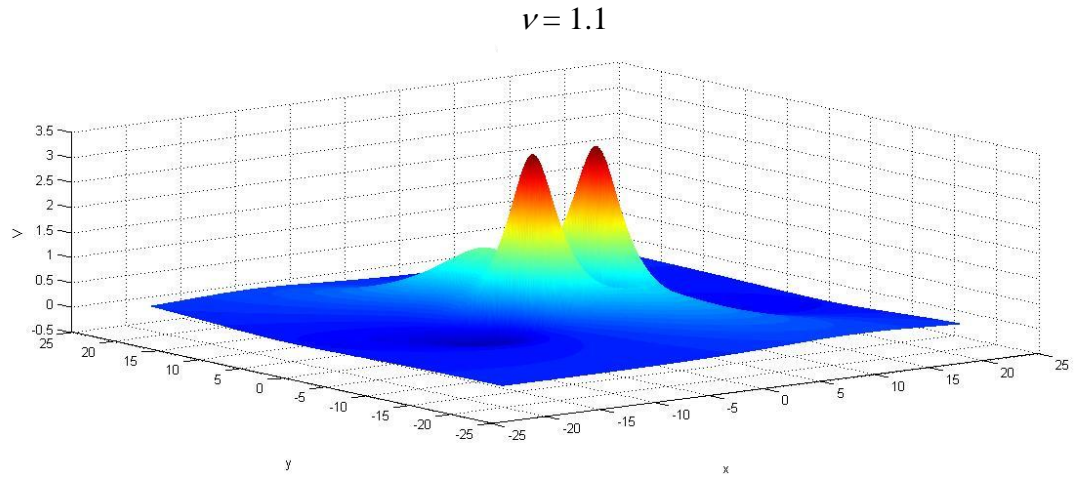


Figure 4.6f: Skew lumps as per Equation (4.18) with $a = 10$, $b = 0$ and $\nu = 1.1$.

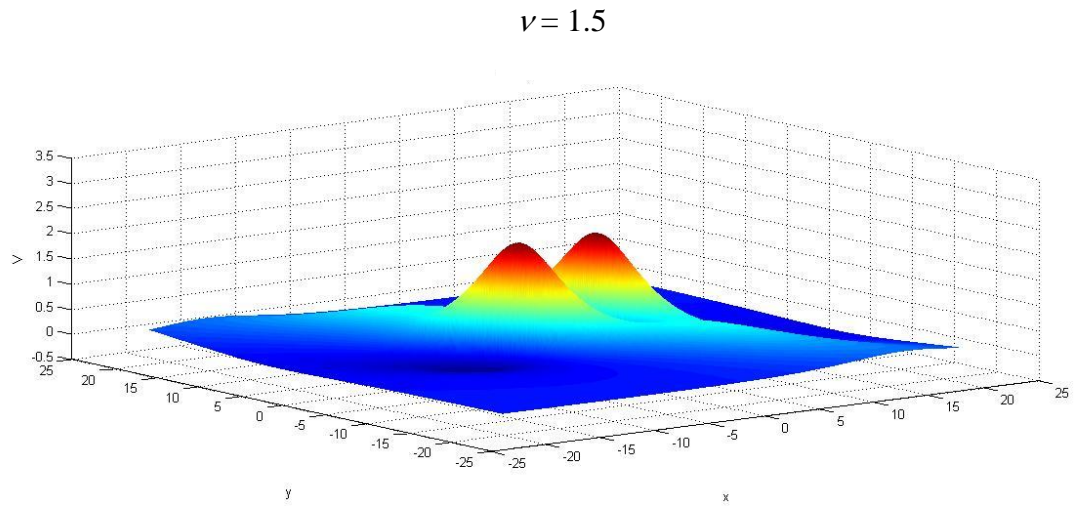


Figure 4.6g: Skew lumps as per Equation (4.18) with $a = 10$, $b = 0$ and $\nu = 1.5$.

$$\nu = 1.9$$

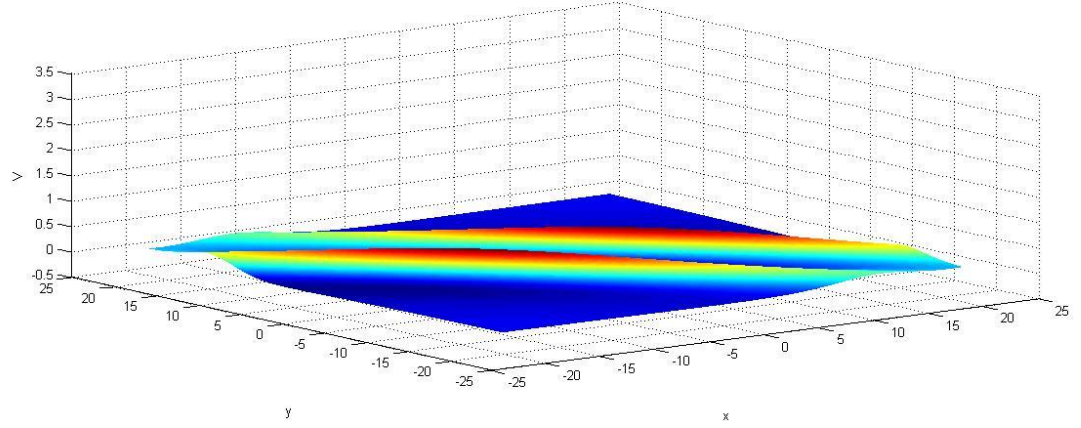


Figure 4.6h: Skew lumps as per Equation (4.18) with $a = 10$, $b = 0$ and $\nu = 1.9$.

As it has been shown in (Pelinovsky & Stepanyants, 1993), the binding energy of lumps in the multi-lump solutions is zero, therefore such stationary solutions are unstable with respect to small perturbations, whereas the stability of single lumps has been proven in (Kuznetsov & Turitsyn, 1982). One can expect that interacting with other perturbations, multi-lumps decay into stable single lumps moving at different angles to each other. Such process of decay and scattering has not been studied yet (this work is currently under way, and results obtained will be published elsewhere).

4.4. Integral Characteristics of Skew Lumps

This section calculates the integral quantities for skew lumps (the components of the momentum and energy), as it can be used in the development of asymptotic theory of interactions of skew lumps and multi-lumps (see, e.g., (Gorshkov, *et al*, 1993) (Gorshkov & Ostrovsky, 1981).

Using representation of lump solution (4.11b), it is easy to check that the total “mass” of the lump $M = \iint_{\infty} u(x, y, t) dx dy$ is zero independently of ν . The components of the lump momentum in the dimensional variables can be defined as follows (Gorshkov, *et al*, 1993) (Gorshkov & Ostrovsky, 1981):

$$P_x = \frac{1}{2} \iint_{\infty} u^2(x, y, t) dx dy = \frac{24\pi\beta c}{\alpha^2} \sqrt{2\left(1 - \frac{V_x}{c}\right) - \left(\frac{V_y}{c}\right)^2} \quad (4.19a)$$

$$P_y = 2\sqrt{2}P_x \frac{V_y}{c} = \frac{48\sqrt{2}\pi\beta c}{\alpha^2} \frac{V_y}{c} \sqrt{2\left(1 - \frac{V_x}{c}\right) - \left(\frac{V_y}{c}\right)^2} \quad (4.19b)$$

The integrals in Equations (4.19a) and (4.19b) can be easily evaluated using again the representation (4.11b). The maximal values of the momentum components are:

$$(P_x)_{\max} = \frac{24\pi\beta c}{\alpha^2} \sqrt{2\left(1 - \frac{V_x}{c}\right)} \text{ at } V_y = 0, \quad (4.20a)$$

$$|P_y|_{\max} = \frac{48\sqrt{2}\pi\beta c}{\alpha^2} \left(1 - \frac{V_x}{c}\right) \text{ at } \left|\frac{V_y}{c}\right|_{\max} = \sqrt{1 - \frac{V_x}{c}} \quad (4.20b)$$

In the dimensionless variables the components of lump momentum read $\tilde{P}_x = 6\pi\sqrt{4 - \nu^2}$ and $\tilde{P}_y = 12\pi\nu\sqrt{4 - \nu^2}$; their maximal values are: $(\tilde{P}_x)_{\max} = 12\pi$ at $\nu = 0$ and $|\tilde{P}_y|_{\max} = 24\pi$ at $\nu = \pm\sqrt{2}$.

One more important lump characteristic which is of the physical interest is its energy (the Hamiltonian):

$$\begin{aligned} H &= \frac{1}{2} \iint_{\infty} \left[\beta \left(\frac{\partial u}{\partial x}\right)^2 + \frac{c}{2} \left(\int \frac{\partial u}{\partial y} dx\right)^2 + \frac{\alpha}{3} u^3 \right] dx dy = \\ &= \frac{2\sqrt{2}\beta c^2}{\alpha^2} \left(1 - \frac{V_x}{c}\right)^{\frac{3}{2}} \frac{1}{2} \iint_{\infty} \left[\left(\frac{\partial v}{\partial X}\right)^2 + \left(\int \frac{\partial v}{\partial Y} dX\right)^2 - \frac{2}{3} v^3 \right] dX dY = \\ &= \frac{144\pi\beta c^2}{\alpha^2} \left(1 - \frac{V_x}{c}\right)^{\frac{3}{2}} \sqrt{\frac{2}{3}(4 - \nu^2)} = \frac{288\pi\beta c^2}{\alpha^2 \sqrt{3}} \left(1 - \frac{V_x}{c}\right) \sqrt{2\left(1 - \frac{V_x}{c}\right) - \left(\frac{V_y}{c}\right)^2} \end{aligned} \quad (4.21)$$

The maximum value of the energy at a given value of V_x is

$$H_{\max} = 96\sqrt{6}\pi \frac{\beta c^2}{\alpha^2} (1 - V_x/c)^{\frac{3}{2}}.$$

The quantities derived in the Section will be useful in the subsequent study of lump interactions with each other and with external fields and potentials.

4.5. Conclusion

The KP equation was derived for quasi-plane waves propagating in isotropic media, e.g., for surface waves in a shallow water or for waves in the Bose–Einstein condensate (Mironov, *et al*, 2010). However, the equation is not symmetrical with respect to the variables x and y . The apparent anisotropy of the equation is associated with the choice of primary direction of wave propagation (oriented, for example, along the axis x) and weak diffraction of the wave field in the perpendicular direction (along the axis y). This explains anisotropic properties of the conventional lump solution Equation (4.6) which is not axisymmetric. But in fact such non-axisymmetric lumps can propagate in any direction in the x,y -plane, being symmetrical in the x,y -plane. Solution anisotropy in the x,y -plane is the intrinsic property, which is not caused, however, by the anisotropy of a medium.

This chapter derives more general solutions describing skew KP1 lumps. Similar single-lump solutions have been obtained in (Lu, *et al*, 2004) (Ma W. -X., 2015) and their interactions have been studied in (Lu, *et al*, 2004). It has been shown that a variety of skew multi-lump solutions can exist in the KP1 equation; examples of simplest of them have been presented. The properties of single skew lumps have been analysed in details. The lumps can move at certain angles to the chosen coordinate axes and certain angles to their own axes of symmetry. In an isotropic medium the skew lumps, apparently, can co-exist with the symmetrical lumps forming a wide class of three-dimensional patterns playing important role in the dynamics of initial perturbation.

Integral characteristics of single lumps (mass, momentum components and energy) have been calculated and presented in terms of lump velocity components. The

detailed pair- or multiple collisions of such lumps is an interesting problem for further analytical and numerical study. Unidirectional interactions of single lumps when they initially aligned and moved along the same x -direction were studied analytically in (Gorshkov, *et al*, 1993) (Ablowitz & Villarroel, 1997), whereas their oblique interactions were studied numerically in (Lu, *et al*, 2004).

This research also obtained a family of skew bi-lump solutions which depend on two free parameters. The structure of two particular, but typical family representatives have been studied in details and illustrated graphically. Even more complicated skew lump solutions can be constructed in the spirit of paper (Pelinovsky & Stepanyants, 1993). It is believed that all these elementary solutions can play important role in the theory of strong wave turbulence when the chaotic wave field can be represented by a big ensemble of interacting lumps.

Chapter 5 Research Outcome and Further Work

5.1. Research Outcome

The objective of this research was to study and investigate the structure and dynamics of solitary waves in fluid media. Various analytical and numerical methods were used to obtain interesting results describing solitary waves under different conditions. The model PDE Gardner–Kawahara equation derived in the Thesis was considered and studied for the first time and provides a contribution to the existing literature. The PDE can be solved by means of well-developed solvers realized in software such as FORTRAN and MATLAB. The numerical results were obtained in the Thesis using the numerical codes for the solution of stationary wave equations designed in FORTRAN, MATLAB and MATHCAD software.

Chapter 2 presents the case of internal waves in two-layer fluid and the range of parameters where they exist. Weakly nonlinear long internal waves in the oceans can be described, in general, by the Korteweg–de Vries equation. It was discovered that at certain circumstances the quadratic nonlinear coefficient can turn to zero. At such critical situations the next (cubic) nonlinear term should be taken into account. In the near-critical situation another model equation – the Gardner–Ostrovsky, alias extended KdV equation, replaces the classical KdV equation. However, in some situations the cubic dispersion coefficient also can vanish both in the KdV and GO equations when the surface tension between the layers is taken into consideration. In such cases the fifth-order dispersion should be taken into consideration. The structure of solitary waves within the framework of GO equation has been studied in the Thesis.

Chapter 3 revisits the problem of modulation stability of quasi-monochromatic wave-trains propagating in a media with the double dispersion occurring both at small and large wave-numbers. Shrira (1981) derived the shallow-water equation which describes both surface and internal long waves in a rotating fluid. The nonlinear Schrödinger equation derived from the unidirectional Gardner–Ostrovsky equation agrees well with the NLS equation derived from the more general Shrira’s equation within the range of validity of the Gardner–Ostrovsky equation. All possible signs of

nonlinear and dispersive coefficient were considered; the Lighthill criterion has been used to classify the zones of modulational stability and instability for all possible signs of nonlinear and dispersive coefficient.

Chapter 4 presents the exact analytical solutions describing skew lumps in the Kadomtsev–Petviashvili (KP1) equation. Stationary single lumps and multi-lumps were constructed analytically and illustrated graphically. Examples of skew bi-lumps were analysed in details. The integral characteristics (momenta components and energy) of skew lumps were calculated.

5.2. Future Work

In this research new stationary solutions for solitary waves were obtained. Conditions of existence and structures of solitary waves have been investigated. However, many aspects of solitary wave dynamics were not studied yet. In particular, it is planned to study within the framework of model equations derived in the Thesis the stability of solitary waves, their interactions with each other and with arbitrary wave perturbation; their evolution from various initial conditions. This pertains to solitary waves of Gardner–Kawahara equation and Kadomtsev–Petviashvili equation. In particular, the dynamics of KP lumps in dissipative media will be studied soon. The interaction of lumps with stationary multi-lumps derived in the Thesis will be also a subject of interesting study.

Another important direction of a future research is a modulation stability of quasi-monochromatic waves in a rotating fluid. It is expected that the results obtained in the Thesis will be validated by direct numerical simulations within the framework of primitive hydrodynamic equation. In the meantime, the one-dimensional theory developed in the Thesis will be generalized for the two-dimensional case. It can be expected that in some domain of parameters both the self-modulation and self-focusing can occur simultaneously. In such case the collapse of water waves may occur, and extremely large waves may be generated. Nowadays this is a very topical problem in the physical oceanography.

In all cases mentioned above the applicability of formal solutions obtained in the Thesis to the real physical situations will be investigated.

Appendix A The Numerical Code for the Construction of Stationary Solutions of the Gardner–Ostrovsky Equation by the Petviashvili Method

C The Gardner–Ostrovsky equation

$$C \quad (u_t + auu_x + a_1u^2u_x - bu_{xxx} + b_1u_{5x})_x = du$$

C In the stationary form the equation reads:

$$C \quad (b_1u'''' - bu'' - Vu + au^2/2 + a_1u^3/3)'' - du = 0$$

C*****

real lright,lleft,mq,mq1,kx

dimension zz(2048), u(2048), uim(2048), usq(2048),

*usqim(2048), ucub(2048), ucubi(2048), fut(2048), futim(2048)

vph(kx) = b1*kx**4 + b*kx**2 + d/kx**2

open(1,file = 'out.dat')

open(2,file = 'mn.dat')

open(3,file = 'in.dat')

open(4,file = 'GOEqPar.dat')

C*****

C PARAMETERS

read(4,*) a, a1, b, b1, d, V, lright, eps, Nmax

6 format(' a a1 b b1 d V lright eps Nmax'/8F11.4, I4)

pi = 3.14159265359

n = 2048

n2 = n/2

lleft = -lright

dx = (lright - lleft)/(n-1)

dkx = 2.*pi/(lright-lleft)

am = 1.

del = 2.

C am, del - THE PARAMETERS OF THE START FUNCTION

print 7, a,a1,b,b1,d,V,eps,lright,n,Nmax

7 format(' a a1 b b1 d V

* eps lright',/8F11.6/,/ N Nmax',

* /3x,I4,4x,I4)

C*****

C INITIALIZATION OF THE START PROCEDURE (ITARATION No 0)

Iter = 0

C*****

C PREPARATION OF THE WORKING ARRAYS AND START FUNCTION u(x)

kx = 0.

amu = 10**(-10)

zz(1) = V - Vph(kx+0.000001)

zz(n2+1) = V - Vph(dkx*n2)

```

do 11 js = 2,n2

kx = kx+dkx

zz(js) = V - Vph(kx)

zz(n+2-js) = V - Vph(-kx)

11  continue

print 8

8  format(/1x,'NWAY = ?'/

*  ' (1 - for analytically given start function;'/

*  ' 2 - for numerically given start function)  ')

read(*,*) nway

if(nway.eq.2) go to 2

C*****
C ANALYTICALY GIVEN START FUNCTION

1  x = lleft

do 10 is = 1,n

fun = am*exp(-x*x/(del*del))

u(is) = fun

usq(is) = fun*fun

ucub(is) = fun**3

uim(is) = 0.

usqim(is) = 0.

```

ucubi(is) = 0.

C write(4,15) x,u(is)

x = x + dx

10 continue

go to 9

C NUMERICALLY GIVEN FUNCTION

2 do 18 is = 1,n

read(3,*) x,u(is)

usq(is) = u(is)*u(is)

ucub(is) = u(is)**3

uim(is) = 0.

usqim(is) = 0.

ucubi(is) = 0.

18 continue

C*****

C CALCULATION OF THE COEFFICIENT mq

9 call fft(u,uim,n,n,n,1)

do 16 is = 1,n

uim(is) = uim(is)/n

16 u(is) = u(is)/n

12 call fft(usq,usqim,n,n,n,1)

```

do 4 is = 1,n

usq(is) = usq(is)/n

4  usqim(is) = usqim(is)/n

call fft(ucub,ucubi,n,n,n,1)

do 40 is = 1,n

ucub(is) = ucub(is)/n

40  ucubi(is) = ucubi(is)/n

chis = 0.

znam = 0.

do 3 is = 1,n

zt = zz(is)

fun = u(is)

chis = chis + zt*fun*fun

fut(is) = (0.5*a*usq(is) + a1*ucub(is)/3.)/zt

futim(is) = 0.

znam = znam + (0.5*a*usq(is) + a1*ucub(is)/3.)*fun

3  continue

mq = chis/znam

mq1 = abs(1. - mq)

write(2,*) iter,mq,mq1

```

C*****

C PREPARATION OF THE NEXT ITERATION

iter = iter + 1

do 17 is = 1,n

f = fut(is)*sqrt(sqrt(abs(mq)**7))

fut(is) = f

u(is) = f

17 uim(is) = 0.

C RECONSTRUCTION OF THE FUNCTION $u(x)$

call fft(fut,futim,n,n,n,-1)

if (iter.gt.Nmax) go to 15

if (abs(mq-1.).gt.eps) then

do 13 is = 1,n

usq(is) = fut(is)**2

ucub(is) = fut(is)**3

ucubi(is) = 0.

13 usqim(is) = 0.

go to 12

else

do 14 ip = 1,n

x = lleft + (ip - 1)*dx

C write(1,*) x,fut(ip)

```

        write(1,23) x,fut(ip)
14  continue

        endif

        go to 5

15  write(*,*) ' THE NUMBER OF ITERATIONS EXCEEDS Nmax'

        do 19 ip = 1,n

        x = lleft + (ip - 1)*dx

C    write(1,*) x,fut(ip)

        write(1,23) x,fut(ip)

19  continue

23  format(1X,E12.6,3X,E12.6)

5   stop

        end

```

Appendix B Derivation of Nonlinear Schrödinger Equation

The nonlinear Schrödinger equation describing the evolution of wave-trains with the central wavenumber k of a carrier wave can be derived from Equation (3.12) following the standard approach (see, e.g., (Ablowitz & Haut, 2009)), therefore details are reproduced here only briefly. Introduce the fast phase variable $\theta = \omega \tau - k \xi$, the slow spatial $X = \varepsilon \xi$ and temporal $T = \varepsilon \tau$ variables, as well as the ‘super-slow’ temporal variable $t = \varepsilon T = \varepsilon^2 \tau$, where $\varepsilon \ll 1$ is a small parameter, and present a solution of Equation (3.12) in the form of the series on small parameter ε :

$$w(\theta, X, T, t) = \varepsilon w_1(\theta, X, T, t) + \varepsilon^2 w_2(\theta, X, T, t) + \varepsilon^3 w_3(\theta, X, T, t) + \dots \quad (\text{B1})$$

Substitution of this series into Equation (3.12) gives

$$\begin{aligned} & \varepsilon \left[\left(\omega^2 - C^2 k^2 \right) \frac{\partial^2 w_1}{\partial \theta^2} - B k^2 \omega^2 \frac{\partial^4 w_1}{\partial \theta^4} + \Gamma w_1 \right] + \varepsilon^2 \left[\left(\omega^2 - C^2 k^2 \right) \frac{\partial^2 w_2}{\partial \theta^2} - B k^2 \omega^2 \frac{\partial^4 w_2}{\partial \theta^4} + \right. \\ & \left. \Gamma w_2 + 3\alpha \omega^2 k \frac{\partial w_1}{\partial \theta} \frac{\partial^2 w_1}{\partial \theta^2} - 2\omega \frac{\partial^2 w_1}{\partial \theta \partial T} - 2C^2 k \frac{\partial^2 w_1}{\partial \theta \partial X} + 2B\omega k \frac{\partial^3}{\partial \theta^3} \left(\omega \frac{\partial w_1}{\partial X} - k \frac{\partial w_1}{\partial T} \right) \right] + \\ & \varepsilon^3 \left\{ \left[\left(\omega^2 - C^2 k^2 \right) \frac{\partial^2 w_3}{\partial \theta^2} - B k^2 \omega^2 \frac{\partial^4 w_3}{\partial \theta^4} + \Gamma w_3 \right] + \frac{\partial^2 w_1}{\partial T^2} - C^2 \frac{\partial^2 w_1}{\partial X^2} + 2C^2 k \frac{\partial^2 w_2}{\partial \theta \partial X} + \right. \\ & B \frac{\partial^2}{\partial \theta^2} \left[2\omega k \frac{\partial}{\partial \theta} \left(\omega \frac{\partial w_2}{\partial X} - k \frac{\partial w_2}{\partial T} \right) + 4\omega k \frac{\partial^2 w_1}{\partial T \partial X} - \omega^2 \frac{\partial^2 w_1}{\partial X^2} - k^2 \frac{\partial^2 w_1}{\partial T^2} - 2\omega k^2 \frac{\partial^2 w_1}{\partial \theta \partial t} \right] + \\ & \omega A \left[3\omega k \left(\frac{\partial w_1}{\partial \theta} \frac{\partial^2 w_2}{\partial \theta^2} + \frac{\partial w_2}{\partial \theta} \frac{\partial^2 w_1}{\partial \theta^2} \right) + 2k \left(\frac{\partial w_1}{\partial T} \frac{\partial^2 w_1}{\partial \theta^2} + 2 \frac{\partial w_1}{\partial \theta} \frac{\partial^2 w_1}{\partial \theta \partial T} \right) - \right. \\ & \left. \omega \left(\frac{\partial w_1}{\partial X} \frac{\partial^2 w_1}{\partial \theta^2} + 2 \frac{\partial w_1}{\partial \theta} \frac{\partial^2 w_1}{\partial \theta \partial X} \right) \right] + 2\omega \frac{\partial}{\partial \theta} \left(\frac{\partial w_2}{\partial T} + \frac{\partial w_1}{\partial t} \right) + 6\Phi \omega^2 k^2 \frac{\partial w_1}{\partial \theta} \frac{\partial^2 w_1}{\partial \theta^2} \left. \right\} + o(\varepsilon^3) = 0 \end{aligned} \quad (\text{B2})$$

Considering a solution to Equation (B2) in the form of quasi-monochromatic wave:

$$w_1(\theta, X, T, t) = W_1(X, T, t) e^{i\theta} + W_1^*(X, T, t) e^{-i\theta} \quad (\text{B3})$$

$$w_2(\theta, X, T, t) = W_2(X, T, t) e^{2i\theta} + W_2^*(X, T, t) e^{-2i\theta} + W_0(X, T, t) + W_0^*(X, T, t) \quad (\text{B4})$$

where star stands for complex conjugate.

Substitute now solutions (B3) and (B4) into Equation (B2) and collect the terms proportional to $e^{i\theta}$. In the leading order with respect to ε , the dispersion relation Equation (3.14) is obtained. Collecting then the terms proportional to ε^2 , it gets to

$$2i \left[-\omega(Bk^2 + 1) \frac{\partial W_1}{\partial T} + k(B\omega^2 - C^2) \frac{\partial W_1}{\partial X} \right] e^{i\theta} + \left[(4C^2k^2 - 4\omega^2 - 16B\omega^2k^2 + \Gamma)W_2 + 3iA\omega^2k|W_1|^2 \right] e^{2i\theta} + \Gamma W_0 + \text{c.c.}, \quad (\text{B5})$$

where c.c. stands for complex conjugate terms.

Equating to zero the coefficient of $e^{i\theta}$, it acquires the simple wave equation:

$$\frac{\partial W_1}{\partial T} + V_g \frac{\partial W_1}{\partial X} = 0 \quad (\text{B6})$$

where V_g is the group speed as per Equation (3.16).

Equating then to zero the coefficient of $e^{2i\theta}$, it gives a relationship between the amplitudes of the first and second harmonics:

$$W_2 = \frac{3iA\omega^2k|W_1|^2}{16B\omega^2k^2 - \Gamma + 4\omega^2 - 4C^2k^2} \quad (\text{B7})$$

In the same approximation, the term W_0 , which is independent of exponent (the mean flow term) vanishes, $W_0 = 0$; this is a specific feature of wave systems with the large-scale dispersion (Shrira, 1981; Obregon & Stepanyants, 1998; Grimshaw & Helfrich, 2008; 2012; Whitfield & Johnson 2015a; 2015b).

In the next order on the parameter ε the coefficient of $e^{i\theta}$ gives:

$$2i\omega(1+Bk^2) \frac{\partial W_1}{\partial t} + (C^2 + BV_g\omega k + B\omega^2) \frac{\partial^2 W_1}{\partial X^2} + 6k\omega^2 (iAW_2 + \Phi k|W_1|^2) W_1 = 0 \quad (\text{B8})$$

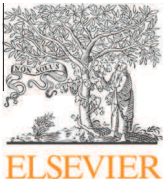
Substituting here W_2 from Equation (B7), it obtains the NLSE in the form:

$$i \frac{\partial W_1}{\partial t} + p(k) \frac{\partial^2 W_1}{\partial X^2} + Q(k) |W_1|^2 W_1 = 0, \quad (\text{B9})$$

where $p(k) = \frac{C^2 + BV_g \omega k + B\omega^2}{2\omega(1+Bk^2)}$ and

$$Q(k) = -3k^2 \omega \frac{3A^2 \omega^2 - \Phi [4k^2 (4B\omega^2 - C^2) + 4\omega^2 - \Gamma]}{(1+Bk^2)(16B\omega^2 k^2 - \Gamma + 4\omega^2 - 4C^2 k^2)}.$$

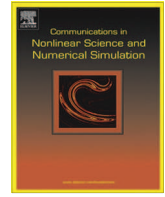
Coming back to the original variables τ and ξ and using the relationship between the variables w and $\zeta = \partial w / \partial \xi$, which in the first approximation for quasi-monochromatic wave reads $\zeta = ikw$, which finally obtains Equation (3.18) with the coefficients $p(k)$ as per Equation (3.19a) and $q(k) = Q(k)/k^2$ as per Equation (3.21a).



Contents lists available at [ScienceDirect](http://www.sciencedirect.com)

Commun Nonlinear Sci Numer Simulat

journal homepage: www.elsevier.com/locate/cnsns



Structure of internal solitary waves in two-layer fluid at near-critical situation



O. Kurkina^a, N. Singh^b, Y. Stepanyants^{a,b,*}

^aNizhny Novgorod State Technical University n.a. R.E. Alexeev, 24 Minin St., Nizhny Novgorod 603950, Russia
^bUniversity of Southern Queensland, West St., Toowoomba, QLD 4350, Australia

ARTICLE INFO

Article history:
 Received 28 June 2014
 Received in revised form 19 September 2014
 Accepted 19 September 2014
 Available online 2 October 2014

Keywords:
 Two-layer fluid
 Internal wave
 Nonlinear evolution equation
 Solitary wave
 Stationary multi-soliton

ABSTRACT

A new model equation describing weakly nonlinear long internal waves at the interface between two thin layers of different density is derived for the specific relationships between the densities, layer thicknesses and surface tension between the layers. The equation derived and dubbed here the Gardner–Kawahara equation represents a natural generalisation of the well-known Korteweg–de Vries (KdV) equation containing the cubic nonlinear term as well as fifth-order dispersion term. Solitary wave solutions are investigated numerically and categorised in terms of two dimensionless parameters, the wave speed and fifth-order dispersion. The equation derived may be applicable to wave description in other media.

© 2014 Elsevier B.V. All rights reserved.

1. Introduction

The governing equation describing long internal waves of small amplitude at the interface in a two-layer fluid is, in general, the well-known Korteweg–de Vries (KdV) equation (see, e.g., [1,3] and references therein):

$$\frac{\partial u}{\partial t} + c \frac{\partial u}{\partial x} + \alpha u \frac{\partial u}{\partial x} + \beta \frac{\partial^3 u}{\partial x^3} = 0. \quad (1.1)$$

Here the coefficients are:

$$c^2 = \frac{g(\rho_2 - \rho_1)h_1 h_2}{\rho_1 h_2 + \rho_2 h_1}, \quad \alpha = \frac{3c}{2h_1 h_2} \frac{\rho_2 h_1^2 - \rho_1 h_2^2}{\rho_1 h_2 + \rho_2 h_1}, \quad \beta = \frac{h_1 h_2}{6} c \frac{\rho_1 h_1 + \rho_2 h_2 - 3\sigma/c^2}{\rho_1 h_2 + \rho_2 h_1}, \quad (1.2)$$

where index 1 pertains to the upper layer, index 2 – to the lower layer (see Fig. 1), $\rho_{1,2}$ are densities of the layers, $h_{1,2}$ are thicknesses of the layers, and σ is the surface tension between the layers. For the sake of simplicity we assume here that the ‘rigid lid’ approximation is used to filter the surface mode [5].

However, at certain conditions equation (1.1) degenerates because some of its coefficients vanish. In particular, the generalisation is required when the density interface is located near the half-depth of the fluid. In this case the coefficient of quadratic nonlinearity α becomes anomalously small, and one should take into consideration the next order nonlinear term,

* Corresponding author.
 E-mail address: Yury.Stepanyants@usq.edu.au (Y. Stepanyants).

the cubic term, to balance the dispersion effect [3]. The corresponding equation is known as the Gardner equation (alias the extended KdV or combKdV equation):

$$\frac{\partial u}{\partial t} + c \frac{\partial u}{\partial x} + \alpha u \frac{\partial u}{\partial x} - \alpha_1 u^2 \frac{\partial u}{\partial x} + \beta \frac{\partial^3 u}{\partial x^3} = 0, \tag{1.3}$$

where the cubic nonlinear coefficient is:

$$\alpha_1 = \frac{21}{8c} \left[\frac{8}{7} \left(\frac{c}{h_1 h_2} \right)^2 \frac{\rho_2 h_1^3 + \rho_1 h_2^3}{\rho_1 h_2 + \rho_2 h_1} - \left(\frac{2\alpha}{3} \right)^2 \right]. \tag{1.4}$$

The KdV and Gardner equations are completely integrable [1]; they possess, in particular, soliton solutions [3] which attract a special interest due to their specific particle-like properties, e.g., they restore their shapes after the interaction with each other and asymptotically evolve from arbitrary pulse-type perturbations. In a two layer fluid the structure of Gardner solitons is very well studied, it varies from the bell-shaped KdV solitons for small amplitude waves to table-top solitons for large-amplitude waves [3].

There are also situations when the dispersion coefficient β vanishes. Such cases are known, for example for gravity-capillary waves with strong surface tension and magnetosonic waves in plasma [15]. In the near critical situation when the dispersive coefficient β becomes anomalously small, the next-order dispersion should be taken into consideration. This leads to the fifth-order KdV equation with the quadratic nonlinearity:

$$\frac{\partial u}{\partial t} + c \frac{\partial u}{\partial x} + \alpha u \frac{\partial u}{\partial x} + \beta \frac{\partial^3 u}{\partial x^3} + \beta_1 \frac{\partial^5 u}{\partial x^5} = 0. \tag{1.5}$$

This equation was derived for the first time by Kakutani and Ono (1969) [14] for magnetosonic waves in plasma and then it was derived for many other types of waves, including gravity-capillary waves on the surface of thin liquid films [21], electromagnetic waves in nonlinear electric transmission lines [10,17], etc. Recently the similar equation was derived for internal waves in two-layer fluid [7] and it was obtained the expression for the coefficient β_1 :

$$\frac{\beta_1}{H^4} = \frac{b[4a(1+b^4) + 19b(1+a^2b^2) + 30ab^2]}{360(a+b)^2(1+b)^4} - \frac{sb^2(1+a)}{32(1+b)^3(a+b)^2} \left[\frac{4}{3}(1+ab) + s(1+a)(1+b) \right], \tag{1.6}$$

where $a = \rho_1/\rho_2$, $b = h_1/h_2$, $H = h_1 + h_2$, and $s = 2\sigma[(\rho_1 + \rho_2)Hc^2]^{-1}$.

Equation (1.5) is currently known as the Kawahara equation, although it was derived by other authors cited above. However, Kawahara [16] investigated its solitary solutions and obtained numerically a family of solitons with non-monotonic, but oscillatory tails.

In the meantime, as has been recently shown [7] in the case of internal waves in two-layer fluid with strong surface tension at the interface the double-critical situation is also possible when both the coefficients of quadratic nonlinearity α and third-order dispersion β become so small that the next order corrections with the coefficients α_1 and β_1 should be taken into consideration. As one can see from Eq. (1.2), in the double critical situation both coefficients α and β vanish when $\rho_1 = \rho_2(h_1/h_2)^2$ and $\sigma = c^2\rho_2h_2[1 + (h_1/h_2)^3]/3$. In this case the coefficients α_1 and β_1 take simple forms:

$$\alpha_1 = \frac{3c}{h_1 h_2}, \quad \beta_1 = cH^4 \frac{1+b^5}{90(1+b)^5}. \tag{1.7}$$

The coefficient β_1 is always positive and has the minimum value at $b = 1$ (i.e. when the thicknesses of the upper and lower layers are equal); its plot is shown in Fig. 2.

In the vicinity of the double critical situation the governing equation reads:

$$\frac{\partial u}{\partial t} + c \frac{\partial u}{\partial x} + \alpha u \frac{\partial u}{\partial x} - \alpha_1 u^2 \frac{\partial u}{\partial x} + \beta \frac{\partial^3 u}{\partial x^3} + \beta_1 \frac{\partial^5 u}{\partial x^5} = 0. \tag{1.8}$$

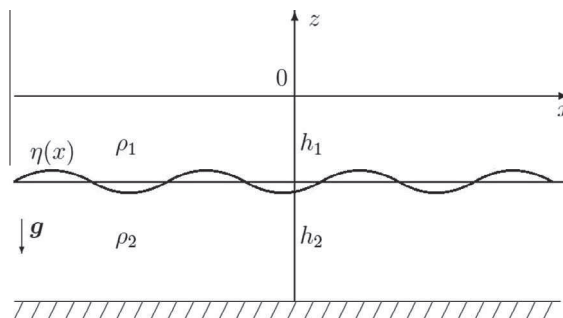


Fig. 1. Sketch of internal waves at the interface between two fluid layers.

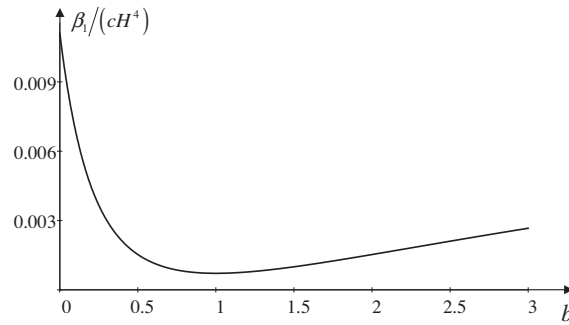


Fig. 2. The dependence of the normalised dispersion coefficient $\beta_1/(cH^4)$ on the ratio of layer thicknesses $b = h_1/h_2$ at the double critical situation.

We will call this equation the Gardner–Kawahara (GK) equation. In this paper we consider stationary solutions of Eq. (1.8) in the form of solitary waves. A family of soliton solutions are constructed numerically by means of the Petviashvili method [20,19] and Yang–Lakoba AITEM (A.N.) method [22]. The properties of such solutions are investigated and discussed.

2. Dispersion relation and stationary solutions to the Gardner–Kawahara equation

First of all, let us present Eq. (1.8) in the dimensionless form using change of variables:

$$\tau = \frac{\alpha^3 t}{\alpha_1 \sqrt{\alpha_1 \beta}}, \quad \xi = \frac{\alpha(x - ct)}{\sqrt{\alpha_1 \beta}}, \quad v = \frac{\alpha_1}{\alpha} u. \tag{2.1}$$

After that the main equation reads:

$$\frac{\partial v}{\partial \tau} + v \frac{\partial v}{\partial \xi} - v^2 \frac{\partial v}{\partial \xi} + \frac{\partial^3 v}{\partial \xi^3} + B \frac{\partial^5 v}{\partial \xi^5} = 0, \tag{2.2}$$

where $B = (\beta_1/\alpha_1)(\alpha/\beta)^2$.

For waves of infinitesimal amplitude, $v \rightarrow 0$, looking for a solution in the form $v \sim e^{i(\tilde{\omega}\tau - \kappa\xi)}$ we obtain the dispersion relation

$$\tilde{\omega} = -\kappa^3 + B\kappa^5. \tag{2.3}$$

Then, it follows that the phase speed of small-amplitude waves is

$$V_{ph}(\kappa) \equiv \frac{\tilde{\omega}}{\kappa} = -\kappa^2 + B\kappa^4. \tag{2.4}$$

The plot of phase speed is shown in Fig. 3 for three values of the parameter B .

In the case $B \leq 0$ the phase speed is a monotonic function of κ , whereas at $B > 0$ it has a minimum, $V_{min} = -1/(4B)$ at the point $\kappa_c = (2B)^{-1/2}$ (see Fig. 3). The concept of phase speed is very important in understanding the process of interaction of a

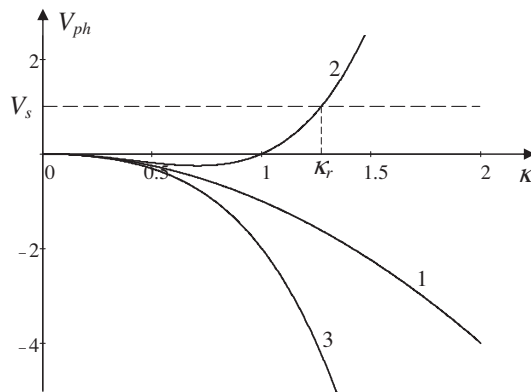


Fig. 3. Plots of phase speed (2.4) for $B = 0$ (line 1, KdV dispersion), $B = 1$ (line 2), and $B = -1$ (line 3). Dashed horizontal line shows the object moving with a constant speed V_s and generating small amplitude wave at the resonant wavenumber κ_r .

moving source with waves. In particular, if the speed of a source is such that there is no resonance with any wave, i.e. there is no intersection of the dashed line in Fig. 3 with the dispersion curve (e.g., with lines 1 or 3), then the source does not loose energy for wave excitation. Otherwise, in the case of the resonance (see the intersection of dashed line with line 2), the source experiences energy losses for wave generation and, as a result, it experiences wave resistance. Without external compensation of energy losses such source cannot move stationary.

Consider now stationary solutions to the wave equation (2.2) depending on one variable only $\zeta = \xi - V\tau$. In this case Eq. (2.2) reduces to the ODE:

$$\frac{d}{d\zeta} \left[-Vv + \frac{v^2}{2} - \frac{v^3}{3} + \frac{d^2v}{d\zeta^2} + B \frac{d^4v}{d\zeta^4} \right] = 0. \tag{2.5}$$

We will focus further on the solitary solutions only; therefore assuming zero asymptotics at the infinity we can integrate Eq. (2.5) once with the zero integration constant:

$$B \frac{d^4v}{d\zeta^4} + \frac{d^2v}{d\zeta^2} - Vv + \frac{v^2}{2} - \frac{v^3}{3} = 0. \tag{2.6}$$

It follows from this equation that the shape of a solitary wave is determined by two parameters, B and V . Considering asymptotic solution of Eq. (2.6) when $\zeta \rightarrow \infty$ and $v \rightarrow 0$, we can linearise this equation (simply omit the nonlinear terms) and seek for its solution in the form $v \sim e^{\mu\zeta}$. Substituting this trial solution into linearised Eq. (2.6), we obtain the equation determining the exponent μ :

$$B\mu^4 + \mu^2 - V = 0. \tag{2.7}$$

The roots to this bi-quadratic equation are:

$$\mu_{1,2} = \pm \sqrt{\frac{-1 + \sqrt{1 + 4BV}}{2B}}; \quad \mu_{3,4} = \pm \sqrt{\frac{-1 - \sqrt{1 + 4BV}}{2B}}. \tag{2.8}$$

Let us analyse the roots in detail. Assume first that B is negative, then for $V < 0$ we have $\sqrt{1 + 4BV} > 1$; therefore the roots $\mu_{1,2}$ are purely imaginary, and the roots $\mu_{3,4}$ are real. Solutions corresponding to purely imaginary roots are not decaying and cannot represent solitary waves with the zero asymptotics. If $V = 0$, then $\mu_{1,2} = 0$ and again we have a solution with non-decaying asymptotics. If $0 < V < -1/(4B)$, then we have $\sqrt{1 + 4BV} > 0$, and all four roots $\mu_{1,2,3,4}$ are real. In this case the soliton solutions are possible with the exponential asymptotics $v \sim \exp(-|\mu_1\zeta|)$. And at last, if $V > -1/(4B)$, then we have $\sqrt{1 + 4BV}$ is complex; all roots are complex-conjugate in pairs $\mu_{1,2} = (p_1 \pm iq_1)$, $\mu_{3,4} = \pm(p_2 \pm iq_2)$. Due to presence of the real parts of the roots $p_{1,2}$, the soliton solutions are also possible with the oscillatory asymptotics. The decay rate of a solitary wave in the far field is determined by the root with the smallest value of $|p_{1,2}|$.

Assume now that B is positive, then it follows from the similar analysis as above that solitary waves with the oscillatory asymptotics are possible only when $V < V_{min} \equiv -1/(4B)$. In the particular case of $B = 0$, Eq. (2.7) has two real roots $\mu_{1,2} = \pm\sqrt{V}$ corresponding to soliton solutions, provided that $V > 0$.

These findings can be summarised with the help of a schematic diagram shown in Fig. 4. It should be noticed that the analysis of roots only predicts possible asymptotics of solitons provided that they exist, but it does not guarantee their existence. In particular, if $B = 0$, then soliton solutions with monotonically decaying exponential asymptotics could exist for any $V > 0$ (see case b) in the diagram), but in fact they exist only for $0 \leq V \leq 1/6$ (see the exact solution (3.1) of the Gardner equation below).

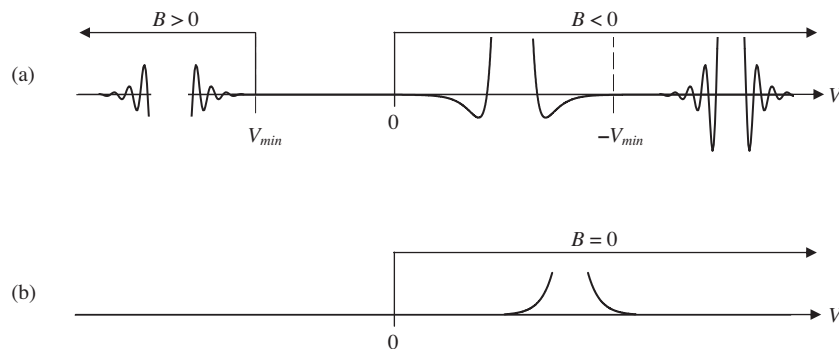


Fig. 4. Schematic structure of solitary wave asymptotics for Eq. (2.6) with different signs of B (frame a). If $B = 0$ only the solitons with monotonic exponential tails are possible as shown in frame b) – see exact solution (3.1).

3. Soliton solutions to the Gardner–Kawahara equation

Consider first the limiting case of $B = 0$ when Eq. (2.6) reduces to the completely integrable Gardner equation. It has a family of soliton solutions which is determined by only one parameter V varying in the interval $0 \leq V \leq 1/6$ (a soliton solution does not exist beyond this interval):

$$v(\zeta) = \frac{\sqrt{6V}}{2} \left[\tanh\left(\frac{\sqrt{V}}{2}\zeta + \phi\right) - \tanh\left(\frac{\sqrt{V}}{2}\zeta - \phi\right) \right]. \tag{3.1}$$

where $\phi(V) = (1/4) \ln[(1 + \sqrt{6V})/(1 - \sqrt{6V})]$, and the amplitude of a soliton $A = 1 - \sqrt{1 - 6V}$.

The family of solitons varies from KdV-type bell-shaped solitons, when $V \rightarrow 0$, to table-top solitons, when $V \rightarrow 1/6$ (see, e.g., [3]); the typical solitons are shown in Fig. 5 for three values of V .

If $B \neq 0$, then exact analytical solutions of Eq. (2.6) are not known. However they can be constructed numerically using, for example, a modified Petviashvili method [20,19] or even more effective Yang–Lakoba method [22]. To this end let us make a Fourier transform of Eq. (2.6) on the variable ζ denoting the Fourier spectrum of function v by $\hat{F}(v)$:

$$(B\kappa^4 - \kappa^2 - V)\hat{F}(v) = \frac{1}{3}\hat{F}(v^3) - \frac{1}{2}\hat{F}(v^2). \tag{3.2}$$

If we multiply Eq. (3.2) by $\hat{F}(v)$ and integrate it then on κ from minus to plus infinity, we obtain the equality:

$$\int_{-\infty}^{+\infty} (B\kappa^4 - \kappa^2 - V)\hat{F}(v)\hat{F}(v)d\kappa = \int_{-\infty}^{+\infty} \left[\frac{1}{3}\hat{F}(v^3) - \frac{1}{2}\hat{F}(v^2) \right] \hat{F}(v)d\kappa. \tag{3.3}$$

If $v(\zeta)$ is an exact solution of Eq. (2.6) and $\hat{F}(v)$ is its Fourier spectrum satisfying Eq. (3.2), then it follows from Eq. (3.3) that the quantity M (the stabilising factor) as defined below should be equal to one:

$$M[v] \equiv \frac{\int_{-\infty}^{+\infty} (B\kappa^4 - \kappa^2 - V)\hat{F}(v)\hat{F}(v)d\kappa}{\int_{-\infty}^{+\infty} \left[\frac{1}{3}\hat{F}(v^3) - \frac{1}{2}\hat{F}(v^2) \right] \hat{F}(v)d\kappa} = 1. \tag{3.4}$$

However, in general, if $v(\zeta)$ is not a solution of Eq. (2.6), then $M[v]$ is a functional of v . In the spirit of the Petviashvili method let us construct the iteration scheme (for details see [20]):

$$\hat{F}(v_{n+1}) = M^r[v_n] \frac{\frac{1}{3}\hat{F}(v_n^3) - \frac{1}{2}\hat{F}(v_n^2)}{V_{ph}(\kappa) - V}, \tag{3.5}$$

where $V_{ph}(\kappa)$ is the phase speed of infinitesimal perturbation as per Eq. (2.4), and the exponent r should be taken in the range $r = [3/2, 2]$ to provide a convergence of the numerical scheme. As has been shown in [19], $r = 3/2$ provides the fastest convergence for pure cubic nonlinearity, whereas $r = 2$ provides the fastest convergence for pure quadratic nonlinearity. In our calculations it was taken $r = 7/4$ which provided the fastest convergence to the stationary solution for the mixed quadratic and cubic nonlinearity. The convergence is controlled by the closeness of parameter M to unity. Starting from the arbitrary pulse function $v_0(z)$ we conducted calculations with the given parameters B and V on the basis of iteration scheme (3.5) until the parameter M attained a unity up to small quantity ε (in our calculations we have chosen $\varepsilon = 10^{-6}$). To avoid a singularity in Eq. (3.5) the speed of a solitary wave should be taken such that at the given value of V_{ph} the fourth-degree polynomial in the denominator of Eq. (2.4) does not have real roots.

As the test case we have considered the Gardner equation (2.6) with $B = 0$. As one can see, there is no singularity in Eq. (3.5) if $V > 0$; this is in agreement with the condition of existence of Gardner solitons (3.1). For relatively small $V \leq 0.1663$ we obtained numerical solutions in a complete agreement with the analytical solution (3.1). But for larger values of V we failed to obtain any solution by means of the modified Petviashvili method as the iteration procedure (3.5) did not converge to

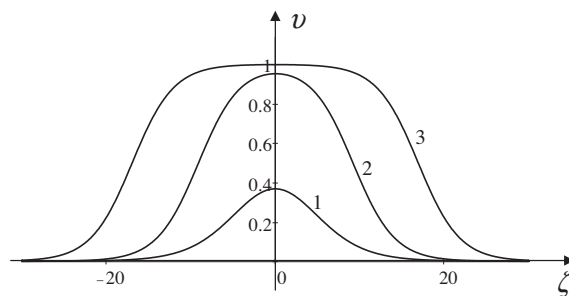


Fig. 5. Solitary wave shapes as per Eq. (3.1) for three values of V . Line 1 pertains to $V = 0.1$ (quasi-KdV case), line 2 pertains to $V = 0.1663$ ('fat soliton'), and line 3 pertains to $V = 0.166666$ (table-top soliton).

something. In the meantime, application of the Yang–Lakoba method [22] enabled us to construct soliton solutions in the complete agreement with the analytical solution (3.1) for any positive value of $V < 1/6$. Thus, we have confirmed that the Yang–Lakoba method is even more efficient and converges faster than the Petviashvili method.

In the case of $B > 0$ the denominator of Eq. (3.5) is positive when $V < V_{min}$. Then, depending on the value of V we have obtained various shapes of solitary waves by the Petviashvili method; they are illustrated by Fig. 6 for $B = 1$. For other positive values of B the soliton structures are qualitatively the same as shown in this figure, but solitons become narrower when $B \rightarrow 0$ and wider when $B \rightarrow \infty$. Their asymptotic behaviour is in agreement with the prediction shown in Fig. 4 for $B > 0$; the oscillatory tails of solitons are clearly seen in this figure.

It is worth noting two features of these solitons. Firstly, at small amplitudes, when $V \rightarrow (V_{min})_-$, solitons reduce to stationary moving wavetrains. Such wavetrains can be described by the higher-order non-linear Schrödinger equation; similar solutions in the form of envelope solitons have been earlier obtained for the Ostrovsky equation [18,12].

Secondly, due to oscillatory character of soliton tails, solitons can form the bound states – stationary propagating bi-solitons and even more complicated multi-solitons [8,18]. We do not consider such structures in details here, but present only one example in Fig. 7. In frame (a) one can see a single soliton with oscillating tails, whereas in frame (b) the bi-soliton is depicted for the same parameters $B = 1$ and $V = -0.5$.

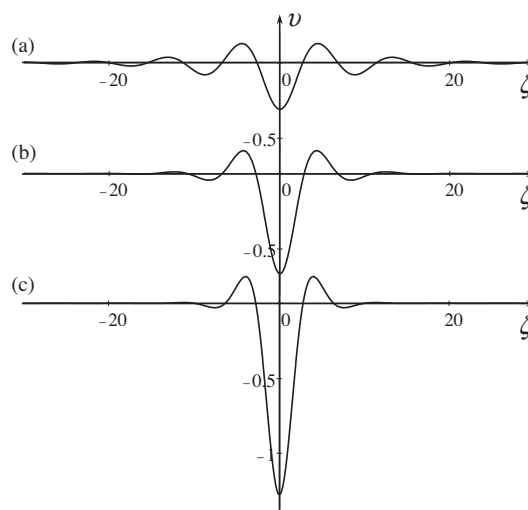


Fig. 6. Solitary wave shapes numerically obtained for $B = 1$ and three values of V . Case (a) – $V = -0.3$, case (b) – $V = -0.5$, case (c) – $V = -1.0$.

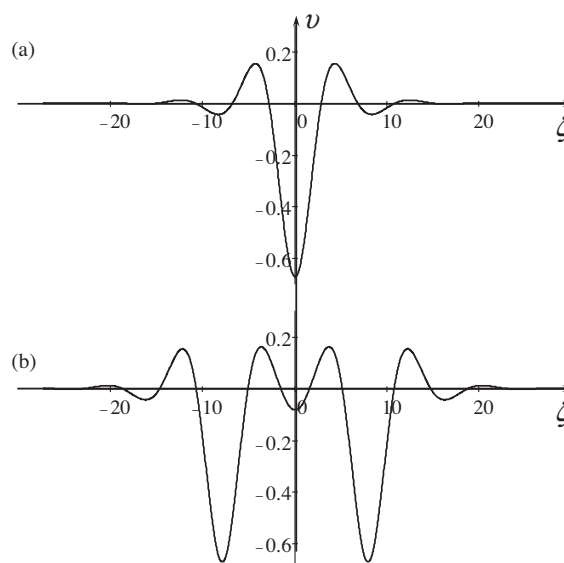


Fig. 7. Examples of single soliton and bi-soliton representing a family of stationary multi-soliton solutions of the GK equation (2.6).

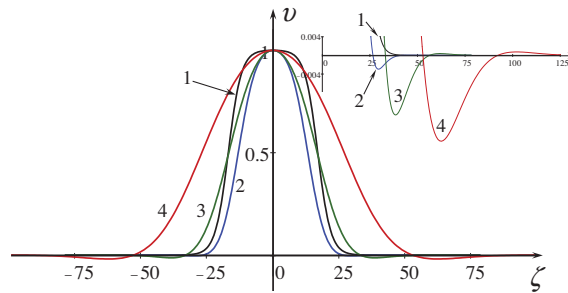


Fig. 8. Solitary wave shapes numerically obtained for the fixed soliton amplitude $A = 0.998$ and four values of B : line 1 – $B = 0$, line 2 – $B = -10$, line 3 – $B = -100$, line 4 – $B = -1000$.

For the sake of completeness, we have investigated a structure of soliton solutions for the negative parameter B too, although in the context of interfacial waves in two-layer fluid this parameter is always positive. When $B < 0$, the denominator of Eq. (3.5) is non-singular, if $V > 0$.

With the help of Petviashvili and Yang–Lakoba numerical methods we have obtained a family of soliton solutions only in the finite range of the parameter V : $0 < V \leq V_{cr}$, where V_{cr} depends on B , but only slightly differs from $1/6$. We did not investigate in details the dependence of soliton speed on its amplitude for different values of B , this can be a matter of a separate study. In Fig. 8 we present several soliton solutions constructed numerically for the fixed amplitude $A = 0.998$ and different B .

As one can see from this figure, the greater the B , the wider the soliton. Again, in accordance with the prediction, soliton asymptotics changes from the exponential aperiodic, when $V < -1/(4B)$, to oscillatory decaying, when $V > -1/(4B)$ (see Fig. 4). However, the oscillations are so small and they decay so fast that are hardly visible in soliton profile. In the insertion one can see the magnified portion of corresponding soliton tails.

Due to oscillatory character of soliton tails the bounded bi-soliton and multi-soliton solutions may exist in this case too. Moreover, even more complicated infinite chains of bounded solitons are possible. Such chains may be both regular and irregular representing quasi-random sequences of bounded solitons [9].

4. Discussion and conclusion

Thus, in this paper we have shown that in the study of interfacial waves between two immiscible fluids there are such situations, when the double critical conditions can occur, i.e. when both the coefficients of quadratic nonlinearity and third-order dispersion vanish simultaneously. In the near-critical situation the basic governing equation is the Gardner–Kawahara equation (1.8). Let us make an estimate of physical applicability of the GK equation to the real case of two-layer system consisting of kerosene in the upper layer and water in the lower layer. Take the following parameters for the kerosene and water at 20 °C: the density of kerosene is $\rho_1 = 0.82 \text{ g/cm}^3$, the density of water is $\rho_2 = 0.998 \text{ g/cm}^3$, and the surface tension at the interface between them is $\sigma = 48 \text{ dyn/cm}$. Then the double critical condition occurs, if the layer thicknesses are $h_1 = 0.82 \text{ cm}$ and $h_2 = 0.9 \text{ cm}$ with the total fluid depth $H = h_1 + h_2 = 1.72 \text{ cm}$. If we choose $h_1 = 0.62 \text{ cm}$ and $h_2 = 1.1 \text{ cm}$ with the same total depth, we will have a near critical condition with $h_1/h_2 \approx 0.56$. In this case the coefficient β_1 is positive and close to its minimum value (see Fig. 2); the dimensionless coefficient B in Eqs. (2.2) and (2.6) is also positive, and Eq. (2.6) possesses soliton solutions of negative polarity with the oscillatory tails as shown in Fig. 6. The shapes of such solitons may vary from quasi-sinusoidal wavetrains, when the amplitude goes to zero, up to narrow pulses, when the amplitude increases. The negative speeds of these solitons (see the diagram in Fig. 4) imply that they travel with the speeds less than the speed of long linear waves c in the immovable coordinate frame (see Eq. (1.2)).

Apparently, the similar GK equation can be applicable for the description of other types of waves in continuous media, for example, in plasma physics. The equation can be further generalised to take into account weak medium rotation in the spirit of the Ostrovsky equation [3,13] and weak wave diffraction in the spirit of the Kadomtsev–Petviashvili equation [20]. In the latter case two-dimensional lump solitons with oscillatory tails can be possible. Such solutions were constructed numerically for the two-dimensional version of the Kawahara equation (1.3) in [2].

It is important to notice in the conclusion that here we investigated the simplest types of soliton solutions of the GK equation – single solitary waves in the strict sense, and only briefly mentioned about existence of more complicated structures like coupled bi-solitons shown in Fig. 7. The stationary GK equation (2.6) is the fourth-order ODE with the 3D phase space (the equation can be reduced to the autonomous third-order ODE (see, e.g. [11]) or non-autonomous second-order ODE). Therefore there is no wonder that such complicated structures as coupled bi-, tri- and, in general, multi-solitons can exist within the framework of this equation. Moreover, even more complicated stationary structures like random sequences of solitary waves, obviously, are possible. They can be considered as examples of a “frozen turbulence” – stationary moving random waves. Such waves may be non-symmetrical in space. Similar classes of solutions have been found already for the related equations, for instance, for the Kawahara equation [8] and Ostrovsky equation [18]. In the latter case it has been shown

[6] that not only symmetric, but also anti-symmetric stationary solutions are also possible within the corresponding fourth-order ODE. (We do not touch here *quasi-stationary* asymmetric solutions, which have central cores and oscillatory tails either behind or in front of the cores. Such *slowly decaying* non-local solitary waves, apparently, are also possible within the GK equation similar to what was obtained for the Kawahara equation in [4]).

One can expect also existence of stationary non-local solitary wave solutions where the central core of the wave is accompanied by co-propagating trailing oscillations from both sides of the core. Such solutions were constructed, in particular, for the Kawahara equation (see, e.g. [11] and references therein). This topic, however, is out of the current paper scope.

Acknowledgment

This study was supported by the State Project of Russian Federation in the field of scientific activity, Task No 5.30.2014/K.

References

- [1] Ablowitz MJ, Segur H. Solitons and the inverse scattering transform. Philadelphia: SIAM; 1981.
- [2] Abramyan LA, Stepanyants YuA. The structure of two-dimensional solitons in media with anomalously small dispersion. Sov Phys JETP 1985;61(5):963–6.
- [3] Apel J, Ostrovsky LA, Stepanyants YA, Lynch JF. Internal solitons in the ocean and their effect on underwater sound. J Acoust Soc Am 2007;121(2):695–722.
- [4] Benilov ES, Grimshaw R, Kuznetsova EP. The generation of radiating waves in a singularly perturbed Korteweg–de Vries equation. Physica D 1993;169:270–8.
- [5] Brekhovskikh LM, Goncharov VV. Mechanics of continua and wave dynamics. Berlin: Springer; 1994.
- [6] Chen GY, Boyd JP. Analytical and numerical studies of weakly nonlocal solitary waves of the rotation-modified Korteweg–de Vries equation. Physica D 2001;155:201–22.
- [7] Giniyatullin AR, Kurkin AA, Kurkina OE, Stepanyants YA. Generalised Korteweg–de Vries equation for internal waves in two-layer fluid. Fundam Appl Hydrophys (in Russian), 2014;4 (in press).
- [8] Gorshkov KA, Ostrovsky LA, Papko VV, Pikovsky AS. On the existence of stationary multisolitons. Phys Lett A 1979;74(3–4):177–9.
- [9] Gorshkov KA, Ostrovsky LA, Stepanyants YuA. Dynamics of soliton chains: from simple to complex and chaotic motions. In: Albert Luo, Valentin Afraimovich, editors. Long-range interactions, stochasticity and fractional dynamics, Springer; 2010. p. 177–218.
- [10] Gorshkov KA, Papko VV. Dynamic and stochastic oscillations of soliton lattices. Zh Eksp Teor Fiz 1977;73(7):178–87 (in Russian. Engl. transl.: Sov. Phys. JETP, 1977, 46, 92–97).
- [11] Grimshaw R, Joshi N. Weakly nonlocal solitary waves in a singularly perturbed Korteweg–de Vries equation. SIAM J Appl Math 1995;55(1):124–35.
- [12] Grimshaw R, Helfrich KR. The effect of rotation on internal solitary waves. IMA J Appl Math 2012;77:326–39.
- [13] Grimshaw RHJ, Ostrovsky LA, Shrira VI, Stepanyants YuA. Long nonlinear surface and internal gravity waves in a rotating ocean. Surv Geophys 1998;19:289–338.
- [14] Kakutani T, Ono H. Weak non-linear electromagnetic waves in a cold, collision-free plasma. J Phys Soc Japan 1969;26:1305–18.
- [15] Karpman VI. Nonlinear waves in dispersive media. Moscow: Nauka; 1973 (in Russian; Engl. transl.: 1975, Pergamon Press, Oxford).
- [16] Kawahara T. Oscillatory solitary waves in dispersive media. J Phys Soc Jpn 1972;33:260–4.
- [17] Nagashima H. Experiment on solitary waves in the non-linear transmission-line described by the equation $du/dt + udu/dz - d^2u/dz^2 = 0$. J Phys Soc Jpn 1979;47:1387–8.
- [18] Obregon MA, Stepanyants YuA. Oblique magneto-acoustic solitons in rotating plasma. Phys Lett A 1998;249(4):315–23.
- [19] Pelinovsky DE, Stepanyants YA. Convergence of Petviashvili's iteration method for numerical approximation of stationary solutions of nonlinear wave equations. SIAM J Numer Anal 2004;42(3):1110–27.
- [20] Petviashvili VI, Pokhotelov OV. Solitary waves in plasmas and in the atmosphere. Philadelphia: Gordon and Breach; 1992.
- [21] Stepanyants YA. Dispersion of long gravity–capillary surface waves and asymptotic equations for solitons. Proc Russ Acad Eng Sci Ser Appl Math Mech 2005;14:33–40 (in Russian).
- [22] Yang J, Lakoba TI. Accelerated imaginary-time evolution methods for the computation of solitary waves. Stud Appl Math 2008;120:265–92.

Modulational stability of weakly nonlinear wave-trains in media with small- and large-scale dispersions

S. Nikitenkova,^{1,a)} N. Singh,^{2,a)} and Y. Stepanyants^{2,3,a),b)}

¹Lobachevsky State University of Nizhny Novgorod, Russia

²University of Southern Queensland, West St., Toowoomba, Queensland 4350, Australia

³Nizhny Novgorod State Technical University, Nizhny Novgorod 603950, Russia

(Received 16 July 2015; accepted 24 November 2015; published online 15 December 2015)

In this paper, we revisit the problem of modulation stability of quasi-monochromatic wave-trains propagating in a media with the double dispersion occurring both at small and large wavenumbers. We start with the shallow-water equations derived by Shrira [Izv., Acad. Sci., USSR, Atmos. Ocean. Phys. (Engl. Transl.) **17**, 55–59 (1981)] which describes both surface and internal long waves in a rotating fluid. The small-scale (Boussinesq-type) dispersion is assumed to be weak, whereas the large-scale (Coriolis-type) dispersion is considered as without any restriction. For unidirectional waves propagating in one direction, only the considered set of equations reduces to the Gardner–Ostrovsky equation which is applicable only within a finite range of wavenumbers. We derive the nonlinear Schrödinger equation (NLSE) which describes the evolution of narrow-band wave-trains and show that within a more general bi-directional equation the wave-trains, similar to that derived from the Ostrovsky equation, are also modulationally stable at relatively small wavenumbers $k < k_c$ and unstable at $k > k_c$, where k_c is some critical wavenumber. The NLSE derived here has a wider range of applicability: it is valid for arbitrarily small wavenumbers. We present the analysis of coefficients of the NLSE for different signs of coefficients of the governing equation and compare them with those derived from the Ostrovsky equation. The analysis shows that for weakly dispersive waves in the range of parameters where the Gardner–Ostrovsky equation is valid, the cubic nonlinearity does not contribute to the nonlinear coefficient of NLSE; therefore, the NLSE can be correctly derived from the Ostrovsky equation. © 2015 AIP Publishing LLC. [<http://dx.doi.org/10.1063/1.4937362>]

It is a well-known fact that plane surface gravity waves on shallow water are stable with respect to self-modulation, when $kh < 1.363$, where k is the wavenumber and h is the water depth. The same remains basically true for gravity-capillary waves, if the surface tension effect is not too strong; however, the criterion of stability in terms of kh becomes more complicated and depends on surface tension (Ablowitz and Segur, 1981). The situation becomes even more complicated for waves in a rotating fluid. In 1981, Shrira derived an equation describing long nonlinear waves in a rotating fluid and, neglecting the small-scale (Boussinesq) dispersion, obtained the nonlinear Schrödinger equation (NLSE) for quasi-harmonic waves. According to the analysis performed within the NLSE, surface waves are unstable to self-modulation due to the influence of rotation at very small wavenumbers $kh \rightarrow 0$. In 2008, Grimshaw and Helfrich found that within the Ostrovsky equation, which is a particular case of Shrira's equation, valid within the certain range of wavenumbers, $k_1 < k < k_2$, the modulation instability occurs for relatively big wavenumbers, when $k_c < k < k_2$, whereas at small wavenumbers $k_1 < k < k_c$, waves are stable. However, their analysis seems incomplete in application to real physical processes, since the cubic nonlinear term is not

included into the Ostrovsky equation, whereas it can contribute to the nonlinear coefficient of NLSE. More accurate analysis based on the Gardner–Ostrovsky equation containing both quadratic and cubic nonlinearities was performed by Whitfield and Johnson (2015a; 2015b). The results obtained in the papers by Shrira (1981), on the one hand, and Grimshaw and Helfrich (2008), as well as Whitfield and Johnson (2015a; 2015b), on the other hand, provide a contradictory conclusion about the modulation instability of large scale waves; the resolution of the issue requires more attention. In this work, we revisit the results obtained in all these papers and derive the NLSE applicable to quasi-monochromatic waves both with very small wavenumbers of carrier wave, up to $k \rightarrow 0$, and with relatively big wavenumbers, when the influence of small-scale Boussinesq dispersion becomes important. We present the governing equation in the dimensionless form containing the dispersion parameters of either sign, so that the equation is applicable not only to water waves in a rotating fluid but also to a wider class of nonlinear waves of any nature. From the derived NLSE,s we determine then the criterion of modulational stability/instability for all possible signs of dispersion coefficients and show that the results obtained agree well with the findings of Grimshaw and Helfrich (2008) within the range of validity of Ostrovsky equation, but contradict to the results obtained by Shrira (1981) at small k . We also show that the correction to the nonlinear coefficient in the

^{a)}S. Nikitenkova, N. Singh, and Y. Stepanyants contributed equally to this work.

^{b)}Author to whom correspondence should be addressed. Electronic mail: Yury.Stepanyants@usq.edu.au.

NLSE due to the cubic nonlinear term in the Gardner–Ostrovsky equation as derived by Whitfield and Johnson (2015a; 2015b) is actually of the next order of smallness and can be usually neglected, unless the coefficient of the quadratic nonlinearity in the Gardner–Ostrovsky equation is not anomalously small (such situation can occur, e.g., for internal waves in two-layer fluid (Ostrovsky *et al.*, 2015)).

I. INTRODUCTION

It is a matter of a well-known fact that unidirectional trains of shallow-water waves (both surface and internal) are modulationally stable except the case of a very strong surface tension effect (Ablowitz and Segur, 1981). This result formally agrees with what follows from the Korteweg–de Vries (KdV) equation

$$\frac{\partial \eta}{\partial t} + c_0 \frac{\partial \eta}{\partial x} + \alpha \eta \frac{\partial \eta}{\partial x} + \beta \frac{\partial^3 \eta}{\partial x^3} = 0, \quad (1)$$

which is applicable to the description of weakly nonlinear long waves. The coefficients α and β may be of either sign depending on the nature of waves. In particular, for the surface gravity-capillary waves the coefficients are (Karpman, 1973)

$$\alpha = \frac{3c_0}{2h}, \quad \beta = \frac{c_0 h^2}{6} \left(1 - \frac{3\sigma}{\rho g h^2} \right), \quad (2)$$

where $c_0 = (gh)^{1/2}$ is the speed of long linear waves, g is the acceleration due to gravity, h is the fluid depth, σ is the surface tension, and ρ is the fluid density. The dispersion relation between the wave frequency ω and wavenumber k for infinitesimal amplitude waves in the linearised equation (1) is well-known (see, e.g., Ablowitz and Segur (1981); Karpman (1973); and Ostrovsky *et al.* (2015))

$$\omega(k) = c_0 k - \beta k^3. \quad (3)$$

It shows that the dispersion appears at relatively large k (small wavelength λ), when the influence of the second term in the right-hand side is not negligibly small. Such small-scale (“Boussinesq”) dispersion is typical for long water waves. The derivation of Eq. (1) is based on the assumption that the dispersion is weak, so that $\beta k^3 \ll c_0 k$ or $k \ll k_1$, where $k_1 = (c_0/|\beta|)^{1/2}$. Depending on the sign of coefficient β , one can distinguish between the negative dispersion, if $\beta > 0$ (the phase speed $V_p \equiv \omega(k)/k = c_0 - \beta k^2$ decreases with k in this case), and positive dispersion, if $\beta < 0$ (the phase speed increases with k).

There are also physical systems containing the large-scale (“Coriolis-type”) dispersion which manifests when $k \rightarrow 0$ and disappears when $k \rightarrow \infty$. In many physical situations the large-scale dispersion is small and of the same order of smallness as the small-scale dispersion, so that the combined dispersion relation can be presented in the form

$$\omega(k) = c_0 k - \beta k^3 + \gamma/k, \quad (4)$$

where γ is some constant which can be of either sign, and $\gamma/k \ll c_0 k$, so that $k \gg k_2$, where $k_2 = (|\gamma|/c_0)^{1/2}$. The corresponding weakly nonlinear evolution equation generalising the KdV equation (1) is known as the Ostrovsky equation (Ostrovsky, 1978; Grimshaw *et al.*, 1998; Grimshaw and Helfrich, 2008; 2012; and Ostrovsky *et al.*, 2015)

$$\frac{\partial}{\partial x} \left(\frac{\partial \eta}{\partial t} + c_0 \frac{\partial \eta}{\partial x} + \alpha \eta \frac{\partial \eta}{\partial x} + \beta \frac{\partial^3 \eta}{\partial x^3} \right) = \gamma \eta. \quad (5)$$

This equation is applicable for waves of intermediate spatial scales

$$\sqrt{|\gamma|/c_0} \ll k \ll \sqrt{c_0/|\beta|}, \quad (6)$$

when both small-scale and large-scale dispersions are relatively small.

Grimshaw and Helfrich (2008; 2012) using Ostrovsky Eq. (5) with $\beta > 0$ and $\gamma > 0$ have shown that the large scale dispersion drastically changes the modulation stability of quasi-harmonic wave-trains. The nonlinear correction to the wave frequency remains negative for all wavenumbers as in the case of KdV equation, but the dispersion coefficient in the NLSE changes its sign at $k = k_c \equiv (\gamma/3\beta)^{1/4}$ when the group velocity $c_g = d\omega/dk$ attains maximum. Therefore, the corresponding NLSE remains modulationally stable for $k < k_c$, but becomes unstable for $k > k_c$. This is in a sharp contrast to the intuition based on the NLSE derived from the KdV equation (1). Indeed, at a first glance one can expect an influence of Coriolis-type dispersion at large scales only, as it vanishes when $k \rightarrow \infty$. At this limit, $k \rightarrow \infty$, the small-scale dispersion predominates, and wave-trains should be modulationally stable as in the case of KdV equation.

The physical explanation of this apparent contradiction is in the crucial role of a zero harmonic (the “mean flow”) generated by the basic wave-train. The nonlinear coefficient in the NLSE usually consists of contributions from both the second and zero harmonics. However, the zero harmonic is beyond the range of applicability of the Ostrovsky equation (see above), which formally requires the zero total “mass” of a perturbation (see, e.g., Grimshaw *et al.* (1998)). Therefore, the zero harmonic cannot contribute to the nonlinear coefficient, and the second harmonic provides the nonlinear coefficient in the NLSE of the opposite sign in comparison with that derived from the KdV equation, where both zero and second harmonics contribute jointly (this will be clearly seen from the analysis presented in the Appendix).

As the Ostrovsky equation is approximate and has a limited range of validity, the issue of modulation stability of wave-trains remained uncertain thus far, because at very small wavenumbers the situation with the modulation stability could be different, and contribution of the zero harmonic into the nonlinear coefficient of NLSE might be important again. Therefore, the problem of modulation stability of wave-trains should be resolved within the framework of more accurate equations in the long-wave limit. Moreover, for the analysis of modulation stability of waves in the real physical systems (e.g., water waves, or plasma waves) the KdV model equation is, obviously, insufficient, because it

contains only the quadratic nonlinear term, whereas cubic nonlinear terms usually provide the same order contribution to the nonlinear coefficient of NLSE.

The analysis of modulation stability of long water waves in a rotating fluid was undertaken as earlier as 1981 by Shrira, who derived a set of shallow-water equations and investigated modulation stability of quasi-monochromatic waves, ignoring however the small-scale dispersion. His analysis predicts the modulation instability of wave-trains at very small wavenumbers; this does not match with the result of Grimshaw and Helfrich (2008; 2012). Thus, the problem of modulation stability of water waves requires thorough consideration which motivates the current study.

Below the problem of modulation stability of quasi-monochromatic wave-trains is re-examined on the basis of the 2D shallow-water model set of equations derived by Shrira (1981) and augmented by the terms representing the Boussinesq dispersion. We derive the 2D NLSE and study a stability of quasi-monochromatic wave-trains with respect to longitudinal and transverse modulations for various signs of coefficients of the NLSE. The results obtained can be applicable not only to water waves, but in the wider context, including plasma waves, waves in solids, in optical media, etc.

II. THE GOVERNING EQUATIONS AND DISPERSION RELATIONS

We start with the following set of equations applicable (after appropriate scaling) both to surface and internal waves in the Boussinesq approximation (Ostrovsky, 1978; Shrira, 1981; and Grimshaw et al., 1998)

$$\frac{\partial \eta}{\partial t} + \nabla_{\perp} [(h + \eta)\mathbf{q}] = 0, \tag{7}$$

$$\frac{\partial \mathbf{q}}{\partial t} + (\mathbf{q} \cdot \nabla_{\perp})\mathbf{q} + [\mathbf{f} \times \mathbf{q}] + \frac{c_0^2}{h} \nabla_{\perp} \eta + s h \frac{\partial^2 \nabla_{\perp} \eta}{\partial t^2} = 0, \tag{8}$$

where η is the perturbation of a free surface in a non-stratified fluid or perturbation of an isopycnal surface (surface of equal density) in a stratified fluid, $\mathbf{q} = (u, v)$ is the depth averaged fluid velocity with two horizontal components, longitudinal u and transverse v , $\mathbf{f} = f\mathbf{n}$, where $f = 2\Omega \sin\varphi$ is the Coriolis parameter, Ω is the angular frequency of Earth rotation, φ is the local geographic latitude, \mathbf{n} is the unit vector normal to the Earth surface, and $\nabla_{\perp} = (\partial/\partial x, \partial/\partial y)$. Other parameters in Eqs. (7), (8) are c_0 —the speed of long linear waves, h —the fluid depth, and s —the dispersion parameter. In the case of surface waves the long-wave speed $c_0 = \sqrt{gh}$, and $s = (1 - 3\sigma/\rho gh^2)/3$, whereas for internal waves in two-layer fluid $c_0 = \sqrt{\frac{\Delta\rho}{\rho} g \frac{h_1 h_2}{h_1 + h_2}}$ and $s = h_1 h_2 / 3h^2$, where h_1 and h_2 are thicknesses of the upper and lower layers correspondingly, and $\Delta\rho = \rho_2 - \rho_1$ is the difference of layer densities (in the Boussinesq approximation both these densities are assumed close to each other ($\rho_1 \approx \rho_2 = \rho$), while the product $\Delta\rho g$ is assumed to be finite).

In one-dimensional case when all variables depend on one spatial coordinate x this set of equations can be reduced to one bi-directional equation for the transverse velocity v (Shrira, 1981). If we put

$$\eta = \frac{h}{f} \frac{\partial v}{\partial x}, \quad u = -\frac{1}{f + v_x} \frac{\partial v}{\partial t}, \tag{9}$$

where indices t and x here and below stand for the corresponding derivatives, then we obtain

$$v_{tt} - c_0^2 v_{xx} + f^2 v - s h^2 v_{ttxx} = \left(\frac{v_t v_x}{f + v_x} \right)_t + \frac{f}{2} \left[\frac{(v_t)^2}{(f + v_x)^2} \right]_x. \tag{10}$$

For perturbations of relatively small amplitude, the nonlinear terms in the right-hand side can be simplified, and Eq. (10) can be reduced to

$$v_{tt} - c_0^2 v_{xx} + f^2 v - s h^2 v_{ttxx} \approx \frac{1}{f} (v_{tt} v_x + 2v_t v_{xt}) - \frac{1}{f^2} [v_{tt} (v_x)^2 + 4v_t v_x v_{xt} + (v_t)^2 v_{xx}]. \tag{11}$$

By introducing new variables $\tau = ft/\sqrt{|\Gamma|}$, $\xi = (x/h)(|B/s|)^{1/2}$, $w = v(|B/s|)^{1/2}/(Ahf)$, where $A = B = \Gamma = 1$, one can present Eq. (11) in the dimensionless form

$$w_{\tau\tau} - C^2 w_{\xi\xi} + \Gamma w - B w_{\tau\tau\xi\xi} = A(w_{\tau\tau} w_{\xi} + 2w_{\tau} w_{\tau\xi}) - \Phi [w_{\tau\tau} (w_{\xi})^2 + 4w_{\tau} w_{\xi} w_{\tau\xi} + (w_{\tau})^2 w_{\xi\xi}], \tag{12}$$

where $C^2 = (c_0/hf)^2(|B\Gamma/s|)$ stands for the normalised characteristic wave speed, and $\Phi = A^2$ (we prefer to keep letter Φ rather than A^2 to track the contribution of nonlinear terms in the final equation). For further estimates we put $C = 34.3$ assuming that $h = 1000$ m, $g = 9.8$ m/s ($c_0 = 99$ m/s), $f = 5 \times 10^{-3}$ s⁻¹, $s = 1/3$, and $B = \Gamma = 1$.

In what follows we will not restrict ourselves to the particular choice of dimensionless coefficients $A = B = \Gamma = 1$ as above, but will assume that these coefficients can be of either sign with the moduli equal to unity. Then Eq. (12) or its unidirectional analogue, the Ostrovsky equation (see below) can be considered in a much wider context. In particular, the coefficient B can be negative for magnetosonic waves in a rotating plasma (Obregon and Stepanyants, 1998) or for capillary waves in a liquid fluid layer (Karpman, 1973) (see Eq. (2)); the coefficient Γ is usually positive, but can be negative in a rotating stratified ocean with shear flows (Alias et al., 2014a; 2014b).

For unidirectional waves propagating, for instance, to the right only, one can derive from Eq. (12) the following Gardner–Ostrovsky equation (Ostrovsky, 1978; Grimshaw et al., 1998; and Ostrovsky et al., 2015)

$$\frac{\partial}{\partial \xi} \left(\frac{\partial w}{\partial t} + C \frac{\partial w}{\partial \xi} + a\zeta \frac{\partial \zeta}{\partial \xi} - a_1 \zeta^2 \frac{\partial \zeta}{\partial \xi} + b \frac{\partial^3 \zeta}{\partial \xi^3} \right) = r\zeta, \tag{13}$$

where $\zeta = \partial w / \partial \xi$ (in terms of Eq. (9) this is just the normalised variable η : $\zeta = (\eta/Afh)(B\Gamma/s)^{1/2}$), $a = 3AC/2$, $a_1 = 3\Phi C$, $b = BC/2$, and $r = \Gamma/2C$.

For perturbations of infinitesimal amplitudes, the nonlinear terms on the right-hand side of Eq. (12) can be omitted,

then the following dispersion relation of the linearised equation can be obtained for $v \sim \exp[i(\omega t - kx)]$:

$$\omega^2 = \frac{C^2 k^2 + \Gamma}{1 + Bk^2}. \tag{14}$$

In the intermediate range of wavenumbers where $\sqrt{|\Gamma|/C} \ll k \ll 1/\sqrt{|B|}$, the dispersion relation can be approximated by the first three terms of the Laurent series (cf. Eq. (4))

$$\omega = Ck - bk^3 + \frac{r}{k} \equiv Ck - \frac{BC}{2}k^3 + \frac{\Gamma}{2Ck}. \tag{15}$$

In particular, when $r = 0$ ($\Gamma = 0$) we obtain from Eq. (15) the dispersion relation (3) in the dimensionless variables. Plots of the dispersion relations (14) and (15) are shown in Fig. 1 for different values of parameters B and Γ and $C = 34.3$. As one can see from these plots, the dispersion relation (15) approximates well the dispersion relation (14) in the intermediate range of wave numbers indicated above. Therefore, the non-physical singularity which appears at $k = 0$ in Eq. (15) with $|\Gamma| = 1$ is actually beyond the range of its applicability and is just an artefact of approximate character of the dispersion relation. The more accurate Eq. (14) does not have such singularity and is valid up to $k = 0$ inclusive.

From dispersion relations (14) and (15), one can readily obtain the group velocities $V_g \equiv d\omega/dk$

$$V_g = \frac{k(C^2 - B\Gamma)}{(1 + Bk^2)^{3/2}\sqrt{C^2k^2 + \Gamma}}; \quad V_{gO} = C - 3bk^2 - \frac{r}{k^2}, \tag{16}$$

where V_g pertains to Eq. (14) and V_{gO} pertains to Eq. (15).

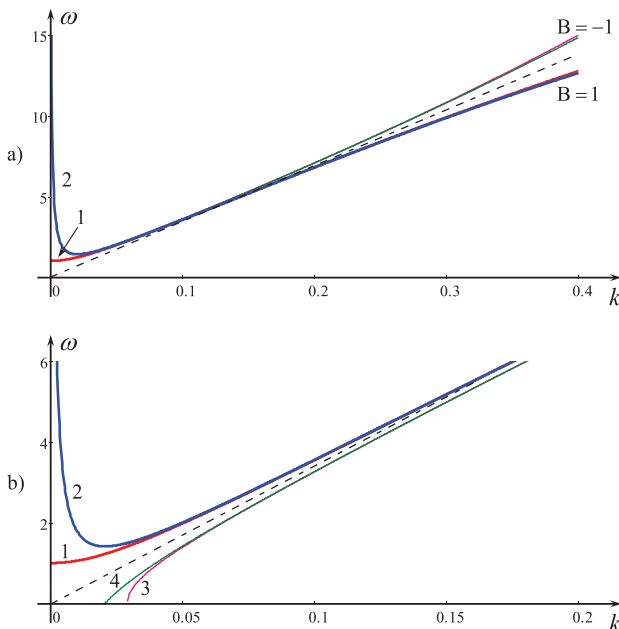


FIG. 1. Dispersion curves as per Eqs. (14) and (15) for different coefficients B and Γ . Lines 1 in panels (a) and (b) pertain to Eq. (14) with $\Gamma = 1$; lines 2 in panels (a) and (b) pertain to Eq. (15) with the same $\Gamma = 1$ ($r = 1.46 \times 10^{-2}$); in panel (b) line 3 pertains to Eq. (14) and line 4 to Eq. (15) with $\Gamma = -1$ ($r = -1.46 \times 10^{-2}$). Dashed lines in panels (a) and (b) represent the dispersionless dependence $\omega = Ck$.

Plots of group velocities are shown in Fig. 2 for $B = \Gamma = 1$ and $B = \Gamma = -1$. All other combinations of signs are not shown in the figure to avoid a mess.

Critical points of group velocities (16) (maxima, minima, or inflection points depending on signs of parameters B and Γ) occur at $k = k_c$ and $k = k_{cO}$, respectively, where

$$k_c = \sqrt{\frac{1}{C} \left[\sqrt{\frac{\Gamma}{3B} \left(1 + \frac{B\Gamma}{3C} \right)} - \frac{\Gamma}{C} \right]}, \quad k_{cO} = \sqrt{\frac{1}{C} \frac{\Gamma}{3B}} \tag{17}$$

(notice that the critical points are real if $\Gamma/B > 0$).

III. THE NONLINEAR SHRODINGER EQUATION AND MODULATION INSTABILITY

In this section, we analyse the stability of quasi-monochromatic wave-trains of small amplitude $\psi \ll 1$ within the framework of NLSE written for the dimensionless variable $\zeta = \partial w / \partial \xi$ in the form

$$i \frac{\partial \psi}{\partial \tau} + p \frac{\partial^2 \psi}{\partial \xi^2} + q |\psi|^2 \psi = 0, \tag{18}$$

where $p(k)$ and $q(k)$ are the dispersion and nonlinear coefficients, respectively; they depend on the central wavenumber of the carrier wave and coefficients of the governing equation. The details of the derivation of this equation from Eq. (12) are presented in the Appendix. Notice that the dispersion coefficient $p(k)$ can be readily obtained directly from the dispersion relations (14), $p(k) = (1/2)(\partial^2 \omega / \partial k^2)$ (see, e.g., Karpman (1973); Ablowitz and Segur (1981); and Ostrovsky and Potapov (1999)). When the NLSE (18) is derived from the Gardner–Ostrovsky equation (13), then the corresponding dispersion coefficient $p_O(k)$ can be obtained from the dispersion relations (15). Thus, we have

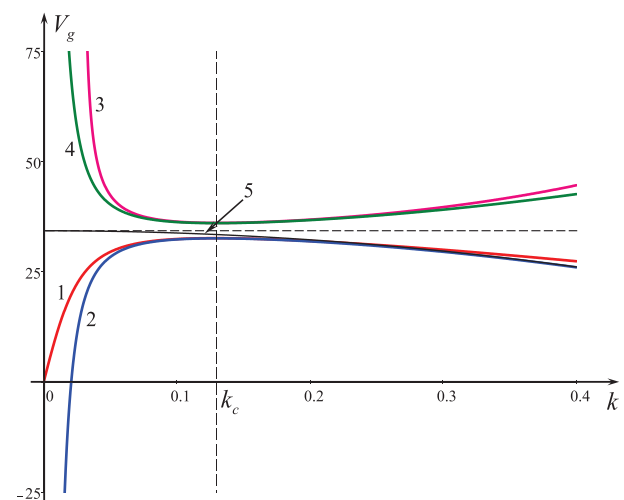


FIG. 2. Group velocities as per Eqs. (16) for different coefficients B and Γ . Line 1 pertains to V_g with $B = \Gamma = 1$; line 2 pertains to V_{gO} with the same parameters B and Γ ; line 3 pertains to V_g with $B = \Gamma = -1$; line 4 pertains to V_{gO} with the same parameters B and Γ ; and line 5 pertains to V_g with $B = 1$ and $\Gamma = 0$. Dashed horizontal line illustrates the limiting dispersionless case $V_g = C$, and dashed vertical line shows the position of maximum in line 2.

$$p(k) = \frac{C^2 - B\Gamma}{2} \frac{\Gamma - 2B\Gamma k^2 - 3BC^2 k^4}{(1 + Bk^2)^{5/2} (C^2 k^2 + \Gamma)^{3/2}}, \quad (19a)$$

$$p_O(k) = -3bk + \frac{r}{k^3} \equiv \frac{C}{2k} \left(-3Bk^2 + \frac{\Gamma}{C^2 k^2} \right). \quad (19b)$$

The expression for the coefficient $p_O(k)$ can be obtained from Eq. (19a) as the first terms of Taylor series on small parameters $Bk^2 \ll 1$ and $\Gamma/C^2 k^2 \ll 1$. Figure 3 shows the comparison of coefficients $p(k)$ and $p_O(k)$ with each other and with the coefficient $p_K(k) = -3bk \equiv -3BCk/2$ that follows from NLSE derived from the KdV equation.

In frame (a) lines 1 and 2 pertain to $p(k)$ and $p_O(k)$ as per Eqs. (19a) and (19b), correspondingly, with $B = \Gamma = 1$; lines 3 and 4 pertain to the case when $B = 1$ and $\Gamma = -1$; line 5 shows the coefficient $p_K(k)$. The insertion in frame (a) shows the same lines in the different scale. It is clearly seen that when k increases, lines 2 and 4 asymptotically approach line 5, whereas lines 1 and 3 become indistinguishable and both of them infinitely increase with k .

In frame (b), lines 1 and 2 pertain to $p(k)$ and $p_O(k)$, correspondingly, with $B = -1$ and $\Gamma = 1$; lines 3 and 4 pertain to the case of $B = \Gamma = -1$; line 5 shows the coefficient

$p_K(k)$. The insertion in frame (b) shows the same lines in the different scale. Again when k increases, lines 2 and 4 asymptotically approach line 5, whereas lines 1 and 3 become indistinguishable and both of them infinitely increase with k .

As one can see, in some cases the dispersion coefficient vanishes at $k = k_{c1,2}$ for Eq. (14) and $k = k_O \approx k_{c1,2}$ for Eq. (15), respectively, where

$$k_{c1,2} = \sqrt{\frac{1}{C} \left[\sqrt{\frac{\Gamma}{3B} \left(1 + \frac{B\Gamma}{3C} \right) - \frac{\Gamma}{C}} \right]}, \quad k_O = \sqrt{\frac{1}{C} \sqrt{\frac{\Gamma}{3B}}}, \quad (20)$$

k_{c1} pertains to the case $B = \Gamma = 1$, whereas k_{c2} pertains to the case $B = \Gamma = -1$, and $k_{c1} < k_O < k_{c2}$. In such cases the NLSE degenerates and it should be augmented by the terms of the next-order of smallness; then the generalised NLSE can be derived for wavenumbers in the vicinity of such points (see, e.g., Obregon and Stepanyants (1998) and Grimshaw and Helfrich (2008; 2012)).

Let us analyse now the nonlinear coefficient $q(k)$. Its formal derivation from Eq. (12) yields

$$q(k) = \frac{-3\sqrt{C^2 k^2 + \Gamma} [\Gamma(A^2 - \Phi) + C^2 k^2 A^2 - B\Phi k^2 (5\Gamma + 4C^2 k^2)]}{(1 + Bk^2)^{3/2} [4BC^2 k^4 + \Gamma(1 + 5Bk^2)]}. \quad (21a)$$

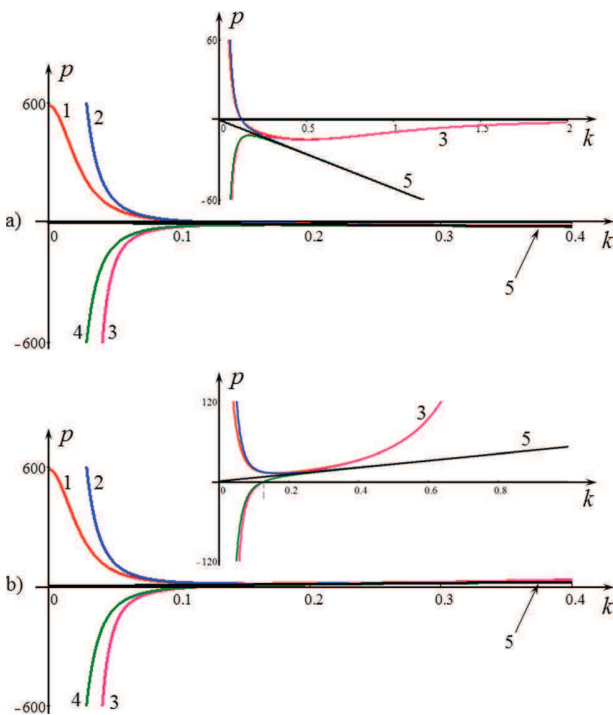


FIG. 3. The dispersion coefficient in the NLSE (18) as a function of wavenumber for different primitive equations.

Bearing in mind that $\Phi = A^2$ (see after Eq. (12)), one can present Eq. (21a) as

$$q_c(k) = \frac{-3k^2 A^2 \sqrt{C^2 k^2 + \Gamma} [C^2(1 - 4Bk^2) - 5B\Gamma]}{(1 + Bk^2)^{3/2} [4BC^2 k^4 + \Gamma(1 + 5Bk^2)]}. \quad (21b)$$

This expression can be compared with the case when the cubic nonlinearity in Eq. (12) is omitted ($\Phi = 0$)

$$q_q(k) = \frac{-3A^2 (C^2 k^2 + \Gamma)^{3/2}}{(1 + Bk^2)^{3/2} [4BC^2 k^4 + \Gamma(1 + 5Bk^2)]}. \quad (21c)$$

As one can see, the coefficients (21b) and (21c) are different, in general, and contribution of the cubic nonlinear term in Eq. (12) into the nonlinear coefficient of NLSE is important. Moreover, in some cases the quadratic nonlinear coefficient can vanish (this occurs, in particular, for internal waves in two-layer fluid with equal layer thicknesses (see, e.g., Grimshaw et al. (1998))), then the only cubic nonlinear term contributes into the NLSE coefficient $q(k)$, which reduces to

$$q_{pc}(k) = \frac{3\Phi \sqrt{C^2 k^2 + \Gamma} [\Gamma + Bk^2 (5\Gamma + 4C^2 k^2)]}{(1 + Bk^2)^{3/2} [4BC^2 k^4 + \Gamma(1 + 5Bk^2)]}. \quad (21d)$$

If we consider, however, the range of wavenumbers when the Ostrovsky equation is applicable, i.e., $\sqrt{|\Gamma|/C} \ll k$

$\ll 1/|B|$ (see above), then we obtain from Eqs. (21b) and (21c) the coefficients of NLSE up to the first-order terms on small parameters ($Bk^2 \sim \Gamma/C^2k^2 \ll 1$)

$$q_{Go}(k) \approx \frac{-3CkA^2}{4Bk^2 + \Gamma/C^2k^2} \left[1 + \frac{\Gamma}{C^2k^2} \left(\frac{3}{2} - \frac{\Phi}{A^2} \right) - \frac{3}{2} Bk^2 \left(1 + \frac{8}{3} \frac{\Phi}{A^2} \right) \right], \quad (22a)$$

if the cubic terms in Eq. (12) are taken into consideration

$$q_o(k) \approx \frac{-3CkA^2}{4Bk^2 + \Gamma/C^2k^2} \left[1 + \frac{3}{2} \left(\frac{\Gamma}{C^2k^2} - Bk^2 \right) \right], \quad (22b)$$

if the cubic terms in Eq. (12) are neglected ($\Phi = 0$), and

$$q_{pc}(k) \approx 3Ck\Phi \left[1 + \frac{B\Gamma/C^2 + \Gamma^2/C^4k^4 - 12B^2k^4}{2(\Gamma/C^2k^2 + 4Bk^2)} \right], \quad (22c)$$

if only the cubic terms in Eq. (12) are taken into consideration and the quadratic terms are ignored.

As one can see, if the quadratic terms do not vanish, then in the lowest order on small parameters the coefficients $q_{Go}(k)$ and $q_o(k)$ do not depend on the cubic terms in Eq. (13) and exactly coincide with the coefficient derived in Grimshaw and Helfrich (2008; 2012) and Whitfield and Johnson (2015a) directly from the Ostrovsky Eq. (13) without cubic nonlinear term ($a_1 = 0$)

$$q_o(k) = q_{Go}(k) = -\frac{2}{3} \frac{a^2k^3}{4bk^4 + r} \equiv \frac{-3CkA^2}{4Bk^2 + \Gamma/C^2k^2}. \quad (22d)$$

However, in the next order on small parameters, the corrections depend on the cubic terms in the original Eq. (12).

Notice that in the recent paper by Whitfield and Johnson (2015b) the NLSE was derived from the Gardner–Ostrovsky equation (15) which was formally considered without the restrictions on the range of its validity. The nonlinear coefficient in that paper formally follows from Eq. (22a) if we assume that $Bk^2 \sim \Gamma/C^2k^2 \ll 1$, but $Bk^2\Phi/A^2 \sim \Gamma\Phi/(ACk)^2 \sim 1$.

Figure 4 illustrates the dependence of the nonlinear coefficient in NLSE on the wavenumber k for different models. The first big difference in the dependences of the coefficients $q(k)$ is seen when $B = \Gamma = 1$. The coefficient $q_c(k)$ changes its sign at the point $k_0 = (C^2/B - 5\Gamma)^{1/2}/2C$ (see line 1 in frame (a)), whereas neither $q_q(k)$ nor $q_o(k)$ changes their signs (see lines 2 and 3 in frame (a)). However, at very small $k \ll 1$ the dependences $q_c(k)$, $q_q(k)$, and $q_o(k)$ are close to each other.

In the case $B = \Gamma = -1$, line 5 for $q_q(k)$ is qualitatively similar to line 4 for $q_c(k)$, but there is an obvious quantitative difference between these curves for relatively big values of $k > 0.2$ (both these lines go to infinity when $k \rightarrow 1/|(-B)| = 1$). As in the first case, at small $k \ll 1$ the dependences $q_c(k)$, $q_q(k)$, and $q_o(k)$ are close to each other.

When the coefficients B and Γ are of opposite sign, then the nonlinear coefficients change their signs at the point of singularity $k = K_{1,2}$ and $k = K_o$, where

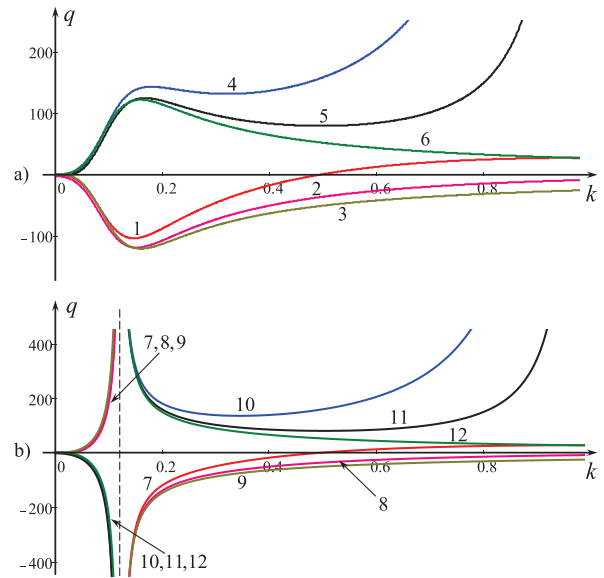


FIG. 4. The nonlinear coefficient in the NLS equation (18) as a function of a wavenumber for different basic equations. In frame (a) lines 1, 2, and 3 are plotted for $B = \Gamma = 1$, lines 4, 5, and 6 are plotted for $B = \Gamma = -1$; in frame (b) lines 7, 8, and 9 are plotted for $B = -\Gamma = 1$, lines 10, 11, and 12 are plotted for $B = -\Gamma = -1$.

$$K_{1,2} = \sqrt{\frac{1}{2C} \sqrt{-\frac{\Gamma}{B} \left(1 - \frac{25B\Gamma}{16C^2} \right)} - \frac{5\Gamma}{8C^2}},$$

$$K_o = \sqrt{\frac{1}{2C} \sqrt{-\frac{\Gamma}{B}}}, \quad (23)$$

K_1 pertains to the case $B = -1, \Gamma = 1$, whereas K_2 pertains to the case $B = 1, \Gamma = -1$ and K_o pertains to Eq. (22d). These three singular points are very close to each other, although they are ordered in the following way $K_1 < K_o < K_2$.

For the wavenumbers greater than the singular point all corresponding lines, except line 7, do not change their signs any more, but line 7 changes its sign at $k_0 = \frac{1}{2C} \sqrt{C^2/B - 5\Gamma}$. The points where the coefficients $p(k)$ and $q(k)$ change their signs are very important from the point of view of wave-trains stability with respect to self-modulation; this will be discussed below.

In the case when the NLSE is derived directly from the KdV equation the nonlinear coefficient $q_{KdV}(k) = 9A^2C/Bk$ depends on the sign of coefficient B and is either positive, when $B > 0$, or negative, when $B < 0$. Notice that the expression for this coefficient does not follow from Eq. (22d), if one formally puts $\Gamma = 0$. As explained above, the nonlinear coefficient in the NLSE derived from the KdV equation contains contributions from both the second harmonic and zero harmonic terms. However, as shown in the Appendix, when $\Gamma \neq 0$ the zero harmonic contributes only into the higher-order terms (see also Grimshaw and Helfrich (2008; 2012)).

As well known (see, e.g., Karpman (1973); Ablowitz and Segur (1981); and Ostrovsky and Potapov (1999)), the stability of quasi-monochromatic wave-trains with respect to small modulations is determined in the NLSE (18) by the

relative sign of nonlinear and dispersive coefficients. According to the well-known Lighthill criterion (Lighthill, 1965; Ostrovsky and Potapov, 1999; and Zakharov and Ostrovsky, 2009), the stability occurs when $p(k)q(k) < 0$, otherwise, when $p(k)q(k) > 0$, the wave-trains are unstable. In the latter case the “bright” envelope solitons can exist, whereas in the former case only “dark” solitons can exist on the background of a sinusoidal wave (see the references cited above).

To determine the range of wave-train stability/instability for the particular choice of parameters B and Γ and present it in the vivid form, let us define function $F(k) = S \text{sign}[p(k)q(k)]$, where $\text{sign}(x) = 1$ if $x > 0$ and $\text{sign}(x) = -1$ if $x < 0$, S is the “amplitude” of function $\text{sign}(x)$ which will help us to distinguish between different lines in Fig. 5. This illustrates the behaviour of function $F(k)$ for the different sets of parameters B and Γ .

Lines 1 in all frames pertain to the NLSE derived from Eq. (12) with the cubic nonlinear term, whereas lines 2 pertain to the NLSE derived from Eq. (12) without cubic nonlinear term ($\Phi = 0$), and lines 3 pertain to the NLSE derived from the Ostrovsky equation (13) without cubic nonlinear term ($a_1 = 0$).

As one can see from this figure, in the case shown in frame (a), the models based on Eq. (12) both with and without cubic nonlinear terms predict the stability of wave trains at $k < k_p \equiv \sqrt{\sqrt{(3C^2 + B\Gamma)\Gamma/B} - \Gamma/C}\sqrt{3}$ and instability at $k > k_p$. In the meantime, the model based on Ostrovsky equation (13) without cubic nonlinear term predicts the boundary between the stability and instability at $k = k_{O1} \equiv \sqrt[4]{\Gamma/3BC^2}$. Note that $k_p \approx k_{O1}(1 - \sqrt{B\Gamma/12C^2})$, if $B\Gamma \ll C^2$. Then, the more accurate model (12) with the cubic nonlinear term predicts one more boundary between the stability and instability at $k = k_{01} \equiv \sqrt{C^2/B - 5\Gamma/2C}$, $k_{01} > k_p$ (see line 1 in frame (a), whereas two other models do not predict stability at high wavenumbers. Note that the case shown in frame (a) pertains to gravity water waves in a rotating fluid.

In the case shown in frame (b), the model (12) with the cubic nonlinearity predicts modulation instability at very small $k < k_{O2} \equiv \sqrt{-\Gamma/C}$, whereas other models do not predict such instability. Then, there is the range of instability at

$k > k_p$ predicted by the models based on Eq. (12) both with and without cubic nonlinear term, as well as by the model based on Ostrovsky equation (13) without cubic nonlinear term at $k > k_{O1}$.

In the case shown in frame (c), the model (12) with the cubic nonlinearity predicts two regions of modulation instability, $0 < k < k_{O2}$ and $k_p < k < k_{01}$, and two regions of stability, $k_{O2} < k < k_p$ and $k > k_{01}$ (see line 1 in frame (c)). In the meantime, other two models predict only one boundary between the stability, $k < k_p$ ($k < k_{O2}$), and instability, $k > k_p$ ($k > k_{O2}$), regions (here $k_{O1} \equiv \sqrt[4]{-\Gamma/4BC^2}$).

And, at last, in the case shown in frame (d), the models with and without cubic nonlinearity predict the same regions of wave-train stability $k < k_p$ ($k < k_{O2}$), and instability, $k > k_p$ ($k > k_{O2}$).

In the case when the NLSE is derived from the KdV equation the product $p(k)q(k) = -27(AC)^2/2 < 0$, so that the wave-trains are stable against self-modulations for all k within the range of validity of KdV equation.

IV. DISCUSSION AND CONCLUSION

Thus, in this paper we have shown that the NLSE derived from the unidirectional Gardner–Ostrovsky equation (13) agrees well with the NLSE derived from the more general Shrira equation (12) within the range of validity of the Gardner–Ostrovsky equation. Moreover, within this range the coefficients of NLSE can be correctly obtained even without the cubic nonlinear terms in the governing equation (12). Beyond the range of validity of the Gardner–Ostrovsky equation the existence of ranges of modulation stability/instability is rather non-trivial and depends on the signs of small-scale and large-scale dispersions characterised by dimensionless coefficients B and Γ . In this paper, we have considered all possible signs of nonlinear and dispersive coefficient and presented the complete analysis of the problem for media with double dispersion. Therefore, our analysis is applicable not only to water waves in rotating or non-rotating fluids (e.g., various oceanic waves) but also to plasma waves, waves in solids, optical fibres, and others.

In application to surface and internal waves in a rotating ocean (see Fig. 5, frame (a)) our analysis shows

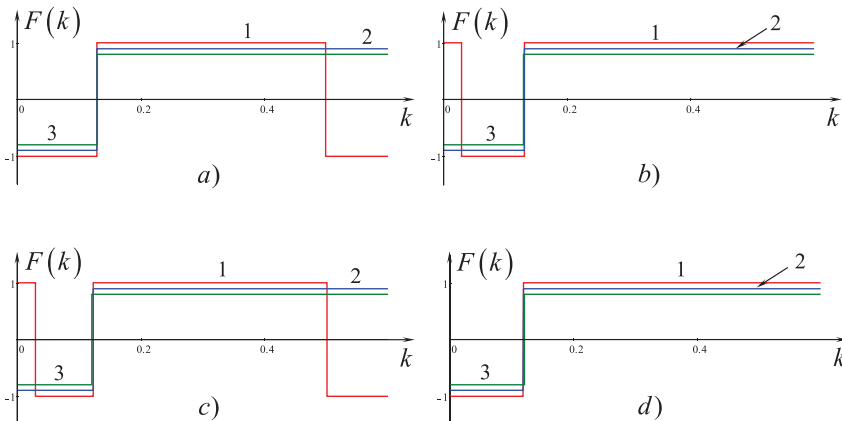


FIG. 5. Ranges of stability (when $F(k) < 0$) and instability (when $F(k) > 0$) of wave-trains against self-modulation. Frame (a) pertains to $B = \Gamma = 1$; frame (b) pertains to $B = \Gamma = -1$; frame (c) pertains to $B = -\Gamma = 1$; and frame (d) pertains to $B = -\Gamma = -1$. For the meaning of lines see the text.

that wave-trains are stable against self-modulation at small wavenumbers less than some critical value $k < k_p \equiv$

$$\sqrt{\sqrt{(3C^2 + B\Gamma)\Gamma/B} - \Gamma/C\sqrt{3}} \quad (k < k_{o1} \equiv \sqrt[4]{\Gamma/3BC^2})$$

which depends on the dispersion coefficients of the governing equations. This is in agreement with the results obtained in Grimshaw and Helfrich (2008; 2012) and Whitfield and Johnson (2015a), where the analysis was performed without cubic nonlinear terms in the limited range of wavenumbers as per Eq. (6).

A similar analysis can be performed in the two-dimensional case when all dependent variables are functions of spatial coordinates x and y , so that Shrira’s set of equations (8), (9) cannot be reduced to one, Equation (10). In contrast to the non-rotating fluid, the 2D NLSE appears in this case alone without a complementary equation for the mean-flow component which is suppressed in the first order by the influence of Coriolis-type dispersion. Therefore, instead of the usual Davey–Stewartson set of equation for a non-rotating fluid of finite depth (Ablowitz and Segur, 1981), we obtain just a single NLSE. The dispersion coefficients $p_x = (1/2)(\partial^2\omega/\partial k_x^2)$ and $p_y = (1/2)(\partial^2\omega/\partial k_y^2)$ of this equation can be easily derived from the dispersion relation (18), where now $k^2 = k_x^2 + k_y^2$. The new feature of the 2D NLSE is the possibility of the collapse phenomenon when self-modulation and self-focussing instabilities occur simultaneously (Zakharov and Kuznetsov, 2012). This interesting problem is currently

under investigation, and results obtained will be published elsewhere.

ACKNOWLEDGMENTS

The authors are thankful to V. I. Shrira for the useful discussions and valuable remarks. This work was supported by the State Project No. 5.30.2014/K of the Russian Federation in the field of scientific activity and by the Grant No. 02.B.49.21.0003 (the agreement between the Ministry of Education and Science of the Russian Federation and Lobachevsky State University of Nizhny Novgorod).

APPENDIX: DERIVATION OF NLS EQUATION

The nonlinear Schrödinger equation describing the evolution of wave-trains with the central wavenumber k of a carrier wave can be derived from Eq. (12) following the standard approach (see, e.g., Ablowitz and Haut (2009)), therefore details are reproduced here only briefly. Introduce the fast phase variable $\theta = \omega \tau - k \xi$, the slow spatial $X = \varepsilon \xi$ and temporal $T = \varepsilon \tau$ variables, as well as the “super-slow” temporal variable $t = \varepsilon T = \varepsilon^2 \tau$, where $\varepsilon \ll 1$ is a small parameter, and present a solution of Eq. (12) in the form of the series on small parameter ε

$$w(\theta, X, T, t) = \varepsilon w_1(\theta, X, T, t) + \varepsilon^2 w_2(\theta, X, T, t) + \varepsilon^3 w_3(\theta, X, T, t) + \dots \tag{A1}$$

Substitution of this series into Eq. (12) gives

$$\begin{aligned} &\varepsilon \left[(\omega^2 - C^2 k^2) \frac{\partial^2 w_1}{\partial \theta^2} - B k^2 \omega^2 \frac{\partial^4 w_1}{\partial \theta^4} + \Gamma w_1 \right] + \varepsilon^2 \left[(\omega^2 - C^2 k^2) \frac{\partial^2 w_2}{\partial \theta^2} - B k^2 \omega^2 \frac{\partial^4 w_2}{\partial \theta^4} + \Gamma w_2 \right. \\ &\quad \left. + 3\alpha\omega^2 k \frac{\partial w_1}{\partial \theta} \frac{\partial^2 w_1}{\partial \theta^2} - 2\omega \frac{\partial^2 w_1}{\partial \theta \partial T} - 2C^2 k \frac{\partial^2 w_1}{\partial \theta \partial X} + 2B\omega k \frac{\partial^3}{\partial \theta^3} \left(\omega \frac{\partial w_1}{\partial X} - k \frac{\partial w_1}{\partial T} \right) \right] \\ &\quad + \varepsilon^3 \left\{ \left[(\omega^2 - C^2 k^2) \frac{\partial^2 w_3}{\partial \theta^2} - B k^2 \omega^2 \frac{\partial^4 w_3}{\partial \theta^4} + \Gamma w_3 \right] + \frac{\partial^2 w_1}{\partial T^2} - C^2 \frac{\partial^2 w_1}{\partial X^2} + 2C^2 k \frac{\partial^2 w_2}{\partial \theta \partial X} \right. \\ &\quad \left. + B \frac{\partial^2}{\partial \theta^2} \left[2\omega k \frac{\partial}{\partial \theta} \left(\omega \frac{\partial w_2}{\partial X} - k \frac{\partial w_2}{\partial T} \right) + 4\omega k \frac{\partial^2 w_1}{\partial T \partial X} - \omega^2 \frac{\partial^2 w_1}{\partial X^2} - k^2 \frac{\partial^2 w_1}{\partial T^2} - 2\omega k^2 \frac{\partial^2 w_1}{\partial \theta \partial t} \right] \right. \\ &\quad \left. + \omega A \left[3\omega k \left(\frac{\partial w_1}{\partial \theta} \frac{\partial^2 w_2}{\partial \theta^2} + \frac{\partial w_2}{\partial \theta} \frac{\partial^2 w_1}{\partial \theta^2} \right) + 2k \left(\frac{\partial w_1}{\partial T} \frac{\partial^2 w_1}{\partial \theta^2} + 2 \frac{\partial w_1}{\partial \theta} \frac{\partial^2 w_1}{\partial \theta \partial T} \right) - \omega \left(\frac{\partial w_1}{\partial X} \frac{\partial^2 w_1}{\partial \theta^2} + 2 \frac{\partial w_1}{\partial \theta} \frac{\partial^2 w_1}{\partial \theta \partial X} \right) \right] \right. \\ &\quad \left. + 2\omega \frac{\partial}{\partial \theta} \left(\frac{\partial w_2}{\partial T} + \frac{\partial w_1}{\partial t} \right) + 6\Phi\omega^2 k^2 \frac{\partial w_1}{\partial \theta} \frac{\partial^2 w_1}{\partial \theta^2} \right\} + o(\varepsilon^3) = 0. \tag{A2} \end{aligned}$$

Let us consider a solution to Eq. (A2) in the form of quasi-monochromatic wave

$$w_1(\theta, X, T, t) = W_1(X, T, t)e^{i\theta} + W_1^*(X, T, t)e^{-i\theta}, \tag{A3}$$

$$w_2(\theta, X, T, t) = W_2(X, T, t)e^{2i\theta} + W_2^*(X, T, t)e^{-2i\theta} + W_0(X, T, t) + W_0^*(X, T, t), \tag{A4}$$

where star stands for complex conjugate.

Substitute now solutions (A3) and (A4) into Eq. (A2) and collect the terms proportional to $e^{i\theta}$. In the leading order with respect to ε , we obtain the dispersion relation (14). Collecting then the terms proportional to ε^2 , we obtain

$$2i \left[-\omega(Bk^2 + 1) \frac{\partial W_1}{\partial T} + k(B\omega^2 - C^2) \frac{\partial W_1}{\partial X} \right] e^{i\theta} + [(4C^2 k^2 - 4\omega^2 - 16B\omega^2 k^2 + \Gamma)W_2 + 3iA\omega^2 k |W_1|^2] e^{2i\theta} + \Gamma W_0 + \text{c.c.}, \tag{A5}$$

where c.c. stands for complex conjugate terms.

Equating to zero the coefficient of $e^{i\theta}$, we obtain the simple wave equation

$$\frac{\partial W_1}{\partial T} + V_g \frac{\partial W_1}{\partial X} = 0, \tag{A6}$$

where V_g is the group speed as per Eq. (16).

Equating then to zero the coefficient of $e^{2i\theta}$, we obtain a relationship between the amplitudes of the first and second harmonics

$$W_2 = \frac{3iA\omega^2 k |W_1|^2}{16B\omega^2 k^2 - \Gamma + 4\omega^2 - 4C^2 k^2}. \tag{A7}$$

In the same approximation, the term W_0 , which is independent of exponent (the mean flow term) vanishes, $W_0 = 0$; this is a specific feature of wave systems with the large-scale dispersion (Shrira, 1981; Obregon and Stepanyants, 1998; Grimshaw and Helfrich, 2008; 2012; and Whitfield and Johnson, 2015a; 2015b).

In the next order on the parameter ε the coefficient of $e^{i\theta}$ gives

$$2i\omega(1 + Bk^2) \frac{\partial W_1}{\partial t} + (C^2 + BV_g \omega k + B\omega^2) \frac{\partial^2 W_1}{\partial X^2} + 6k\omega^2 (iAW_2 + \Phi k |W_1|^2) W_1 = 0. \tag{A8}$$

Substituting here W_2 from Eq. (A7), we obtain the NLSE in the form

$$i \frac{\partial W_1}{\partial t} + p(k) \frac{\partial^2 W_1}{\partial X^2} + Q(k) |W_1|^2 W_1 = 0, \tag{A9}$$

where $p(k) = \frac{C^2 + BV_g \omega k + B\omega^2}{2\omega(1 + Bk^2)}$ and $Q(k) = -3k^2 \omega \frac{3A^2 \omega^2 - \Phi [4k^2(4B\omega^2 - C^2) + 4\omega^2 - \Gamma]}{(1 + Bk^2)(16B\omega^2 k^2 - \Gamma + 4\omega^2 - 4C^2 k^2)}$. Coming back to the original variables τ and ξ and using the relationship between the variables w and $\zeta = \partial w / \partial \xi$, which in the first approximation for

quasi-monochromatic wave reads $\zeta = ikw$, we finally obtain Eq. (18) with the coefficients $p(k)$ as per Eq. (19a) and $q(k) = Q(k)/k^2$ as per Eq. (21a).

Ablowitz, M. J. and Haut, T. S., "Coupled nonlinear Schrödinger equations for interfacial fluids with a free surface," *Theor. Math. Phys.* **159**, 689–697 (2009).

Ablowitz, M. J. and Segur, H., *Solitons and the Inverse Scattering Transform* (SIAM, Philadelphia, 1981).

Alias, A., Grimshaw, R. H. J., and Khusnutdinova, K. R., "Coupled Ostrovsky equations for internal waves with a background shear flow," *Proc. IUTAM* **11**, 3–14 (2014a).

Alias, A., Grimshaw, R. H. J., and Khusnutdinova, K. R., "Coupled Ostrovsky equations for internal waves in a shear flow," *Phys. Fluids* **26**, 126603 (2014b).

Grimshaw, R. and Helfrich, K., "Long-time solutions of the Ostrovsky equation," *Stud. Appl. Math.* **121**, 71–88 (2008).

Grimshaw, R. and Helfrich, K., "The effect of rotation on internal solitary waves," *IMA J. Appl. Math.* **77**, 326–339 (2012).

Grimshaw, R. H. J., Ostrovsky, L. A., Shrira, V. I., and Stepanyants, Yu. A., "Long nonlinear surface and internal gravity waves in a rotating ocean," *Surv. Geophys.* **19**, 289–338 (1998).

Karpman, V. I., *Nonlinear Waves in Dispersive Media* (Nauka, Moscow, 1973; Engl. Transl.: Pergamon Press, Oxford, 1975).

Lighthill, M. J., "Contribution to the theory of waves in non-linear dispersive systems," *J. Inst. Math. Its Appl.* **1**, 269–306 (1965).

Obregon, M. A. and Stepanyants, Yu. A., "Oblique magneto-acoustic solitons in a rotating plasma," *Phys. Lett. A* **249**, 315–323 (1998).

Ostrovskiy, L. A., "Nonlinear internal waves in a rotating ocean," *Oceanology* **18**, 119–125 (1978).

Ostrovsky, L., Pelinovsky, E., Shrira, V., and Stepanyants, Y., "Beyond the KDV: Post-explosion development," *Chaos* **25**, 097620 (2015).

Ostrovsky, L. A. and Potapov, A. I., *Modulated Waves: Theory and Applications* (Johns Hopkins University Press, Baltimore, London, 1999).

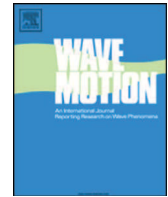
Shrira, V. I., "Propagation of long nonlinear waves in a layer of rotating fluid," *Izv. Acad. Sci., USSR, Atmos. Ocean. Phys. (Engl. Transl.)* **17**, 55–59 (1981).

Whitfield, A. J. and Johnson, E. R., "Modulational instability of co-propagating internal wavetrains under rotation," *Chaos* **25**, 023109 (2015a).

Whitfield, A. J. and Johnson, E. R., "Wave-packet formation at the zero-dispersion point in the Gardner-Ostrovsky equation," *Phys. Rev. E* **91**, 051201(R) (2015b).

Zakharov, V. E. and Kuznetsov, E. A., "Solitons and collapses: Two evolution scenarios of nonlinear wave systems," *Phys. Usp.* **55**, 535–556 (2012).

Zakharov, V. E. and Ostrovsky, L. A., "Modulation instability: The beginning," *Physica D* **238**, 540–548 (2009).



Obliquely propagating skew KP lumps



N. Singh¹, Y. Stepanyants^{*,1}

University of Southern Queensland, Toowoomba, Australia

ARTICLE INFO

Article history:

Received 16 January 2016

Received in revised form 27 March 2016

Accepted 28 March 2016

Available online 6 April 2016

Keywords:

Skew lump

Kadomtsev–Petviashvili equation

Soliton

Multi-lumps

ABSTRACT

Obliquely propagating skew lumps are studied within the framework of the Kadomtsev–Petviashvili equation with a positive dispersion (the KP1 equation). Specific features of such lumps are analysed in detail. It is shown that skew multi-lump solutions can be also constructed within the framework of such an equation. As an example, the bi-lump solution is presented in the explicit form, analysed and illustrated graphically. The relevance of skew lumps to the real physical systems is discussed.

© 2016 Elsevier B.V. All rights reserved.

1. Introduction

The Kadomtsev–Petviashvili (KP) equation is one of the well-studied models of nonlinear waves in dispersive media (see, e.g., [1,2]). In the immovable “laboratory” coordinate frame it can be presented in the form

$$\frac{\partial}{\partial x} \left(\frac{\partial u}{\partial t} + c \frac{\partial u}{\partial x} + \alpha u \frac{\partial u}{\partial x} - \beta \frac{\partial^3 u}{\partial x^3} \right) = -\frac{c}{2} \frac{\partial^2 u}{\partial y^2}, \quad (1)$$

where c is the velocity of long linear perturbations, and α and β are the nonlinear and dispersive coefficients which are determined by the specific type of wave and medium properties.

The properties of solutions to this equation depend on the sign of the dispersion coefficient β . In media with positive dispersion ($\beta > 0$) the equation possesses fully localised solitary wave solutions which are dubbed the lumps [1]. V.I. Petviashvili was the first who discovered such solutions numerically and suggested very effective numerical method to construct stationary solutions of nonlinear wave equations [3] (the method was rigorously substantiated later in Ref. [4]). Then, symmetric lump solutions were found analytically [5,6], and more general solutions representing skew lumps were obtained in [7,8]. Later, even more complex analytical solutions (bi-solitons, triple solitons, etc.) were found in [9,10]. Then it was developed a symbolic computation approach to search for lumps, and more generally, rational solutions (see, e.g., [8,11,12]).

Lump solutions describe nonlinear patterns in plasma [1,13,2], on the surface of a shallow water with the dominated surface tension [13–15], in nonlinear optic media [16], in the Bose–Einstein condensate [17], in solids with inner microstructure [18], etc. They can play a role of elementary wave excitations, and their ensembles with nontrivial internal interaction between lumps can represent a model of a strong wave turbulence.

* Corresponding author.

E-mail address: Yury.Stepanyants@usq.edu.au (Y. Stepanyants).

¹ The authors adhere to the principle of alphabetical order of the names.

However, even in the simplest case of one-lump solution [5–8], the properties of such solution were not thoroughly analysed so far. Meanwhile, it is of interest to analyse lump solutions in detail in the view of their physical applicability to different areas. In this paper such analysis is presented and some interesting features are found for skew lumps and bi-lumps obliquely propagating with respect to the main axis of motion. In isotropic media the main axis of motion can be chosen arbitrarily [19], therefore skew lumps, apparently, can co-exist with the symmetrical lumps forming a wide class of three-dimensional patterns. The role of skew lumps in the dynamics of localised initial perturbation is not clear yet; we believe, it will be studied in the nearest future. The main aim of this paper is to describe the characteristic features of elementary skew lumps and draw attention to their possible role in the dynamic of arbitrary initial perturbations.

2. Skew lumps

Let us consider the KP1 equation (1) with the positive dispersion parameter β . We shall study a stationary solution representing a pulse fully localised in the space. Assume that the pulse moves in the x, y -plane with the constant velocity $\mathbf{V} = (V_x, V_y)$. For such solution function $u(x, y, t)$ in Eq. (1) depends only on two variables $\xi = x - V_x t$ and $\eta = y - V_y t$, and the equation can be rewritten in the form

$$(c - V_x) \frac{\partial^2 u}{\partial \xi^2} + \frac{c}{2} \frac{\partial^2 u}{\partial \eta^2} - V_y \frac{\partial^2 u}{\partial \xi \partial \eta} = -\frac{\partial^2}{\partial \xi^2} \left[\frac{\alpha u^2}{2} - \beta \frac{\partial^2 u}{\partial \xi^2} \right]. \tag{2}$$

This equation under the transformation

$$\xi_n = \xi + V_y \eta, \quad \eta_n = \eta \tag{3}$$

can be reduced to the form which does not contain the mixed second derivative, but contains effective velocity along the ξ_n -axis only $V_{eff} = V_x + V_y^2/2c$. Notice that the transformation is not orthogonal, therefore it does not represent just a rotation of the coordinate system.

For further study it is convenient to convert Eq. (2) to the dimensionless form:

$$\frac{\partial^2 v}{\partial X^2} + \frac{\partial^2 v}{\partial Y^2} - v \frac{\partial^2 v}{\partial X \partial Y} = \frac{\partial^2}{\partial X^2} \left[v^2 + \frac{\partial^2 v}{\partial X^2} \right], \quad \text{where } v = \frac{V_y}{c} \sqrt{\frac{2}{1 - V_x/c}}, \tag{4}$$

with the help of transformation

$$X = \xi \sqrt{\frac{c - V_x}{\beta}}; \quad Y = \eta \sqrt{\frac{2(c - V_x)^2}{\beta c}}; \quad v = \frac{-\alpha u}{2(c - V_x)}. \tag{5}$$

From the transformation it follows the important relationships between the solitary wave amplitude A , velocity component V_x and characteristic widths along axes x and y , Δ_x and Δ_y respectively:

$$V_x = c \left(1 + \frac{1}{2c} \frac{\alpha A}{v_{max}} \right); \quad \Delta_x = \delta_x \sqrt{-2\beta \frac{v_{max}}{\alpha A}}; \quad \Delta_y = -\delta_y \sqrt{2\beta c \frac{v_{max}}{\alpha A}}. \tag{6}$$

Here the dimensionless amplitude v_{max} and characteristic widths δ_x and δ_y depend on the parameter v . Note that in the case of a positive dispersion, $\beta > 0$, we have $V_x < c$, and $v_{max}/(\alpha A) < 0$ [see Eqs. (3) and (4)]. Then, the larger the amplitude of a solitary wave $|A|$ the smaller its characteristic widths both in the x - and y -directions, but $\Delta_y \sim |A|^{-1}$ decreases faster than $\Delta_x \sim |A|^{-1/2}$ when $|A|$ increases. For a lump moving along the axis x , the parameter v is zero; then, the well-known symmetrical lump solution to the KP1 equation is [5,6,1,9] (see Fig. 1):

$$v(X, Y) = 4 \frac{1 - \frac{1}{3}(X^2 - Y^2)}{\left[1 + \frac{1}{3}(X^2 + Y^2) \right]^2}. \tag{7}$$

This solution does not contain any free parameter and can be treated as the nonlinear eigenfunction of Eq. (4) with $v = 0$. In the dimensionless variables the lump amplitude and characteristic widths are $v_{max} = 4$, $\delta_x = \sqrt{3}$; $\delta_y = \sqrt{3}$. The corresponding dimensional parameters are

$$V_x = c \left(1 + \frac{\alpha A}{8c} \right) < c; \quad \Delta_x = \sqrt{\frac{-24\beta}{\alpha A}}; \quad \Delta_y = -\frac{4}{\alpha A} \sqrt{6\beta c}. \tag{8}$$

In general for the obliquely propagating lumps, i.e., when $v \neq 0$, all these parameters are functions of v .

To find a lump solution in the general case, let us use the Hirota ansatz $v = 6 \frac{\partial^2 \ln f(X, Y)}{\partial X^2}$ and transform Eq. (6) into the bilinear form [6,1,7,8]:

$$f(f_{XX} + f_{YY} - v f_{XY}) - (f_X)^2 - (f_Y)^2 + v f_X f_Y = 3(f_{XX})^2 + f f_{XXXX} - 4f_X f_{XXX}. \tag{9}$$

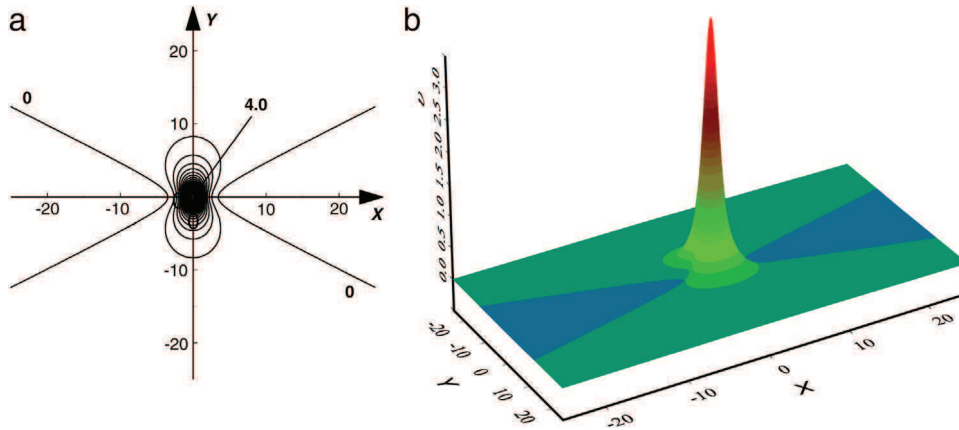


Fig. 1. Contour plot of the conventional KP1 lump (a) and its 3D profile (b). (For interpretation of the references to colour in this figure legend, the reader is referred to the web version of this article.)

Substitute into this equation the quadratic function $f = (X - X_0)^2 + p(Y - Y_0)^2 + qXY + r$, where X_0 and Y_0 are arbitrary constants which determine the initial position of the lump (they are omitted further without loss of generality), p , q , and r are some unknown parameters which can be determined after substitution of the trial quadratic function into Eq. (9). The substitution gives a set of equations for the coefficients:

$$2(p - 1) + q(\nu - q) = 0; \tag{10a}$$

$$2p(p - 1) + q(q - p\nu) = 0; \tag{10b}$$

$$2\nu p - q(p + 1) = 0; \tag{10c}$$

$$2r(p + 1) - \nu q r - 12 = 0. \tag{10d}$$

The solution to this system can be readily found: $p = 1$; $q = \nu$; $r = 12/(4 - \nu^2)$, which yields $f(X, Y) = X^2 + Y^2 + \nu XY + 12/(4 - \nu^2)$. The corresponding function $\nu(X, Y)$ generalises the known lump solution (7) and reduces to it when $\nu = 0$ (see also [7,8]):

$$\nu(X, Y) = (4 - \nu^2) \frac{1 + \frac{4-\nu^2}{12} \left[\frac{4-\nu^2}{4} Y^2 - \left(X + \frac{\nu}{2} Y\right)^2 \right]}{\left\{ 1 + \frac{4-\nu^2}{12} \left[\frac{4-\nu^2}{4} Y^2 + \left(X + \frac{\nu}{2} Y\right)^2 \right] \right\}^2}. \tag{11a}$$

Alternatively, this solution can be presented in another form which is useful for calculation of integral lump characteristics (the total lump mass, momentum, energy, etc.):

$$\nu(X, Y) = \frac{-6}{\left(X + \frac{\nu}{2} Y - i\sqrt{\frac{12}{4-\nu^2} + \frac{4-\nu^2}{12} Y^2}\right)^2} + \frac{-6}{\left(X + \frac{\nu}{2} Y + i\sqrt{\frac{12}{4-\nu^2} + \frac{4-\nu^2}{12} Y^2}\right)^2}, \tag{11b}$$

where i is the imaginary unit.

The solution is non-singular when ν varies in the range $-2 \leq \nu \leq 2$. This condition together with the definition of ν [see Eq. (4)] imposes the restriction on the possible velocity components in the dimensional variables:

$$\frac{V_x}{c} < 1 - \frac{1}{2} \left(\frac{V_y}{c}\right)^2. \tag{12}$$

The domain of possible velocity components of a single lump is shown in Fig. 2.

The dimensionless amplitude of the obliquely moving lump is $\nu_{\max} = 4 - \nu^2$. Thus, the lump amplitude is maximal and equals 4 when $\nu = 0$, i.e., when it moves along the axis x . The lump has an asymmetrical shape (it is skew) and moves obliquely with respect to the axes x ; the angle of lump inclination depends on the parameter ν . The similar skew-lump solution has been obtained in [7,8], but as has been mentioned above, the properties of such solution were not discussed in detail. Fig. 3 shows the contour plots of skew lumps for various values of ν .

Note that the parameter ν does not reflect precisely the direction of motion although it pertains to the oblique lump motion; it determines the orientation of the lump on the X, Y -plane (or, correspondingly, on the physical x, y -plane). The

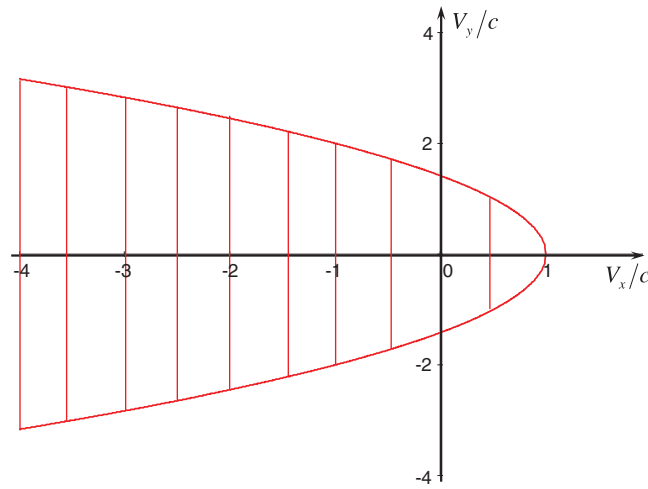


Fig. 2. (colour online). The domain of possible velocity components (shaded) of a single lump as per Eq. (12).

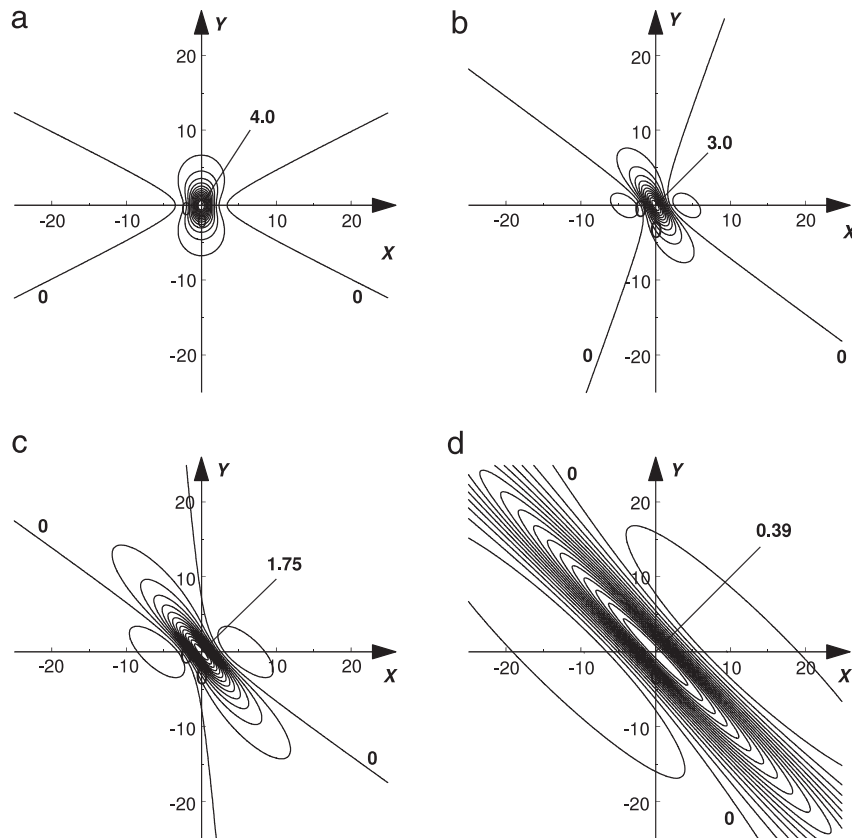


Fig. 3. Contour plots of lumps for different values of ν . (a) $-\nu = 0.5$; (b) $-\nu = 1.0$; (c) $-\nu = 1.5$; and (d) $-\nu = 1.9$. Arrows show maximum values, zero isolines are also indicated.

inclination of the lump trajectory to the axis x is determined by the angle θ , which is such that $\tan \theta = V_y/V_x$. As follows from the definition of the parameter ν [see Eq. (6)],

$$\tan^2 \theta = \frac{\nu^2}{2} \left(\frac{c}{V_x} \right)^2 \left(1 - \frac{V_x}{c} \right). \tag{13}$$

Thus, the oblique lumps with $\nu \neq 0$ move at certain angles to the axes x and y and; as will be shown below, they are antisymmetric in the moving coordinate system.

The isolines of lump zeros are determined by the equation:

$$X^2 - \left(1 - \frac{v^2}{2}\right) Y^2 + vXY = \frac{12}{4 - v^2}. \quad (14)$$

With the help of the orthogonal transformation of coordinates $X = X_n \cos \varphi - Y_n \sin \varphi$, $Y = X_n \sin \varphi + Y_n \cos \varphi$ this equation can be reduced to the canonical form $\frac{X_n^2}{A^2} - \frac{Y_n^2}{B^2} = 1$ which represents the hyperbola. The angle φ between old and new coordinate systems is determined in this case by the equation $\tan 2\varphi = \frac{2v}{4-v^2}$; it can vary in the range $-\pi/4 \leq \varphi \leq \pi/4$ when v varies from -2 to 2 . The parameters A and B determining the ‘semi-axes’ of the hyperbola are functions of v :

$$A^2 = \frac{48\sqrt{(4-v^2)^2 + 4v^2}}{(4-v^2) \left[v^2\sqrt{(4-v^2)^2 + 4v^2} + (4-v^2)^2 - 4v^2 \right]},$$

$$B^2 = \frac{48\sqrt{(4-v^2)^2 + 4v^2}}{v^4\sqrt{(4-v^2)^2 + 4v^2} + (4-v^2)^3}. \quad (15)$$

However even in this coordinate system where the zero line level of the lump is symmetrical with respect to the new coordinate axes X_n and Y_n , the lump itself is antisymmetric in the X_n, Y_n -plane as shown in Fig. 4 for the particular value of $v = 1.5$ (verily skew lump!). In the meantime, in the non-orthogonal coordinates as per Eq. (3) the lump looks symmetrical in the main cross-sections.

Having got a solution (11) in the dimensionless variables, one can present skew lump solution of the KP1 equation in the original variables:

$$u(x, y, t) = -\frac{2c}{\alpha} (1 - V_x/c) v \left[\sqrt{\frac{c}{\beta}} (1 - V_x/c) (x - V_x t), \sqrt{\frac{2c}{\beta}} (1 - V_x/c) (y - V_y t) \right]. \quad (16)$$

To illustrate the oblique and skew character of lump motion, let us consider a particular case when $V_x = 0$. Then, the lump can be either in the rest in the coordinate system moving with the speed c or it may move along axis y with any velocity in the range $-\sqrt{2} < V_y/c < \sqrt{2}$ (see Fig. 2). For the moving lump the parameter $v \neq 0$, therefore the lump is inclined to the axes x and y . The lump shape is very close to the shape of the conventional symmetric lump (see Fig. 1), if its velocity V_y is small, but it propagates in the y - rather than in the x -direction.

3. Obliquely propagating skew multi-lump solutions

In the similar way as in Section 2 one can construct more complicated skew bi-lump, triple lump, ..., multi-lump solutions in the spirit of papers [9,10]. It can be shown (see [10] and references therein) that the number of lumps M constituting a multi-lump solution is $M = N(N+1)/2 = 1, 3, 6, 10, \dots$, where N is an integer number. Such multi-lump solutions are described by Eq. (9) with a polynomial function $f(X, Y)$ of the degree $2M$. The simplest nontrivial rational solution of Eq. (9) after that quadratic function which describes the single lump (see above) can be constructed on the basis of six degree polynomial of X and Y with undetermined coefficients. Substituting such polynomial into Eq. (9) and equating to zero the coefficients of like terms one can find the solution containing two arbitrary parameters, a and b :

$$f(X, Y) = X^6 + Y^6 + \frac{100}{4-v^2} X^4 + 4 \frac{17+14v^2-3v^4}{4-v^2} Y^4 + bX^3 + aY^3 - \frac{2000}{(4-v^2)^2} X^2 + 400 \frac{19-6v^2}{(4-v^2)^2} Y^2$$

$$- \frac{4b}{4-v^2} X - 4 \frac{5a+8bv-3bv^3}{(4-v^2)(1-v^2)} Y - \frac{2000v}{(4-v^2)^2} XY + 60 \frac{6+v^2}{4-v^2} X^2 Y^2 + v(6+v) X^3 Y^3$$

$$+ 3XY \left[v(X^4 + Y^4) + (1+v^2)XY(X^2 + Y^2) + \frac{40v}{3} \frac{5X^2 + (9-v^2)Y^2}{4-v^2} - \frac{(a+bv)X + (b+av)Y}{1-v^2} \right]$$

$$+ \frac{1}{4-v^2} \left[\frac{abv(3-v^2) + (a^2 + b^2)}{(1-v^2)^2} + \frac{120000}{(4-v^2)^2} \right]. \quad (17)$$

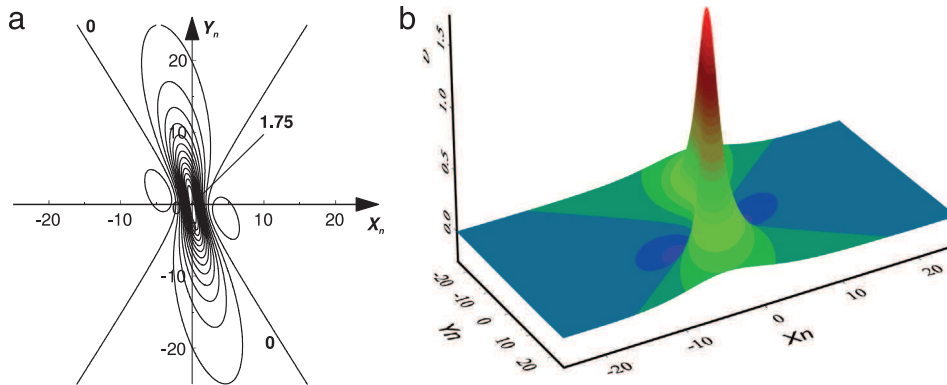


Fig. 4. (colour online). (a) Contour plot of a skew lump with $\nu = 1.5$ in the coordinate system where the zero isolines are symmetrical with respect to the coordinate axes (see the hyperbolic lines); (b) 3D profile of the same lump.

Depending on the parameters a, b and ν , this solution can represent either bi- or triple-lump. In the particular case $\nu = 0$, solution (17) reduces to the solution found in Ref. [10].

Playing with the parameters a and b , one can obtain a big variety of interesting stationary solutions representing coupled lumps moving at some angles to the axis x . Choosing in particular $a = b = 0$, we obtain from Eq. (17)

$$\begin{aligned}
 f = & X^6 + Y^6 + \frac{100}{4 - \nu^2} X^4 + 4 \frac{17 + 14\nu^2 - 3\nu^4}{4 - \nu^2} Y^4 - \frac{2000}{(4 - \nu^2)^2} X^2 + 400 \frac{19 - 6\nu^2}{(4 - \nu^2)^2} Y^2 - \frac{4b}{4 - \nu^2} X \\
 & - \frac{2000\nu}{(4 - \nu^2)^2} XY + 60 \frac{6 + \nu^2}{4 - \nu^2} X^2 Y^2 + \nu(6 + \nu) X^3 Y^3 \\
 & + 3XY \left[\nu(X^4 + Y^4) + (1 + \nu^2)XY(X^2 + Y^2) + \frac{40\nu}{3} \frac{5X^2 + (9 - \nu^2)Y^2}{4 - \nu^2} \right] + \frac{120000}{(4 - \nu^2)^3}. \tag{18}
 \end{aligned}$$

In this case function $f(X, Y)$ has singularities only at $\nu = \pm 2$, but when $|\nu| \rightarrow 2$, the solution for $\nu(X, Y)$ reduces to a very wide bi-lump of small amplitude (see Fig. 5(e)), which completely vanishes in the limit $|\nu| = 2$. Fig. 5 illustrates a solution as per Eq. (18) presented in terms of the variable $\nu(X, Y)$. This solution represents a bi-lump whose shape monotonically depends on the parameter ν .

If however $a^2 + b^2 \neq 0$, then function $f(X, Y)$ has two more singularities at $\nu = \pm 1$. The structure of the solution changes around these singular values. In Fig. 6 we illustrate the function changes for the particular case of $a = 10, b = 0$. When ν increases and approaches 1, the solution being quasi-symmetrical at $\nu = 0$ and having two strongly pronounced maxima (see Fig. 6(a)), becomes more and more asymmetrical. The third small maximum appears at $\nu \approx 0.9$ (see Fig. 6(c)) and gradually grows when $\nu \rightarrow 1$ (see Fig. 6(d)), but the distances between the maxima increase. In the limit $\nu = 1$, the distance becomes infinite, so that all three humps move off to the infinity, and the wave field between them goes to zero; the solution degenerates to zero at this value of ν .

When ν is slightly greater than one, then the solution represents again the three-hump pattern with a big distance between the humps (see Fig. 6(e)). The distance decreases when ν increases; one of the humps becomes smaller than two others and gradually disappears at $\nu > 1.1$ (see Fig. 6(f)). When ν increases further from 1 to 2, the solution becomes more and more symmetrical (see Fig. 6(g)); eventually it reduces to a very wide bi-lump of a small amplitude (see Fig. 6(h)), which completely vanishes in the limit $|\nu| = 2$.

As has been shown in [9], the binding energy of lumps in the multi-lump solutions is zero, therefore such stationary solutions are unstable with respect to small perturbations, whereas the stability of single lumps has been proven in [20]. One can expect that interacting with other perturbations, multi-lumps decay into stable single lumps moving at different angles to each other. Such process of decay and scattering has not been studied yet (this work is currently under way, and results obtained will be published elsewhere).

4. Integral characteristics of skew lumps

In this section we calculate the integral quantities for skew lumps (the components of the momentum and energy), as they can be used in the development of asymptotic theory of interactions of skew lumps and multi-lumps (see, e.g., [10,21]).

Using representation of lump solution (11b), it is easy to check that the total “mass” of the lump $M = \iint_{\infty} u(x, y, t) dx dy$ is zero independently of ν . The components of the lump momentum in the dimensional variables can be defined as

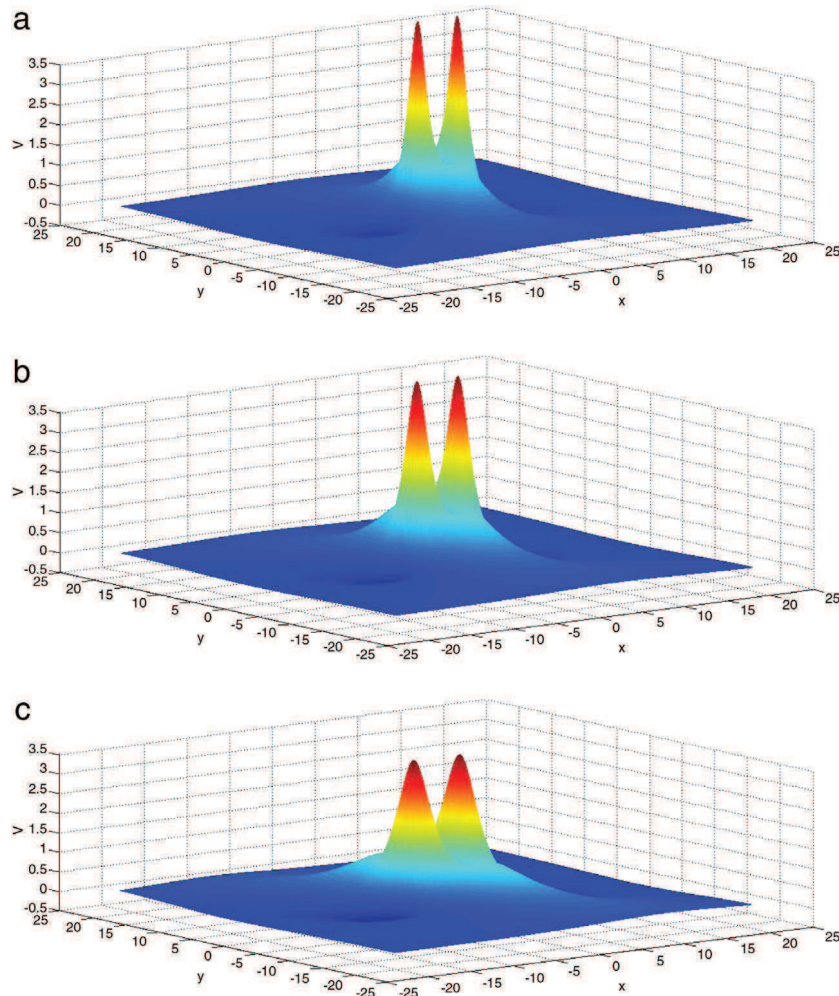


Fig. 5. (colour online). Skew lumps as per Eq. (18) with $a = b = 0$ and different values of ν : (a) $-\nu = 0$; (b) $-\nu = 0.5$; (c) $-\nu = 0.9$; (d) $-\nu = 1.0$; (e) $-\nu = 1.1$; (f) $-\nu = 1.5$; (g) $-\nu = 1.9$.

follows [21, 10]:

$$P_x = \frac{1}{2} \iint_{\infty} u^2(x, y, t) dx dy = \frac{24\pi \beta c}{\alpha^2} \sqrt{2 \left(1 - \frac{V_x}{c}\right) - \left(\frac{V_y}{c}\right)^2}, \tag{19a}$$

$$P_y = 2\sqrt{2} P_x \frac{V_y}{c} = \frac{48\sqrt{2}\pi \beta c}{\alpha^2} \frac{V_y}{c} \sqrt{2 \left(1 - \frac{V_x}{c}\right) - \left(\frac{V_y}{c}\right)^2}. \tag{19b}$$

The integrals in Eqs. (19a) and (19b) can be easily evaluated using again the representation (11b). The maximal values of the momentum components are:

$$(P_x)_{\max} = \frac{24\pi \beta c}{\alpha^2} \sqrt{2 \left(1 - \frac{V_x}{c}\right)} \quad \text{at } V_y = 0, \tag{20a}$$

$$|P_y|_{\max} = \frac{48\sqrt{2}\pi \beta c}{\alpha^2} \left(1 - \frac{V_x}{c}\right) \quad \text{at } \left|\frac{V_y}{c}\right|_{\max} = \sqrt{1 - \frac{V_x}{c}}. \tag{20b}$$

In the dimensionless variables the components of lump momentum read $\tilde{P}_x = 6\pi \sqrt{4 - \nu^2}$ and $\tilde{P}_y = 12\pi \nu \sqrt{4 - \nu^2}$; their maximal values are: $(\tilde{P}_x)_{\max} = 12\pi$ at $\nu = 0$ and $|\tilde{P}_y|_{\max} = 24\pi$ at $\nu = \pm\sqrt{2}$.

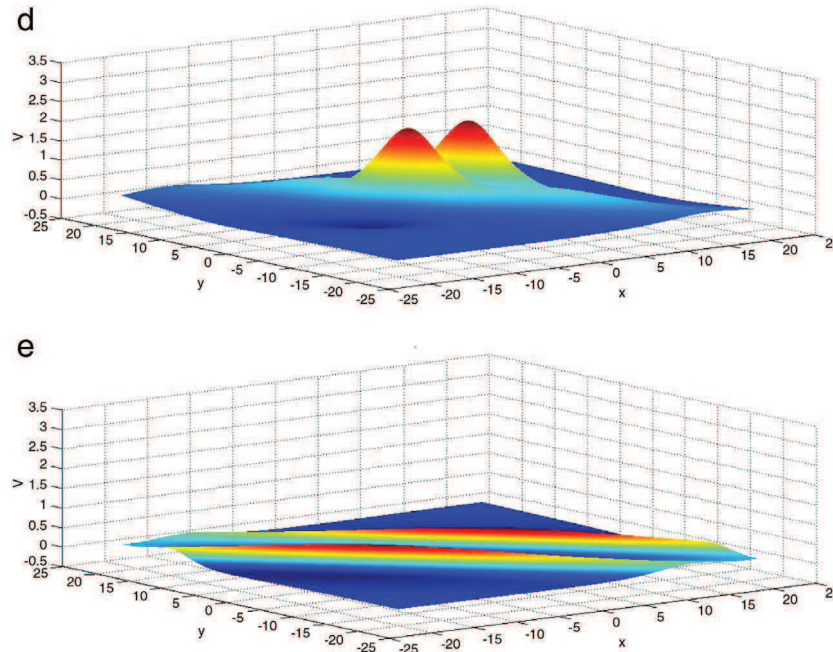


Fig. 5. (continued)

One more important lump characteristics which is of the physical interest is its energy (the Hamiltonian):

$$\begin{aligned}
 H &= \frac{1}{2} \iint_{-\infty}^{\infty} \left[\beta \left(\frac{\partial u}{\partial x} \right)^2 + \frac{c}{2} \left(\int \frac{\partial u}{\partial y} dx \right)^2 + \frac{\alpha}{3} u^3 \right] dx dy \\
 &= \frac{2\sqrt{2}\beta c^2}{\alpha^2} \left(1 - \frac{V_x}{c} \right)^{\frac{3}{2}} \frac{1}{2} \iint_{-\infty}^{\infty} \left[\left(\frac{\partial v}{\partial X} \right)^2 + \left(\int \frac{\partial v}{\partial Y} dX \right)^2 - \frac{2}{3} v^3 \right] dXdY \\
 &= \frac{144\pi\beta c^2}{\alpha^2} \left(1 - \frac{V_x}{c} \right)^{\frac{3}{2}} \sqrt{\frac{2}{3}(4 - v^2)} = \frac{288\pi\beta c^2}{\alpha^2\sqrt{3}} \left(1 - \frac{V_x}{c} \right) \sqrt{2 \left(1 - \frac{V_x}{c} \right) - \left(\frac{V_x}{c} \right)^2}. \tag{21}
 \end{aligned}$$

The maximum value of the energy at a given value of V_x is $H_{\max} = 96\sqrt{6}\pi \frac{\beta c^2}{\alpha^2} \left(1 - \frac{V_x}{c} \right)^{\frac{3}{2}}$. The quantities derived in the section can be useful in the subsequent study of lump interactions with each other and with external fields and potentials.

5. Discussion and conclusion

The KP equation was derived for quasi-plane waves propagating in isotropic media, e.g., for surface waves in a shallow water or for waves in the Bose–Einstein condensate [17]. However, the equation is not symmetrical with respect to the variables x and y . The apparent anisotropy of the equation is associated with the choice of primary direction of wave propagation (oriented, for example, along the axis x) and weak diffraction of the wave field in the perpendicular direction (along the axis y). This explains anisotropic properties of the conventional lump solution (6) which is not axisymmetric. But in fact such non-axisymmetric lumps can propagate in any direction in the x, y -plane, being symmetrical in the x, y -plane. Solution anisotropy in the x, y -plane is the intrinsic property, which is not caused, however, by the anisotropy of a medium.

In this paper we have derived more general solutions describing skew KP1 lumps. Similar single-lump solutions have been obtained in [7,8], and their interactions have been studied in [7]. In the current paper it has been shown that a variety of skew multi-lump solutions can exist in the KP1 equation; examples of simplest of them have been presented. The properties of single skew lumps have been analysed in detail. The lumps can move at certain angles to the chosen coordinate axes and certain angles to their own axes of symmetry. In an isotropic medium the skew lumps, apparently, can co-exist with the symmetrical lumps forming a wide class of three-dimensional patterns playing important role in the dynamics of initial perturbation.

Integral characteristics of single lumps (mass, momentum components and energy) have been calculated and presented in terms of lump velocity components. The detailed pair- or multiple collisions of such lumps is an interesting problem for

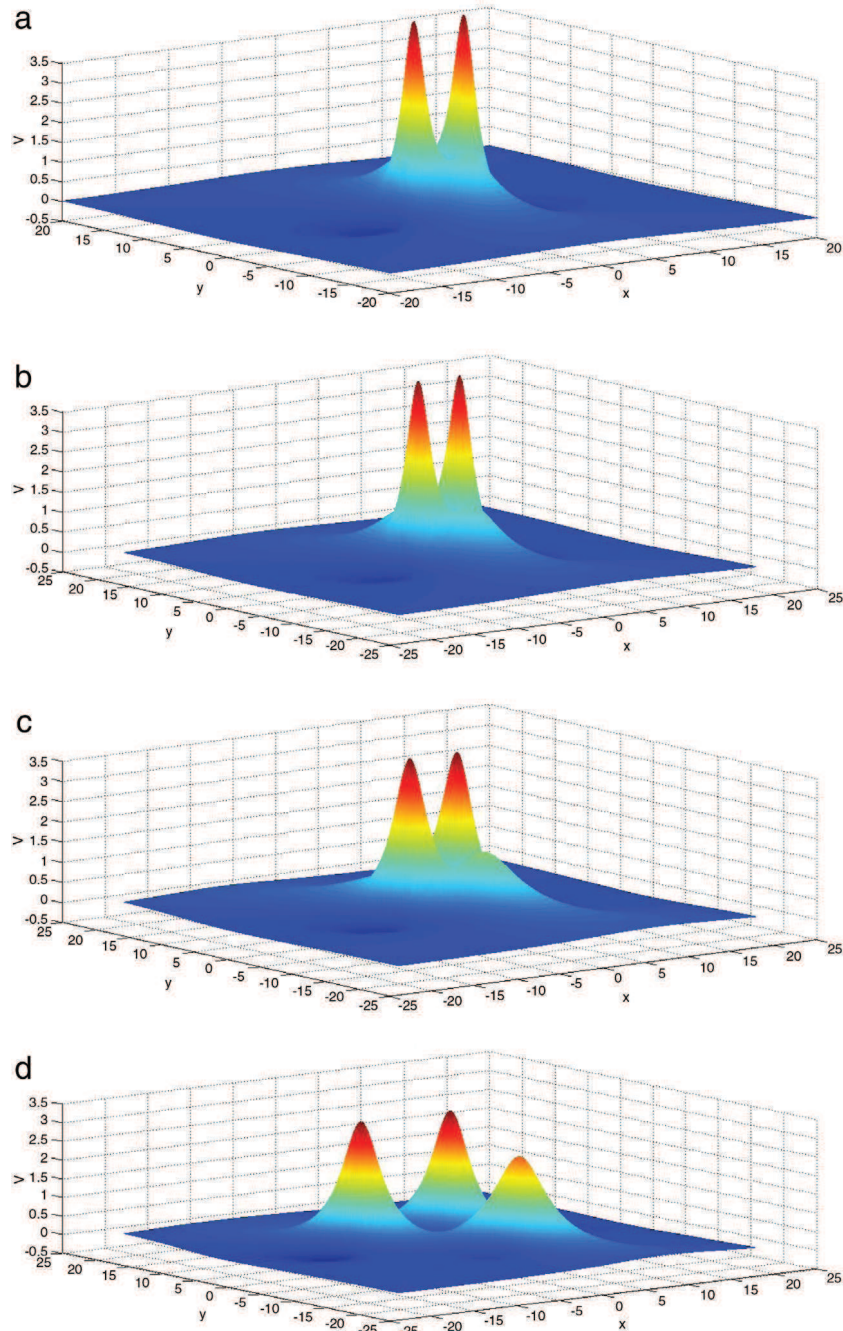


Fig. 6. (colour online). Skew lumps as per Eq. (18) with $a = 10$, $b = 0$ and different values of ν : (a) $-\nu = 0$; (b) $-\nu = 0.5$; (c) $-\nu = 0.9$; (d) $-\nu = 0.99$; (e) $-\nu = 1.01$; (f) $-\nu = 1.1$; (g) $-\nu = 1.5$; (h) $-\nu = 1.9$.

further analytical and numerical study. Unidirectional interactions of single lumps when they initially aligned and moved along the same x -direction were studied analytically in [10,22], whereas their oblique interactions were studied numerically in [7].

We have obtained also a family of skew bi-lump solutions which depend on two free parameters. The structure of two particular, but typical family representatives have been studied in detail and illustrated graphically. Even more complicated skew lump solutions can be constructed in the spirit of paper [9]. It is believed that all these elementary solutions can play important role in the theory of strong wave turbulence when the chaotic wave field can be represented by a big ensemble of interacting lumps.

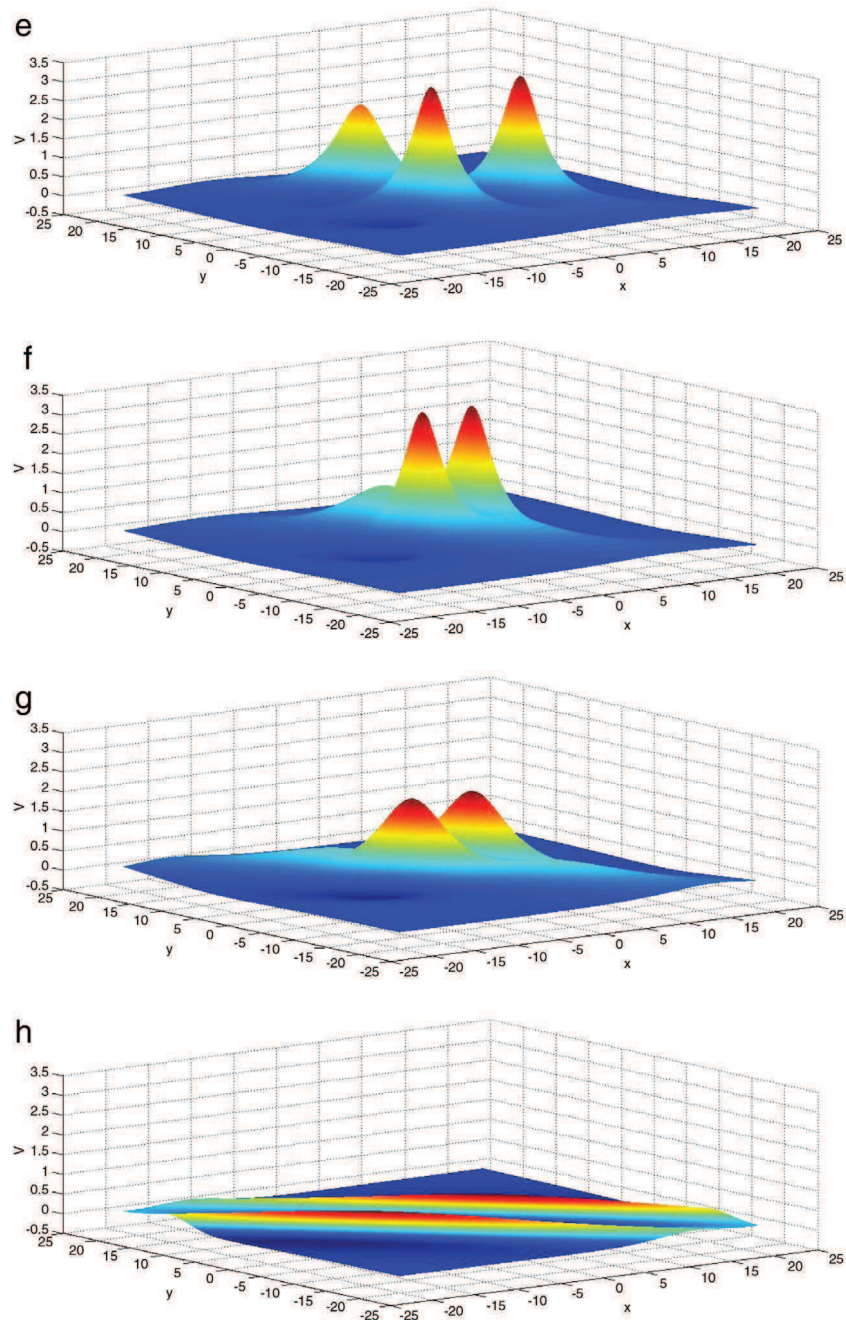


Fig. 6. (continued)

References

- [1] M.J. Ablowitz, H. Segur, *Solitons and the Inverse Scattering Transform*, SIAM, Philadelphia, 1981.
- [2] V.I. Petviashvili, O.V. Pokhotelov, *Solitary Waves in Plasmas and in the Atmosphere*, Energoatomizdat, Moscow, 1989 (in Russian); Gordon and Breach, Philadelphia, 1992, Engl. transl.
- [3] V.I. Petviashvili, Equation of an extraordinary soliton, *Soviet J. Plasma Phys.* 2 (1976) 257–260.
- [4] D.E. Pelinovsky, Y.A. Stepanyants, Convergence of Petviashvili's iteration method for numerical approximation of stationary solutions of nonlinear wave equations, *SIAM J. Numer. Anal.* 42 (2004) 1110–1127.
- [5] S.V. Manakov, V.E. Zakharov, L.A. Bordag, A.R. Its, V.B. Matveev, Two-dimensional solitons of the Kadomtsev–Petviashvili equation and their interaction, *Phys. Lett. A* 63 (1977) 205–206.
- [6] M.J. Ablowitz, J. Satsuma, Solitons and rational solutions of nonlinear evolution equations, *J. Math. Phys.* 19 (1978) 2180–2186.
- [7] Z. Lu, E.M. Tian, R. Grimshaw, Interaction of two lump solitons described by the Kadomtsev–Petviashvili I equation, *Wave Motion* 40 (2004) 95–120.
- [8] W.-X. Ma, Lump solutions to the Kadomtsev–Petviashvili equation, *Phys. Lett. A* 379 (2015) 1975–1978.
- [9] D.E. Pelinovsky, Y.A. Stepanyants, New multisoliton solutions of the Kadomtsev–Petviashvili equation, *JETP Lett.* 57 (1993) 24–28.

- [10] K.A. Gorshkov, D.E. Pelinovsky, Yu.A. Stepanyants, Normal and anomalous scattering, formation and decay of bound-states of two-dimensional solitons described by the Kadomtsev–Petviashvili equation, *J. Exp. Theor. Phys.* 77 (1993) 237–245.
- [11] W.-X. Ma, Zh. Qin, X. Lü, Lump solutions to dimensionally reduced \mathbf{p} -gKP and \mathbf{p} -gBKP equations, *Nonlinear Dynam.* (2015) 1–9.
- [12] Y. Zhang, W.-X. Ma, Rational solutions to a KdV-like equation, *Appl. Math. Comput.* 256 (2015) 252–256.
- [13] V.I. Karpman, *Nonlinear Waves in Dispersive Media*, Nauka, Moscow, 1973 (in Russian); Pergamon Press, Oxford, 1975, Engl. transl.
- [14] L.A. Abramyan, Yu.A. Stepanyants, The structure of two-dimensional solitons in media with anomalously small dispersion, *Sov. Phys.–JETP* 61 (1985) 963–966.
- [15] E. Falcon, C. Laroche, S. Fauve, Observation of depression solitary surface waves on a thin fluid layer, *Phys. Rev. Lett.* 89 (2002) 204501.
- [16] D.E. Pelinovsky, Yu.A. Stepanyants, Yu.S. Kivshar, Self-focusing of plane dark solitons in nonlinear defocusing media, *Phys. Rev. E* 51 (1995) 5016–5026.
- [17] V.A. Mironov, A.I. Smirnov, L.A. Smirnov, Structure of vortex shedding past potential barriers moving in a Bose–Einstein condensate, *J. Exp. Theor. Phys.* 110 (2010) 877–889.
- [18] T.R. Tauchert, A.N. Guzelsu, An experimental study of dispersion of stress waves in a fiber-reinforced composite, *Trans. ASME E* 39 (1972) 98–102.
- [19] K.M. Berger, P.A. Milewski, The generation and evolution of lump solitary waves in surface-tension-dominated flows, *SIAM J. Appl. Math.* 61 (2000) 731–750.
- [20] E.A. Kuznetsov, S.K. Turitsyn, Two- and three-dimensional solitons in weakly dispersive media, *J. Exp. Theor. Phys.* 55 (1982) 844–847.
- [21] K.A. Gorshkov, L.A. Ostrovsky, Interaction of solitons in nonintegrable systems: direct perturbation method and applications, *Physica D* 3 (1981) 428–438.
- [22] M.J. Ablowitz, J. Villarroel, Solutions to the time dependent Schrödinger and the Kadomtsev–Petviashvili equations, *Phys. Rev. Lett.* 78 (1997) 570–573.

Bibliography

- Ablowitz, M. J., & Haut, T. S. (2009). Coupled nonlinear Schrodinger equations for interfacial fluids with a free surface. *Theor. and Math. Phys.*, 689–697.
- Ablowitz, M. J., & Segur, H. (1981). *Solitons and the Inverse Scattering Transform*. Philadelphia: SIAM.
- Ablowitz, M., & Satsuma, J. (1978). Solitons and rational solutions of nonlinear evolution equations. *Math. Phys.*, 19, 2180–2186.
- Ablowitz, M., & Villarroel, J. (1997). Solutions to the time dependent Schrödinger and the Kadomtsev–Petviashvili equations. *Phys. Rev. Lett.*, 78, 570–573.
- Abramyan, L., & Stepanyants, Y. (1985). The structure of two-dimensional soliton in media with anomalously small dispersion. *Sov. Phys. JETP*, 61(5), 963–966.
- Alias, A., Grimshaw, R. H., & Khusnutdinova, K. R. (2014a). Coupled Ostrovsky equations for internal waves with a background shear flow. *Procedia IUTAM*, 3–14.
- Alias, A., Grimshaw, R. H., & Khusnutdinova, K. R. (2014b). Coupled Ostrovsky equations for internal waves in a shear flow. *Phys. Fluids*, 126603.
- Allen, J. E. (1998). The Early History of Solitons (Solitary Waves). *Physica Scripta*, 57(3), 436–441.
- Alpers, W. (1985). Theory of Radar Imaging of Internal Waves. *Nature*, v.314, 245–247.
- Apel, J. R., Byrne, H. M., Proni, J. R., & Charnell, R. L. (1975). Observation of Oceanic Internal and Surface Waves from the Earth Resources Technology Satellite. *Geophys. Res.*, v. 80, 865–881.
- Apel, J. R., Ostrovsky, L. A., Stepanyants, Y. A., & Lynch, J. F. (2006). *Internal Soliton in the Ocean*. Woods Hole, MA: Woods Hole Oceanographic Institute.
- Apel, J., Ostrovsky, L. A., Stepanyants, Y. A., & Lynch, J. F. (2007). Internal Solitons in the Ocean and their Effect on Underwater Sound. *J. Acoust. Soc. Am.*, 121(2), 695–722.
- Baines, P. G. (1973). The Generation of internal tides by flat-bump topography. *Deep-Sea Research*, 20, 179–205.

- Berger, K. M., & Milewski, P. A. (2000). The generation and evolution of lump solitary waves in surface-tension-dominated flows. *SIAM J. Appl. Math.*, 731–750.
- Brekhovskikh, L., & Goncharov, V. (1994). *Mechanics of Continua and Wave Dynamics*. Berlin: Springer.
- Campbell, D. K., Flach, S., & Kivshar, Y. S. (2004). Localizing Energy Through Nonlinearity and Discreteness. *Physics Today*, 43–49.
- Chaplygin, S. A. (2007). One Case of Vortex Motion on Fluid. *Regular and Chaotic Dynamics*, v.12, No.2, 219–232.
- Churaev, E. N., Semin, S. V., & Stepanyants, Y. A. (2015). Transformation of Internal Waves Passing over a Bottom Step. *Fluid Mech.*, v. 768, R3.
- Falcon, E., Laroche, C., & Fauve, S. (2002). Observation of depression solitary surface waves on a thin fluid layer. *Phys. Rev. Lett.*, 204501,4pp.
- Farmer, D. M., & Armi, L. (1988). The flow of Atlantic water through the Straits of Gibraltar. *Progress in Oceanography*, 21, 1–105.
- Gardner, C. S., Green, J. M., Kruskal, M. D., & Miura, R. M. (1967). Method for Solving the Korteweg De Vries Equation. *Phys. Rev. Lett.*, 19, 1095–1097.
- Garrett, C. (2003b). Internal tides and ocean mixing. *Nature*, 477–478.
- Gerkema, T., & Zimmerman, J. T. (2008). *An Introduction to Internal Waves*. Texel: Royal NIOZ.
- Gorshkov, K. A., & Ostrovsky, L. A. (1981). Interactions of solitons in nonintegrable systems: direct perturbation method and applications. *Physica D* 3, 428–438.
- Gorshkov, K. A., & Papko, V. V. (1977). Dynamic and stochastic oscillations of soliton lattices. *Zh. Eksp. Teor. Fiz.*, 73(7), 178–187 (in Russian. Engl. transl.: Sov. Phys. JETP, 1977, 46, 92–97).
- Gorshkov, K. A., Pelinovsky, D. E., & Stepanyants, Y. A. (1993). Normal and anomalous scattering, formation and decay of bound-states of two-dimensional solitons described by the Kadomtsev–Petviashvili equation. *JETP*, 77((Eng. transl. from the Russian journal ZhETF, 104 (1993) 2704).), 237–245.
- Grimshaw, R. (1996). *Internal Solitary Waves, in Advances in Coastal and Ocean Engineering*. edited by P. L.-F. Liu, Singapore: World Scientific.
- Grimshaw, R., & Helfrich, K. (2008). Long-Time Solutions of the Ostrovsky Equation. *Stud. Appl. Math.*, 121, 71–88.

- Grimshaw, R., & Helfrich, K. (2012). The effect of rotation on internal solitary waves. *IMA J. Appl. Math.*, 77, 326–329.
- Grimshaw, R., Ostrovsky, L. A., Shrira, V. I., & Stepanyants, Y. A. (1998b). Long Nonlinear Surface and Internal Gravity Waves in a Rotating Ocean. *Surveys in Geophys.*, 19, 289–338.
- Hasimoto, H. (1970). *Kagaku*, 40, 401 - 403 (in Japanese).
- Helfrich, K. R., & Melville, W. K. (1986). On long Nonlinear Internal Waves over Slope-shelf Topography. *Fluid Mech.*, v. 167, 285–308.
- Helland-Hansen, B., & Nansen, F. (1909). *The Norwegian Sea - its physical oceanography based upon the Norwegian researches 1900-1904*. Kristiania: Det Mallingske Bogtrykkeri.
- Holloway, P., Pelinovsky, E., & Talipova, T. (1999). A Generalised Korteweg-de Vries Model of Internal Tide Transformation in the Coastal Zone. *Geophys Research*, 104(18), 333–350.
- Hughes, B. A. (1978). The Effect of Internal Waves on Surface Wing Waves, 2, Theoretical Analysis. *Geophys. Res.*, v. 83, 455–465.
- Kakutani, T., & Ono, H. (1969). Weak non-linear electromagnetic waves in a cold, collision-free plasma. *J Phys Soc Japan*, 26: 1305–18.
- Karpman, V. I. (1975). *Nonlinear Waves in Dispersive Media*. Oxford: Pergamon Press (Eng. transl. from Russian journal Nauka, Moscow 1973).
- Kawahara, T. (1972). Oscillatory solitary waves in dispersive media. *J. Phys. Soc*, 33, 260–264.
- Kerner, B. S., & Osipov, V. V. (1994). *Autosolitons. A New Approach to Problems of Self-Organization and Turbulence*. Springer.
- Korteweg, D. J., & De Vries, G. (1895). On the Change of Form of long Waves Advancing in a Rectangular Channel and on a New type of Long Stationary Waves. *Phil. Mag.*, 39(5), 442–443.
- Kuznetsov, E., & Turitsyn, S. (1982). *JETP*, 55, 844 (Eng. transl. from the Russian journal ZhETF, 82 (1982) 1457).
- Lamb, H. (1932). *Hydrodynamics, 6th edn*. Cambridge University Press.

- Lamb, K. G. (1994). Numerical Experiments of Internal Wave Generation by Strong Tidal Flow across a Finite Amplitude Bank Edge. *Geophys. Res.*, v. 99, 843–864.
- Lu, Z., Tian, E., & Grimshaw, R. (2004). Interaction of two lump solitons described by the Kadomtsev–Petviashvili I equation. *Wave Motion*, 40, 95–120.
- Ma, W. -X. (2015). Lump solutions to the Kadomtsev-Petviashvili equation. *Physics Lett A*, 1978–1978.
- Ma, W.-X., Qin, Z., & Lü, X. (2015). Lump solutions to dimensionally reduced p-gKP and p-gBKP equations. *Nonlin. Dynamics*, 1–9.
- Manakov, S., Zakharov, V., Bordag, L., & Its, A. (1977). Two-dimensional solitons of the Kadomtsev–Petviashvili equation and their interaction. *Phys. Lett. A.*, 63, 205–206.
- Maxworthy, T. (1979). A note on the Internal Solitary Waves produced by Tidal Flow over Three-dimensional Ridge. *Geophys. Res.*, v. 84, 338–346.
- Mironov, V. A., Smirnov, A. I., & Smirnov, L. A. (2010). Structure of vortex shedding past potential barriers moving in a Bose-Einstein condensate. *JETP*, 877–889.
- Mourachkine, A. (2004). Nonlinear Excitations: Solitons. arXiv:cond-mat/0411452v1.
- Nagashima, H. (1979). Experiment on Solitary waves in the non-linear transmission-line described by the equation $du/dt + udu/dz - d^2u/dz^2 = 0$. *Phys. Soc. Japan*, 47, 1387–1388.
- Obregon, M., & Stepanyants, Y. (1998). Oblique magneto-acoustic solitons in rotating plasma. *Phys. Lett. A.*, 249(4), 315–323.
- Obregon, M., & Stepanyants, Y. (2012). On Numerical Solution of the Gardner-Ostrovsky Equation. *Mathematical Modeling of Natural Phenomena*, 7(2), 113–130.
- Ostrovsky, L. (1978). Nonlinear Internal Waves in a Rotating Ocean. *Oceanography*, 18(2), 119–125.
- Ostrovsky, L. A. (2015). *Asymptotic Perturbation Theory of Waves*. Imperial College press.
- Ostrovsky, L. A., & Stepanyants, Y. A. (1989). Do Internal Solitons Exist in the Ocean? *Rev. Geophys.*, 27, 293.

- Ostrovsky, L., Pelinovsky, E., Shrira, V., & Stepanyants, Y. (2015). Beyond the KDV: Post-explosion development. *Chaos*, 097620.
- Pelinovsky, D., & Stepanyants, Y. (1993). New multisoliton solutions of the Kadomtsev–Petviashvili equation. *JETP Lett.*, 57, 24–28 (Engl. transl. from the Russian journal *Pis'ma v ZhETF* 57 (1993) 25).
- Pelinovsky, D., & Stepanyants, Y. (2004). Convergence of Petviashvili's iteration method for numerical approximation of stationary solutions of nonlinear wave equations. *SIAM J. Numerical Analysis*, 42(3), 1110–1127.
- Pelinovsky, D., Stepanyants, Y., & Kivshar, Y. (1995). Self-focusing of plane dark solitons in nonlinear defocusing media. *Phys. Rev. E*, 51, 5016–5026.
- Petviashvili, V. (1976). Equation of an extraordinary soliton. *Soviet J. Plasma Phys*, 2, 257–260 (Engl. transl. from the Russian journal *Fizika Plazmy*, 2 (1976) 469).
- Petviashvili, V., & Pokhotelov, O. (1992). *Solitary waves in the plasma and in the Atmosphere*. Philadelphia: Gordon and Breach (Eng. transl. from Russian journal *Energoatomizdat*, Moscow, 1989).
- Remoissenet, M. (1999). *Waves Called Solitons*. Berlin: Springer.
- Russell, J. S. (1844). Report on Waves. *Rep. 14th Meet. British Assoc. Adv. Sci.*
- Scott, A. C. (Ed.). (2005). *Encyclopedia of Nonlinear Science*. New York and London: Routledge.
- Shrira, V. I. (1981). Propagation of long nonlinear waves in a layer of rotating fluid. *Izvestiya. Atmos. Ocean. Phys.*, 55–59.
- Stepanyants, Y. A. (2005). Dispersion of long gravity-capillary surface waves and asymptotic equations for Solitons. *Proc. Russ. Acad. Eng. Sci. Ser. Appl. Math.*, 14, 33–40 (in Russian).
- Tauchert, T. R., & Guzelsu, A. N. (1972). An experimental study of dispersion of stress waves in a fiber-reinforced composite. *Trans. ASME, Ser. E, J. Appl. Mech*, 39, 98–102.
- Toda, M. (1989a). *Theory of Nonlinear Lattices* (2nd ed.). Berlin: Springer.
- Whitfield, A. J., & Johnson, E. R. (2015a). Modulational instability of co-propagating internal wavetrains under rotation. *Chaos*, 023109.
- Whitfield, A. J., & Johnson, E. R. (2015b). Wave-packet formation at the zero-dispersion point in the Gardner-Ostrovsky equation. *Phys. Rev. E*, 051201.

- Yang, J., & Lakoba, T. I. (2008). Accelerated imaginary-time evolution methods for the computation of solitary waves. *Stud Appl Math*, 120: 265–92.
- Zhang, Y., & Ma, W.-X. (2015). Rational Solutions to KdV-like equation. *Appl. Math. Comp.*, 252–256.